

**DEVELOPMENT AND ANALYSIS OF ULTRASONIC ASSISTED  
FRICTION STIR WELDING PROCESS**

by

**Kwanghyun Park**

A dissertation submitted in partial fulfillment  
of the requirements for the degree of  
Doctor of Philosophy  
(Mechanical Engineering)  
in The University of Michigan  
2009

Doctoral Committee:

Professor Jun Ni, Chair  
Professor James R. Barber  
Professor Jyotirmoy Mazumder  
Professor Jwo Pan  
Professor Nickolas Vlahopoulos

© Kwanghyun Park  

---

All rights reserved  
2009

To Jinhee

## **ACKNOWLEDGEMENTS**

I would like to acknowledge Professor Jun Ni, my graduate advisor and committee chairman, for initiating my research at S. M. Wu Manufacturing Research Center. Without his continuous support and guidance, this work would not have been possible.

I would also like to extend my sincere gratitude to Professor James Barber, Professor Jyoti Mazumder, Professor Jwo Pan, and Professor Nickolas Vlahopoulos for serving on my doctoral committee. I appreciate the technical assistance received from Xianli Qiao and Steve Erskine on handling machines. I would like to express gratitude to Britt Diver in Weber ultrasonics USA for lending ultrasonic system.

I would also like to thank friends in Wu Manufacturing Research Center for the help and interaction, and my friends Dr. Ho Choi, Dr. Bong-suk Kim, Dr. Gap-Yong Kim, Jae-Wook Oh, and Seungchul Lee for the wonderful moments we have shared.

I am grateful to my parents and parents-in-laws for their care of me throughout the years. Last but not least I would like to thank my lovely wife, Jinhee Han and my adorable children, Shinyoung and Yoonyoung for supporting me and encouraging me to pursue this degree.

## TABLE OF CONTENTS

<b>DEDICATION.....</b>	<b>ii</b>
<b>ACKNOWLEDGEMENTS .....</b>	<b>iii</b>
<b>LIST OF FIGURES .....</b>	<b>vi</b>
<b>LIST OF TABLES.....</b>	<b>xi</b>
<b>ABSTRACT.....</b>	<b>xii</b>
<b>CHAPTER 1 - INTRODUCTION.....</b>	<b>1</b>
1.1 BACKGROUND AND MOTIVATION .....	1
1.2 RESEARCH OBJECTIVES.....	3
1.3 DISSERTATION ORGANIZATION .....	5
<b>CHAPTER 2 - LITERATURE REVIEW ON FRICTION STIR WELDING AND ULTRASONIC ASSISTED PROCESSING .....</b>	<b>6</b>
2.1 GENERAL OVERVIEW OF FRICTION STIR WELDING .....	6
2.2 ULTRASONIC ASSISTED PROCESSING.....	13
2.2.1 Ultrasonic assisted forming .....	14
2.2.2 Ultrasonic Machining .....	18
2.2.3 Ultrasonic welding.....	22
<b>CHAPTER 3 - PRELIMINARY EVALUATION FOR ULTRASONIC ASSISTED FRICTION STIR WELDING .....</b>	<b>25</b>
3.1 OVERVIEW OF FRICTION STIR WELDING EXPERIMENTAL SET-UP AND ITS OPERATION	25
3.2 EXPERIMENTAL INVESTIGATIONS OF THE ULTRASONIC ASSISTED FRICTION STIR WELDING PROCESS .....	28
3.2.1 Force measurement during friction stir welding.....	28
3.2.2 Mechanical testing of friction stir welded material .....	32
3.2.2.1 Tensile test.....	33
3.2.2.2 Microhardness test .....	35
3.2.2.3 Defect analysis .....	37
3.3 FE MODELING OF THE ULTRASONIC ASSISTED FRICTION STIR WELDING .....	39
3.3.1 FE model of the friction stir welding process.....	39
3.3.2 Heat generation due to ultrasonic vibration.....	42
3.3.3 Result and discussion.....	43
3.4 CONCLUSIONS .....	47

<b>CHAPTER 4 - THERMO-MECHANICAL FE MODEL OF ULTRASONIC ASSISTED FRICTION STIR WELDING .....</b>	<b>49</b>
4.1 INTRODUCTION.....	49
4.2 FEM MODELING .....	52
4.2.1 Thermal models .....	52
4.2.2 FE model description.....	53
4.2.2.1 FE mesh and geometry.....	54
4.2.2.2 Material model and interface properties .....	55
4.2.2.3 Boundary conditions .....	57
4.3 EXPERIMENTAL SETUP AND DESIGN .....	58
4.4 VALIDATION OF FEM MODELING OF FSW IN TERMS OF THE WELDING FORCE .....	59
4.5 EFFECT OF ULTRASONIC ASSISTANCE ON FSW OF LOW MELTING TEMPERATURE MATERIALS.....	62
4.6 EFFECT OF ULTRASONIC ASSISTANCE ON FSW OF HIGH MELTING TEMPERATURE MATERIALS.....	64
4.7 CONCLUSIONS .....	68
<b>CHAPTER 5 - EXPERIMENTAL INVESTIGATIONS OF THE ULTRASONIC ASSISTED FRICTION STIR WELDING PROCESS.....</b>	<b>69</b>
5.1 INTRODUCTION.....	69
5.2 DESIGN CONCEPT OF THE ULTRASONIC ASSISTED FSW PROCESS .....	70
5.3 ULTRASONIC HORN DESIGN AND FABRICATION .....	72
5.3.1 Horn design procedure.....	73
5.3.2 Design and fabrication of 40kHz ultrasonic horn.....	75
5.3.2.1 Horn type selection .....	75
5.3.2.2 Tuning process .....	78
5.3.2.3 Actual measurement of resonant frequency and amplitude .....	80
5.3.3 Design and fabrication of 20 kHz ultrasonic horn.....	82
5.4 UAFSW OF 6061-T651 ALUMINUM ALLOY .....	85
5.4.1 Experimental setup .....	85
5.4.2 Results with 40 kHz ultrasonic system.....	88
5.4.3 Results with 20 kHz ultrasonic system.....	94
5.5 ULTRASONIC ASSISTED FSW OF HIGH MELTING TEMPERATURE MATERIALS.....	96
5.6 CONCLUSIONS .....	101
<b>CHAPTER 6 - CONCLUSIONS AND FUTURE WORK .....</b>	<b>102</b>
6.1 CONCLUSIONS .....	102
6.2 RECOMMENDATIONS FOR FUTURE WORK.....	104
<b>BIBLIOGRAPHY.....</b>	<b>106</b>

## LIST OF FIGURES

Figure 2-1 : Schematic drawing of the friction stir welding (Thomas et al. 1991).....	6
Figure 2-2 : Schematic drawing of the FSW tool (Mishra and Ma 2005) .....	7
Figure 2-3 : (a) Worl tool (b) MX triflute tool (Thomas et al. 2003).....	8
Figure 2-4 : (a) Schematic diagram of microstructural zones in friction stir welds in aluminum (b) micrograph showing various micro-structural zones (Threadgill 1999) .....	9
Figure 2-5 : Peak temperature distribution adjacent to a friction stir weld in 7075AL (Mahoney et al. 1998).....	10
Figure 2-6 : Dependence of travel speed on alloy type and thickness.....	13
Figure 2-7 : The reduction in forming force based on superposition mechanism (a) Force reduction by impulses of ultrasonic in the drawing (Pohlman and Lehfeldt 1966) (b) Standing longitudinal wave induced in the sample (Winsper and Sansome 1969) .....	15
Figure 2-8 : Material softening with ultrasound (Langenecker 1966) (a) Stress reduction of aluminum in a tensile test during ultrasound irradiation (b) Temperature profile of standard tensile samples after the beginning of ultrasonic irradiation .....	16
Figure 2-9 : Burrs produced after drilling: 3.18mm drill 6000 RPM, 1.90mm/s federate (Chang and Bone 2005) .....	18
Figure 2-10 : (a) Average thrust force (b) flank wear progression at the outer edge of the cutting tips of four drills (Chang and Bone 2005) .....	19
Figure 2-11 : (a) Relationship between the drilling force and low ultrasonic frequency vibration (b) Drilling force vs. drilling time continuous drilling (Ishikawa et al. 1998).....	20
Figure 2-12 : (a) Simulated contact lengths; approaching (I) penetration (II) unloading (III) withdrawal (IV) (Mitrofanov et al. 2003) (b) Temperature evolution for the cutting tip (Mitrofanov et al. 2004).....	21

Figure 2-13 : Principle of ultrasonic welding set up for spot welding (Edgar de Vries 2004) .....	23
Figure 2-14 : Evolution of bonded area due to ultrasonic vibration (Chang and Bone 1974) .....	23
Figure 3-1 : FSW equipment by the use of Moriseiki CNC machining center.....	25
Figure 3-2 : Schematic of fixture .....	26
Figure 3-3 : Friction stir welding tool (a) tool clamped in a collar (b) tool size(mm).....	28
Figure 3-4 : Axial force (z-direction) and traverse force (x-direction) with respect to time at 1500 rpm rotational speed and 1 in/min translational speed.....	30
Figure 3-5 : Plot of the axial force vs. translational speed (a) at constant rotation speed (1500rpm) (b) at constant rotation speed (1800rpm).....	31
Figure 3-6 : Plot of the axial force vs. rotational speed at constant translational speed of 25 mm/min (left top), 50 mm/min (right top), 75 mm/min (left bottom), and 100 mm/min (right bottom) .....	32
Figure 3-7 : Schematic of a tensile test specimen.....	33
Figure 3-8 : (a) Changes in tensile strength and (b) tensile elongation of friction stir welded Aluminum 6061-T651 as a function of rotational and translational speed.....	34
Figure 3-9 : Top view of the failed tensile specimens showing a failure location.....	35
Figure 3-10 : Vickers hardness and matching cross-section view of the weld at 1800 rpm rotational speed and 75 mm/min translational speed .....	36
Figure 3-11 : Surface appearances of the welds (a) weld which has excessive weld flash (b) good weld (c) groove type defect .....	37
Figure 3-12 : Void defect from the cross sectional view.....	38
Figure 3-13 : Schematic diagram of the FSW system considered in the model .....	40
Figure 3-14 : Temperature-dependant stress-strain curve of 6061-T6 aluminum alloy [Chen and Kovacevic 2003].....	40
Figure 3-15 : Overview of ultrasonic assisted FSW process .....	42
Figure 3-16 : Comparison of temperature time curve for the location 10mm to the weld centerline and 1.6mm below the top surface of the plate.....	44
Figure 3-17 : Comparison of temperature time curve along the lateral direction for	



node lists 1.6mm below the top surface of the plate (time=3.5s) .....	45
Figure 3-18 : Comparison of temperature time curve according to different conditions at the location 10mm to the weld centerline and 1.6mm below the top surface of the plate .....	46
Figure 3-19 : Comparison of predicted principal stress(z-direction) with respect to time according to different conditions at the location 10mm to the weld centerline and 1.6mm below the top surface of the plate .....	47
Figure 4-1 : Friction stir welding process (Mahoney et al. 1998) .....	50
Figure 4-2 : Finite element meshes for workpieces, FSW tool, and backing place.....	55
Figure 4-3 : The effect of the friction coefficients with 0.2, 0.3, and 0.4 on the plunge forces.....	56
Figure 4-4 : Axial and traverse force profiles during the plunging and welding phases.....	58
Figure 4-5 : Comparison of forces-time curves between experiment and simulation results .....	59
Figure 4-6 : Temperature distribution during three steps of the tool travel .....	60
Figure 4-7 : Comparison of the experiment vs. simulated plunge force in FSW for 1500 and 1800 rpm speed, and 1 and 2 in/min translational speed .....	61
Figure 4-8 : Variations of the plunge forces with the tool motion of 1500 rpm rotational speed and 25 mm/min feed rate by imposing ultrasonic vibrations for two amplitudes .....	62
Figure 4-9 : Temperature profiles of welding region with and without ultrasonic effect .....	63
Figure 4-10 : Axial force comparison in FSW (1018 steel, Rotational speed of 650rpm; translational speed of 50 mm/min).....	66
Figure 4-11 : Axial force comparison with ultrasonic assistance (1018 steel, Rotational speed of 650rpm; translational speed of 50 mm/min).....	66
Figure 4-12 : Axial force comparison with ultrasonic assistance (304 stainless steel, Rotational speed of 1000rpm; translational speed of 50 mm/min).....	67
Figure 5-1 : Concept configuration of UaFSW.....	71
Figure 5-2 : Ultrasonic generator by Webber ultrasonics .....	71
Figure 5-3 : Ultrasonic transducer .....	72

Figure 5-4 : Assembly configuration of ultrasonic horn used in this study .....	74
Figure 5-5 : Criterion of horn dimension.....	74
Figure 5-6 : Different types of horn design: (a) Taper type with rectangular section, (b) Stepped type with rectangular section, and (c) Stepped type with circular section.....	75
Figure 5-7 : Amplitude of horn tip displacement with respect to frequency. Left and right plots describe the amplitude acquired from left and right tip of bearings, respectively.....	77
Figure 5-8 : Change in resonant frequency of longitudinal vibration mode after cutting laterally (y-direction).....	79
Figure 5-9 : Change in resonant frequency of longitudinal vibration mode after cutting longitudinally (z-direction).....	79
Figure 5-10 : Estimated modal frequencies for 40 kHz horn.....	80
Figure 5-11 : Actual measurement of (a) impedance and (b) phase using HP4192A.....	81
Figure 5-12 : 40 kHz ultrasonic horn amplitude measured by laser vibrometer .....	82
Figure 5-13 : Result of modal and harmonic analysis of the stepped type with rectangular section .....	83
Figure 5-14 : Result of modal and harmonic analysis of the stepped type with circular section.....	83
Figure 5-15 : Change in resonant frequency of longitudinal vibration mode after shortening and the final prototype .....	84
Figure 5-16 : 20 kHz ultrasonic horn amplitude measured by laser vibrometer .....	85
Figure 5-17 : (a) Schematic drawing of the assembly including a holder and (b) Fabricated horn and fixture.....	86
Figure 5-18 : Experimental set-up for UaFSW using Mori Seiki CNC machine .....	87
Figure 5-19 : Axial forces with respect to time.....	90
Figure 5-20 : Stress strain curve of welded parts.....	91
Figure 5-21 : Macroscopic views of weld zone at (a) 1500 rpm, 25mm/min, and without ultrasonics; (b) 1500 rpm, 25mm/min, and with ultrasonics; (c) 1500 rpm, 50mm/min, and without ultrasonics; (d) 1500 rpm, 50mm/min, and with ultrasonics; (e) 1800 rpm, 25mm/min, and without ultrasonics; (f) 1800 rpm, 25mm/min, and with ultrasonics.....	92

Figure 5-22 : Vickers hardness profiles in weld zone along centerline at different conditions.....	94
Figure 5-23 : Axial forces with respect to time (Rotational speed of 1500rpm; translational speed of 25 mm/min) .....	95
Figure 5-24 : Stress strain curve of welded parts (Rotational speed of 1500rpm; translational speed of 25 mm/min) .....	95
Figure 5-25 : Experimental setup for UaFSW using horizontal CNC machine.....	96
Figure 5-26 : The view of tool used: (a) made of A2 tool steel (b) made of tungsten carbide (10% cobalt).....	97
Figure 5-27 : Top view of friction stir welded 1018 steel; Upper joint is with ultrasonic and lower one is without ultrasonic .....	98
Figure 5-28 : Effect of ultrasonic vibration on axial forces (Rotational speed of 650 rpm; translational speed of 50 mm/min).....	99
Figure 5-29 : Effect of ultrasonic vibration on temperature profiles (Rotational speed of 650 rpm; translational speed of 50 mm/min).....	99
Figure 5-30 : Axial forces with respect to time (Rotational speed of 650 rpm; translational speed of 25 mm/min) .....	100

## LIST OF TABLES

Table 2-1 : Overview of friction stir welding process .....	11
Table 3-1 : Nominal compositions of aluminum alloy 6061-T651.....	26
Table 3-2 : Mechanical properties of aluminum alloy 6061-T651 .....	27
Table 3-3 : Guideline for tempering A2 Tool Steel.....	27
Table 3-4 : Geometry and process variables used for FEA.....	41
Table 3-5 : Material properties of A2 tool steel and 6061-T651 aluminum alloy (Alcan 1970; Chen and Kovacevic 2003).....	41
Table 3-6 : Heat flux conditions due to ultrasonic vibration.....	45
Table 4-1 : Material properties and Johnson-Cook parameters for 1018 steel and 304 stainless steel used in the numerical analysis (Mori et al. 2007; Vural et al, 2003) .....	65
Table 4-2 : Temperature dependent friction coefficient of steel (Awang et al. 2005).....	65
Table 5-1 : Specifications of the 40 kHz ultrasonic generator.....	72
Table 5-2 : Processing parameters .....	87

## **ABSTRACT**

Friction stir welding (FSW) has been used for joining low melting temperature materials successfully. However, applications in high strength alloys, such as titanium and stainless steel, remain limited due to large welding force and consequent tool wear. Ultrasonic-assisted processes have been coupled with tooling in various manufacturing processes in order to enhance the performance of conventional machining and bonding processes. We suggest ultrasonic assisted friction stir welding (UaFSW), as a hybrid system, in order to improve the weld quality and welding efficiency of high melting temperature materials.

For successful and effective implementation of the UaFSW process, integration of the ultrasonics on the FSW equipment is necessary, while minimizing vibratory effects on the remaining machine assembly. The UaFSW system is being developed and its mechanism needs to be understood using both the experiments and the numerical simulations. FE simulations of the UaFSW using ABAQUS are carried out to examine plunge forces and temperature profiles during the plunge stage of the process. To gain the fundamental understanding and insights of the process, force and temperature measurement, mechanical testing, and defect analysis are used in studying the influence of the ultrasonic oscillations on the conventional FSW system.

Taking advantage of the characteristics of ultrasonic vibration, the UaFSW of aluminum alloy enables us to decrease the welding force and enhance mechanical

properties of welded part in terms of elongation and yield strength. It was shown that ultrasonic integration on FSW tool helps to decrease the chance of formation of welding defect. It could be also observed from the experimental results that ultrasonic vibration helps to decrease the welding forces for welding of high melting temperature material. Force reduction of 6% during the peak region and 12.5% during the welding one was observed. For FE analysis of UaFSW, it was predicted that the plunge forces were reduced by using the ultrasonic vibrations. In addition, it was shown that the plunge forces could be decreased by increasing the amplitude of vibrations.

## **CHAPTER 1 - INTRODUCTION**

### **1.1 BACKGROUND AND MOTIVATION**

A variety of joining processes for metal parts have been employed in various fields of the manufacturing industry. Depending on the types or combinations of energy, metal welding processes may be divided into two major groups: (1) fusion welding and (2) solid-state welding. Fusion welding processes use intense localized heat source to melt the base metal. Solid-state welding is completed under pressure alone or a combination of heat and pressure. If heat is used, the temperature in the solid-state welding process is below the melting temperature.

Friction Stir Welding (FSW) falls in the category of solid state welding which was invented by The Welding Institute (TWI) in 1991 for joining low melting temperature alloys like aluminum, magnesium and copper (Thomas et al. 1991). The basic principle of FSW involves plunging a spinning tool that has a specially designed pin and shoulder into the workpieces that are intended for welding. Since melting of materials is avoided, FSW avoids problems such as distortion and metallurgical reactions which typically appear in conventional fusion welding processes. It is reported that the strength of the FSW weld is 30% to 50% greater than those produced by arc welding and resistance spot welding while maintaining the fatigue life comparable to riveted panels (Mendez and Eagar 2001). However, applications with high temperature materials like steel and titanium remain limited. Compared with joining of low temperature materials, FSW of steel requires large plunging and stirring forces, which dictate the use of large FSW

equipment. More importantly, the life of a spin tool is significantly reduced in the FSW of high temperature materials. Frequent replacement of worn-out tools leads to high production cost, which results in additional cost due to reduced production rate. Moreover, the use of the damaged tool brings about another problem in terms of welding quality.

Several variations of FSW are being developed to address these problems. One is to use an induction coil in front of the rotating tool (Reitz 2002; Tweedy et al. 2005). But it is difficult to focus the induction coil on a specific location, and coil heats all conductive materials including the tool. Others are using fusion welding apparatus such as laser and plasma torch (Kohn et al. 2002; Able and Pfefferkorn 2005). These technologies, however, are still under investigations and are inefficient in terms of energy consumption.

Since the 1950s, the application of ultrasonic energy to the plastic deformation of metals has been widely investigated. Claims have been made that ultrasonic oscillations in the tooling reduce static deformation forces, increase processing speeds, and improve the quality of the product (Sansome 1973). These effects have been demonstrated in various manufacturing processes such as machining, drilling, welding, etc (Kremer 1981; Tsujino et al. 2002; Neugebauer and Stoll 2004). Ultrasonic machining and drilling processes have been successfully demonstrated in machining tough-to-cut alloys such as titanium (Singh and Khamba 2006).

In this research, we are introducing a new hybrid technology which integrates ultrasonics to FSW. By integrating the ultrasonics to the FSW process, many benefits are expected in terms of welding quality, welding force, and tool life.



## 1.2 RESEARCH OBJECTIVES

This research aims to develop a novel ultrasonic-assisted friction stir welding (UaFSW) technique which may improve the welding process and enhance the welded part quality. Since the proposed ultrasonic assisted FSW process is a new solid-state welding process, guidelines for the design and control of the process need to be developed using theoretical and numerical models. In pursuit of fundamental understanding of the ultrasonic assisted FSW process and addressing the underlying scientific and technical challenges systematically, the following key objectives have been identified: (1) Development of the ultrasonic assisted FSW system. (2) Investigation of the influence of ultrasonic energy on FSW process. (3) Numerical and experimental studies of the ultrasonic assisted FSW process, and (4) Application of ultrasonic assisted FSW in high temperature materials. Specific objectives can be summarized as follows:

- 1) Development of FSW system and preliminary evaluation of UaFSW process: FSW system will be established using an in-house CNC drilling machine. Several welding parameters such as rotational speed, feed rate, and plunge depth will be measured and analyzed as a function of welding conditions. The FE models of UaFSW will be developed by using additional heat flux equation. Through the comparison with experimental results in the literature, the effectiveness of the FE model will be validated.
- 2) Thermo-mechanical model of UaFSW process: UaFSW is a hybrid welding technique, where high frequency vibration is superimposed on the movement of a rotating tool. The UaFSW system is being developed and its mechanism needs to

be understood using both the experiments and the numerical simulations. FE models of FSW process with ultrasonic assistance will be developed using available material and friction data in the literature. FE simulations of FSW and UaFSW using ABAQUS/Explicit will be carried out to examine plunge forces and temperature profiles during the plunge phase of FSW and UaFSW, respectively. Once the accuracy of the FSW model is validated by experiments, further FEA will be performed to gain a comprehensive understanding and to expand guidelines for the UaFSW process.

- 3) Development of the ultrasonic assisted FSW system: Ultrasonic energy can be transmitted into the welding region in a variety of ways. A good design will consider whether ultrasonic energy should be added to the shoulder, pin, workpiece, or backing table directly. The optimal means of transmitting the ultrasonic energy into the welding region while minimizing the vibration leakage into the rest of the machine must be determined for various geometrical and material configurations. To gain the fundamental understanding and insights of the process, it is essential to measure temperature, and welding force generated during the process. In this study, thrust force measurement, mechanical testing, and defect analysis will be used in studying the influence of the ultrasonic oscillations on the conventional FSW system. One of the most critical issues in FSW of steels is the life of FSW tool. Forces generated during FSW process are known to be one of important factors in causing the tool breakage. Therefore, the force and temperature investigations will be carried out for the UaFSW of high temperature materials.

### **1.3 DISSERTATION ORGANIZATION**

Chapter 2 presents the literature review on the friction stir welding and ultrasonic assisted processes. Chapter 3 presents experimental results of the FSW of 6061 aluminum alloy and preliminary results on the validation of FE model on the enhancement of FSW by means of ultrasonics. Chapter 4 concentrates on FE model of UaFSW process carried out to investigate the mechanism of the process. In Chapter 5, experimental investigations of the UaFSW process are addressed. In the final chapter, the accomplished work is summarized and the proposed future work is presented.

## CHAPTER 2 - LITERATURE REVIEW ON FRICTION STIR WELDING AND ULTRASONIC ASSISTED PROCESSING

### 2.1 GENERAL OVERVIEW OF FRICTION STIR WELDING

Friction Stir Welding (FSW) was invented by TWI in 1991 (Thomas et al. 1991). The basic principle of FSW involves plunging a spinning tool that has a specially designed pin and shoulder into the workpieces that are to be welded as shown in Figure 2-1. Heat is generated by friction and plastic deformation of the material, and thus localized heating softens the material surrounding the pin. Tool rotation and traverse motion causes movement of material from the front of the pin to the back with the weld forming in the solid state condition. Then, the deformed material cools producing a joint. Key benefits of FSW over fusion welding methods are:

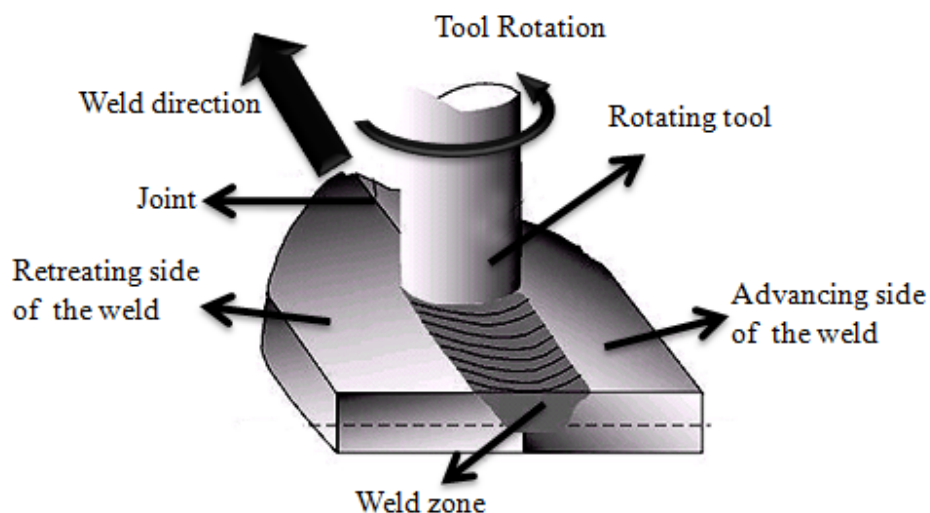
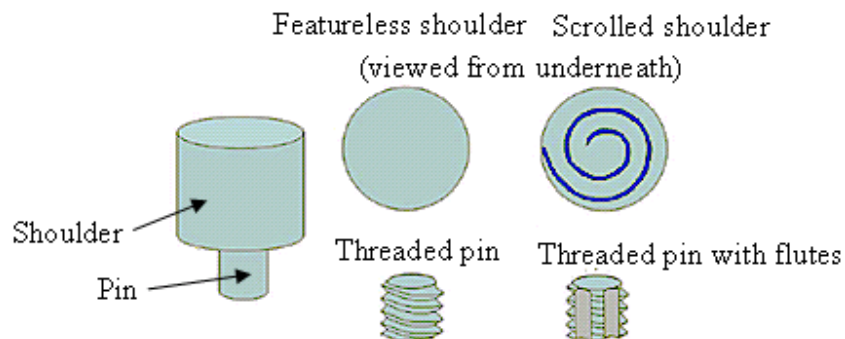


Figure 2-1 : Schematic drawing of the friction stir welding (Thomas et al. 1991)

- Low distortion of the workpiece
- Excellent metallurgical properties in the joint
- No shielding gas
- No surface cleaning preparation
- Energy efficiency

The emergence of the FSW alters the traditional approach for producing lightweight assemblies. Boeing has reduced cost and production time with the FSW on pressure vessels (Johnsen 1999). Likewise, Eclipse aviation began using FSW to join skin structures and Hitachi has applied this technology to the welding of aluminum skin structures in their trains in anticipation of large cost and time savings (Ohba et al. 2001). Complex material movement and plastic deformation contribute significantly to the physical mechanism of FSW. Tool geometry, welding parameters, and joint design significantly influence the material flow. Figure 2-2 shows the FSW tool which consists of a shoulder and a pin. The shape and relative size of the pin and the shoulder are important for maximizing the heat generation, which aids the material flow and reduces welding force.



**Figure 2-2 : Schematic drawing of the FSW tool (Mishra and Ma 2005)**

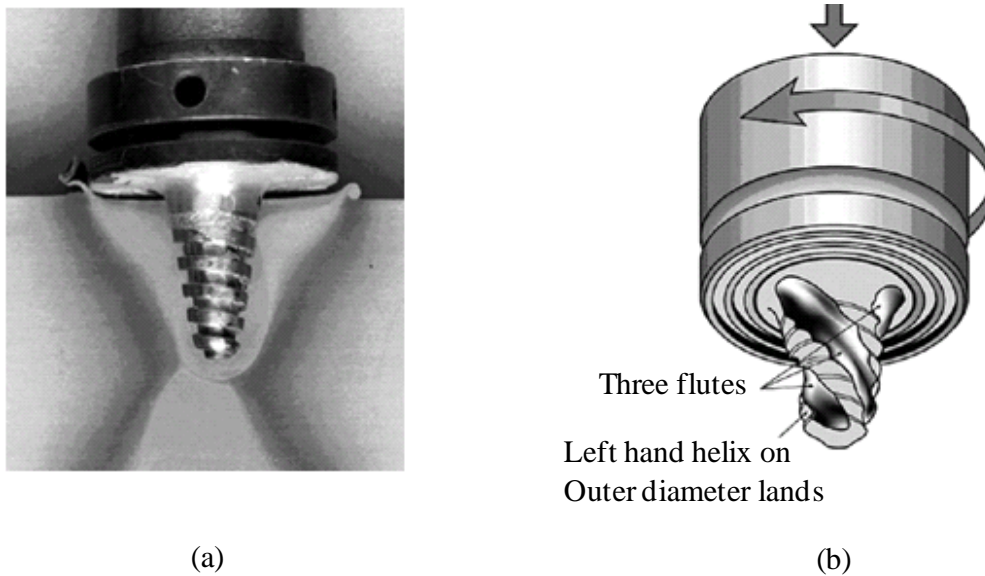


**Figure 2-3 : (a) Worl tool (b) MX triflute tool (Thomas et al. 2003)**

TWI (Thomas et al. 2003) has developed several types of tools like the worl and MX triflute tools as shown in Figure 2-3. It has been suggested that these design features reduce required welding forces, enable easier flow of plasticized material, facilitate a downward auguring effect, and increase the interface surface area between the pin and material. Zhao et al. (Zhao et al. 2005) investigated the influence of the pin geometry on bonding and mechanical properties in friction stir welded Al alloys. He claimed that pin design affects the flow of the plastic material strongly. The best quality weld was acquired using a tapered screw threaded pin.

Figure 2-4 shows the four visually distinct microstructural zones in which welds in aluminum are typically divided into: (a) unaffected parent material, (b) heat affected zone, (c) thermo-mechanically affected zone, and (d) weld nugget. In the heat affected zone, properties and microstructure are affected by the heat from the weld, although there is no mechanical deformation. This zone retains the same grain structure as the parent

materials. The thermo-mechanically affected zone shows characteristics that suggest that it underwent plastic deformation but recrystallization did not occur in this zone due to insufficient deformation strain. In weld nugget zone, intense plastic deformation and frictional heating during FSW result in recrystallized fine-grained microstructure (Threadgill 1999).

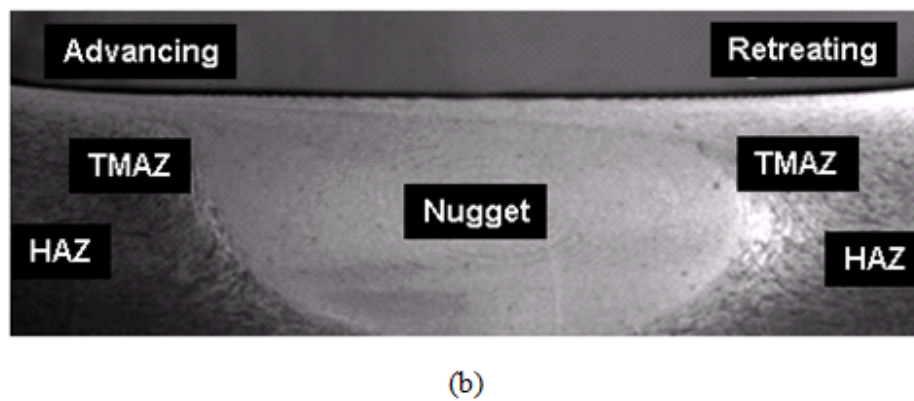
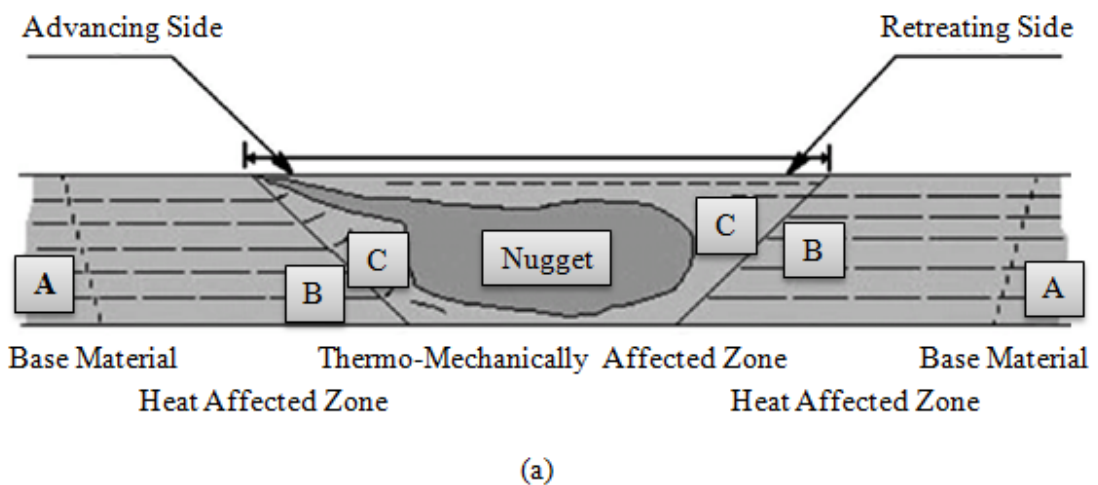


**Figure 2-4 : (a) Schematic diagram of microstructural zones in friction stir welds in aluminum (b) micrograph showing various micro-structural zones (Threadgill 1999)**

In FSW, it is important to analyze temperature distribution during FSW because the temperature distribution helps us to understand the microstructural characteristics such as

grain size, grain boundary, and mechanical properties of the welds. Mahoney et al (Mahoney et al. 1998) measured the temperature distribution near the weld nugget and observed that maximum temperature was measured at the locations close to the weld nugget as shown in Figure 2-5. Tang et al (Tang et al. 1998) also conducted the measurement of the heat input and temperature distribution and observed that maximum temperature increases with increasing tool rotation rate while decreasing with increasing traverse speed. Friction stir spot welding is a new process that has received considerable attention from automotive and other industries. Mazda reported the first application of the FSSW on their 2003 RX-8 (Mazda 2003) and they reported over 90% operation energy savings and over 40% capital investment reductions.

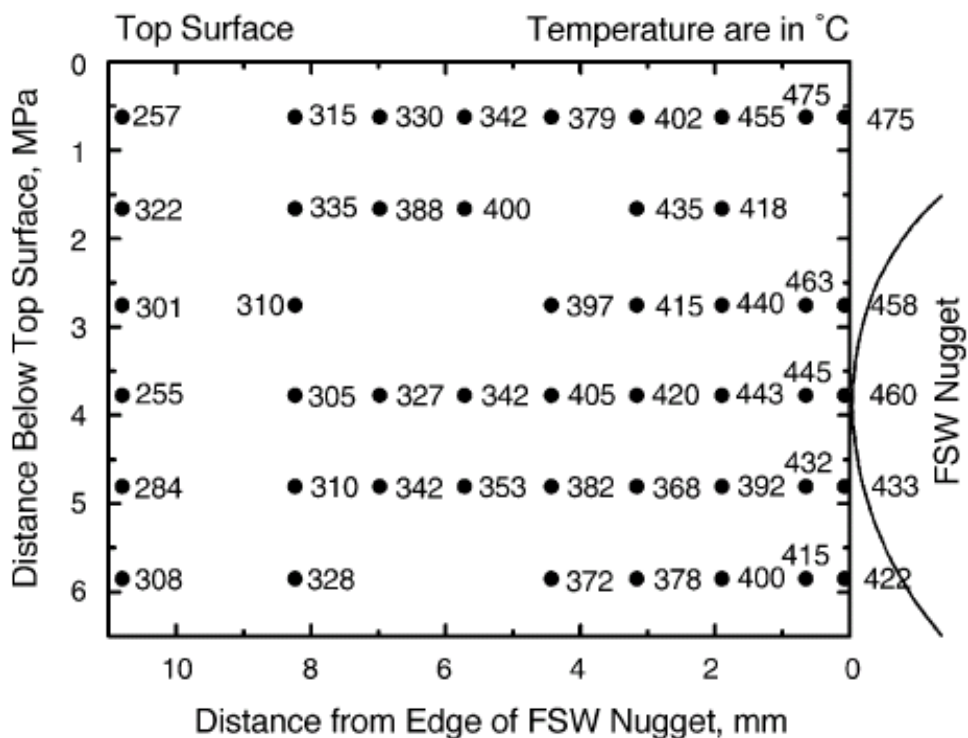


**Figure 2-5 : Peak temperature distribution adjacent to a friction stir weld in 7075AL (Mahoney et al. 1998)**

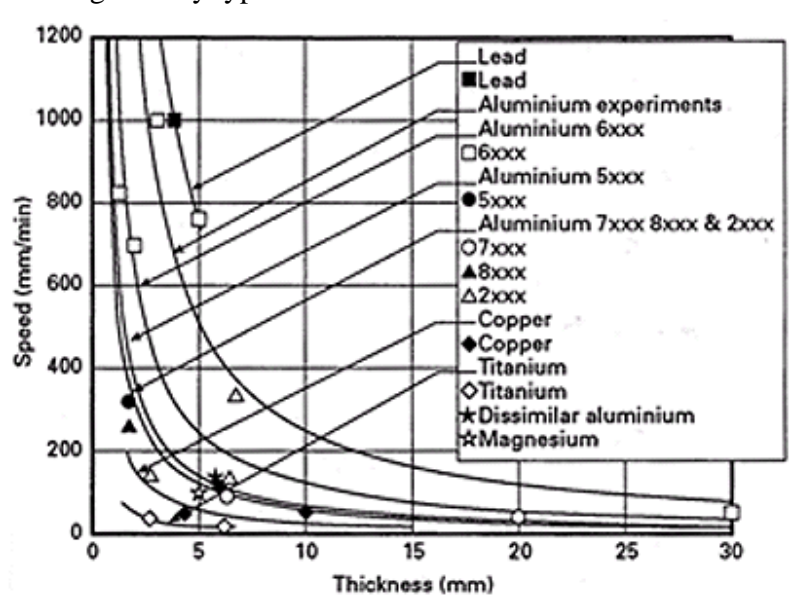


Due to the fact that material flow characteristics during FSW affects weld quality so extensively, a complete understanding of material flow around the rotating tool is crucial to the optimization of FSW parameters and tool design. So far, most tool designs have been carried out with intuitive concepts. It is important that tool wear is more objectively and scientifically understood in order to optimize the tool material and geometry. For microstructural stability, processing parameters such as the tool rotation rate and traverse speed must be investigated thoroughly (Mishra and Ma 2005). An overview of the friction stir welding is summarized in Table 2-1.

**Table 2-1 : Overview of friction stir welding process**

Mode	Description
Strengths	<ul style="list-style-type: none"> <li>▪ Ability to weld materials which are difficult to weld by other processes</li> <li>▪ Relatively simple welding procedure with no consumables or filler metal</li> <li>▪ Low distortion and low shrinkage → Excellent mechanical properties</li> <li>▪ No welding fumes or spatter hazards</li> <li>▪ Low energy consumption</li> <li>▪ No gas shielding required</li> </ul>
Weaknesses	<ul style="list-style-type: none"> <li>▪ High forces required to achieve welding process</li> <li>▪ Need for powerful fixtures to clamp the work-piece in place</li> <li>▪ Backing plate normally required</li> <li>▪ Keyhole usually left at the end of each weld</li> <li>▪ Cannot make fillet welds</li> </ul>
Application	<ul style="list-style-type: none"> <li>▪ NASA/Lockheed martin: Space shuttle external fuel tank</li> <li>▪ Boeing: Delta rocket fuel tanks, etc</li> <li>▪ Marine aluminum: Helidecks, bulkheads and decks for ships</li> <li>▪ Hitachi: A-type train</li> <li>▪ Eclipse aviation: 500 personal jets</li> <li>▪ Ford GT team : Joint extrusion</li> </ul>

Material (Thickness)	<ul style="list-style-type: none"> <li>▪ 1xxx,2xxx,5xxx,6xxx,7xxx,8xxx series aluminum alloy <ul style="list-style-type: none"> <li>○ 6-25mm has been generally reported</li> <li>○ 6082-T6 → up to 50mm (single pass), 75mm (two passes)</li> <li>○ 5xxx, 6xxx → 1mm or slightly less</li> </ul> </li> <li>▪ Steel(mild steel, austenitic, martensitic and duplex SS) <ul style="list-style-type: none"> <li>○ 3.2-6.4mm thick steel plates (single pass)</li> <li>○ 6.4mm thick 304L steel and steel plates of &gt;6.4mm (two passes)</li> </ul> </li> <li>▪ Copper and its alloys (2-50mm)</li> <li>▪ Lead and its alloy (3mm)</li> <li>▪ Zinc (0.88mm)</li> <li>▪ Magnesium alloys/Titanium and its alloy/ Nickel alloys/ Metal matrix composites</li> </ul>
Joint geometry	<ul style="list-style-type: none"> <li>▪ Butt welds (dissimilar thickness, non-linear, circumferential)</li> <li>▪ Lap welds</li> <li>▪ Circumferential lap welds</li> <li>▪ Corner joints</li> <li>▪ T joints</li> <li>▪ Pipe to flange welds</li> </ul>
Welding force (Power Input)	<ul style="list-style-type: none"> <li>▪ 6082-T6 aluminum alloy (6.3mm thick) <ul style="list-style-type: none"> <li>○ Rotational speed: 710-1000rpm, Traverse speed: 40-224mm/min</li> <li>○ <i>Downward force</i>: 5.5-10kN Torque 10-14Nm</li> </ul> </li> <li>▪ 6082/7075 aluminum alloy (25mm thick) <ul style="list-style-type: none"> <li>○ <i>Downward force</i>: 46-54kN (6082), 54-56kN (7075)</li> </ul> </li> <li>▪ 6061-T651 aluminum alloy (6.4mm thick) <ul style="list-style-type: none"> <li>○ Rotational speed: 1000-2500 rpm, Traverse speed: 204-816 mm/min</li> <li>○ <i>Downward force</i>: 3-7 kN</li> <li>○ <i>Spindle power</i>: 1.3-1.9 kW</li> </ul> </li> <li>▪ 2024-T351 aluminum alloy (6.4mm thick) <ul style="list-style-type: none"> <li>○ <i>Power</i>: 3.3kW (Fast weld), 2.9kW (Medium weld), 2.1kW (Slow weld)</li> </ul> </li> <li>▪ 2524-T351 aluminum alloy (6.4mm thick) <ul style="list-style-type: none"> <li>○ <i>Power</i>: 2.3kW (Fast weld), 2.1kW (Medium weld), 1.6kW (Slow weld)</li> </ul> </li> <li>▪ Mild steel (6-12mm thick) <ul style="list-style-type: none"> <li>○ <i>Maximum z-axis load</i>: 89Kn, <i>Machine horsepower</i>: 15kW</li> </ul> </li> <li>▪ 6000 series aluminum alloy(12.5mm) <ul style="list-style-type: none"> <li>▪ <i>Power</i>: 3kW</li> </ul> </li> </ul>

<p>Welding speed</p>	<ul style="list-style-type: none"> <li>▪ Welding speed depends on the tool geometry, the material, and other process parameters. Figure 2-6 shows a general result of travel speed according to alloy type and thickness</li> </ul>  <p><b>Figure 2-6 : Dependence of travel speed on alloy type and thickness</b></p>
<p>Tool life</p>	<ul style="list-style-type: none"> <li>▪ 6000 series aluminum alloy → up to 1000m</li> <li>▪ 6061 aluminum alloy → no measurable tool wear</li> <li>▪ 6061 AA + Al<sub>2</sub>O<sub>3</sub> MMC → 0.64%/cm wear rate(1000rpm), 0.42(1500rpm), 0.56(2000rpm)</li> <li>▪ It has been reported that tools were replaced after they were used to produce 1.5-2.0m of weld of steel</li> <li>▪ PCBN tool → 10m in HSLA-65, 30m in 304 Stainless steel, 80m in A36 steel</li> <li>▪ Tool replacement usually occurs in response to severe tool wear, and pin and shoulder fracture.</li> </ul>

## 2.2 ULTRASONIC ASSISTED PROCESSING

It was noted here that the ultrasonic energy influenced the performance of conventional manufacturing processes such as the forming, machining, and welding.

### 2.2.1 ULTRASONIC ASSISTED FORMING

Reports indicate that applying ultrasonic energy to a tool and/or workpiece in various metal-forming processes affects those processes in such a way that process forces can be reduced, processing speeds can be increased, and product quality is improved. These benefits have been attributed to superposition and local heating which occur when oscillatory energy is applied during the plastic deformation of metals. In most studies, superposition has been considered to be the major mechanism responsible for the reduction in forming force. The static force reduction during forming was found to be equal to the periodic force amplitude induced in the workpiece. Pohlman and Lehfeldt (Pohlman and Lehfeldt 1966) performed simple drawing experiments on pure polycrystalline copper with superimposed ultrasonic oscillation (Figure 2-7a). When the sample was subjected to impulses of ultrasound along the axial direction, the drawing force dropped immediately and remained low for the duration of the impulses. The amount of force reduction agreed with the value of the acoustic stress amplitude in the sample, which could be calculated from the displacement amplitude of the sample. Winsper (Winsper 1969; Winsper and Sansome 1969) reported that the optimum die-to-drum distance,  $d$ , during the wire drawing of mild metal should be obtained based on the following formula to achieve the maximum load reduction. The distance,  $a + \lambda_r/2$ , was found to be optimum value, where  $a$  is the constant determined empirically based on the acoustic impedance of the die/transducer assembly, and  $\lambda$  is the longitudinal wavelength in the wire (Figure 2-7b). The reduction in force could be also attributed to the superposition mechanism. However, Sansome (Sansome 1973) found that the peak of the oscillatory force exceeded the conventional process force in most cases even though the

mean force could be reduced when the ultrasonic vibration is applied. Hence, he concluded that if the superposition occurs alone in oscillatory metal working, it only has limited advantages for the industrial applications.

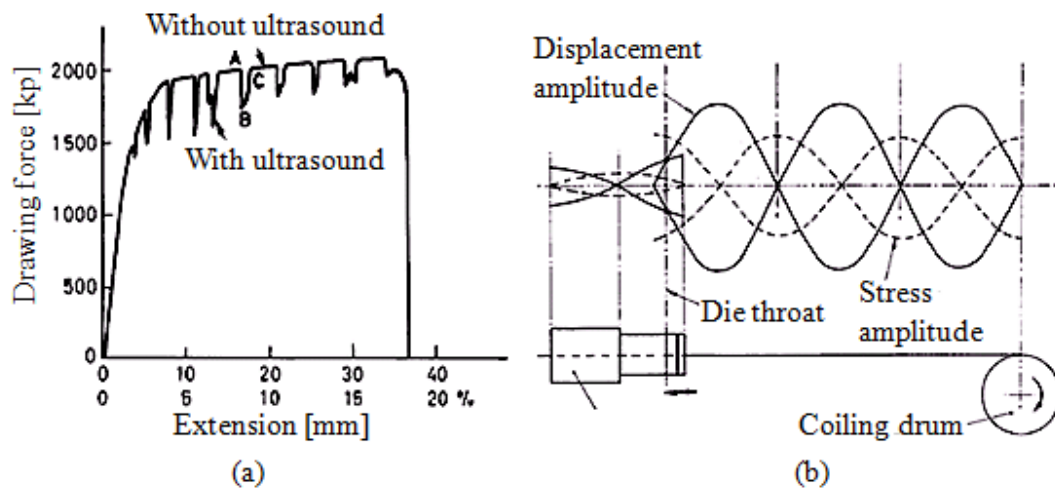


**Figure 2-7 : The reduction in forming force based on superposition mechanism (a) Force reduction by impulses of ultrasonic in the drawing (Pohlman and Lehfeldt 1966) (b) Standing longitudinal wave induced in the sample (Winsper and Sansome 1969)**

In the late 1960's and early '70's, Langenecker (Langenecker 1965; Langenecker 1966; Langenecker and Jones 1970) conducted tensile, wire drawing, and tube bending experiments of various metals (Al, Cu, SAE 1019 Steel, etc), and found that the reduction of process force was much larger than the acoustic stress in the sample when high intensity ultrasound was applied (Figure 2-8a). By using infrared radiometry, he discovered a notable temperature gradient that was built up in the sample within a few seconds (Figure 2-8b).

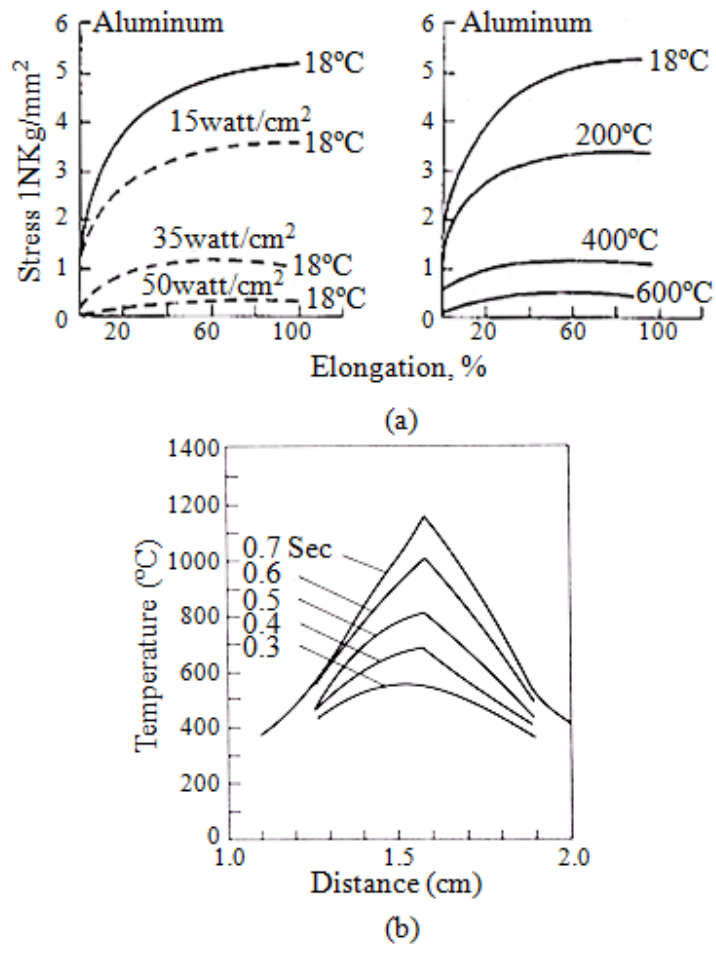


**Figure 2-8 : Material softening with ultrasound (Langenecker 1966) (a) Stress reduction of aluminum in a tensile test during ultrasound irradiation (b) Temperature profile of standard tensile samples after the beginning of ultrasonic irradiation**

It was determined that acoustic softening occurred via a local heating mechanism since a large portion of the energy transmitted from the sonotrode into the workpiece was converted into heat. When compared with the density of thermal energy required to heat the samples without ultrasound, ultrasonic irradiation was proven to be more efficient ( $10^{22} \text{ eV/cm}^3$  in the case of conventional heating vs.  $10^{15} \text{ eV/cm}^3$  when heated by ultrasound). Similar thermal softening was reported for various materials by other

researchers (Severdenko and Petrenko 1969; Izumi et al. 1966) and the reductions in hardness, work hardening rate, and residual stress which were not accounted for by the superposition mechanism could be explained as a result of heating the test-piece. Hence, it would be expected that present forming techniques will be improved by establishment of optimum working parameters for coupling ultrasonic energy into the deformation zone.

Many investigators have claimed that the change in friction force was caused by an actual change of the friction coefficient. Huang et al. (Huang et al. 2002) observed that the maximum forming force during the interval of vibration was much less than the static force without vibration in the upsetting process of plasticine. He concluded that further reduction in the forming force was realized by the reduction of the interfacial friction coefficient and presented the reduced barreling of the finished specimen under ultrasonics as supporting evidence. However, a conflicting result was reported by Pohlman and Lehfeldt (Pohlman and Lehfeldt 1966). When the oscillation direction was normal to the friction direction and the contact surface, no apparent reduction of friction force was observed. Sansome (Sansome 1973) indicated that the coefficient of friction might have been reduced due to: (1) asperities that were softened, (2) pumped lubricant, (3) chemical activation of the lubricant, and (4) surface separation. However, further studies will be required to explain the details for each mechanism. Biddell and Sansome (Biddell and Sansome 1974) also outlined the historical development of oscillating metal forming equipment and its application to the deep drawing, wire drawing, and plug drawing processes. However, at that time (1970s), a clear understanding of the deformation mode, acoustic effect, and production technology (i.e., cost, reliability, and cycle time) were not fully developed, and some misleading conclusions were found pertaining to the

application of ultrasonics (Biddell and Sansome 1974). Since the vibration characteristic changes depending on the process, material, and tooling system, guidelines for the design of this system and its coupling method with the tools and workpiece need to be developed considering such challenges as cost, space, and flexibility for industrial applications.

### 2.2.2 ULTRASONIC MACHINING

Ultrasonics has been successfully applied to machining processes such as drilling, turning, cutting, and EDM. Like other ultrasonic assisted processes, the principle of ultrasonic drilling involves adding high-frequency and low amplitude vibration in the feed direction of the tool or workpiece. Chang and Bone (Chang and Bone 2005) investigated the effect of ultrasonic assistance on burr size, chip formation, thrust forces and tool wear. Usually, large burrs affect part quality and impede assembly. Chang and Bone observed that burr height and width were reduced with ultrasonic assistance (Figure 2-9). He also observed a reduction in thrust force (a). However, the ultrasonic assisted drilling did introduce some disadvantages in terms of tool strength and life (b).

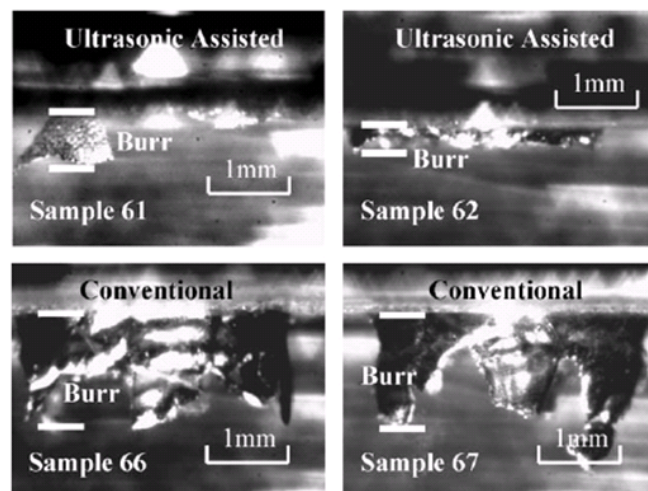


**Figure 2-9 : Burrs produced after drilling: 3.18mm drill 6000 RPM, 1.90mm/s federate (Chang and Bone 2005)**



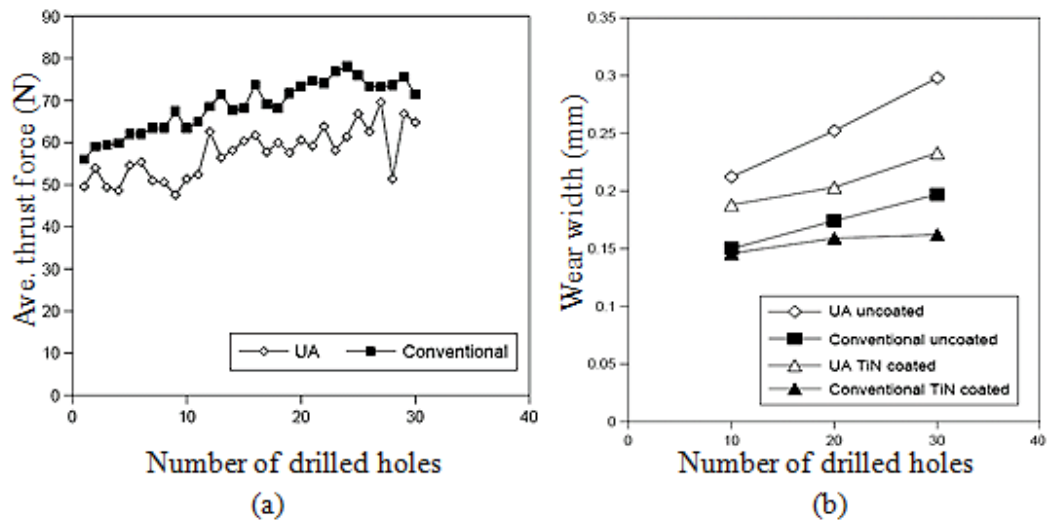


**Figure 2-10 : (a) Average thrust force (b) flank wear progression at the outer edge of the cutting tips of four drills (Chang and Bone 2005)**

Ishikawa et al. (Ishikawa et al. 1998) reported the effect of combined vibration drilling by applying ultrasonic vibration to the core drill and low-frequency vibration to the workpiece. Their research focused on trends in drilling force and hole accuracy. Figure 2-11a shows the relationship between the drilling force and low ultrasonic frequency vibration, which was conducted at three amplitudes. It was observed that drilling force decreased as low frequency vibration and ultrasonic vibration amplitude were increased. Figure 2-11b shows the drilling force vs. drilling times during continuous drilling. In the case of a non-vibration drilling, the drilling force increased greatly as the drilling times increased, while the drilling force didn't change even after drilling 100 times in the combined vibration drilling.

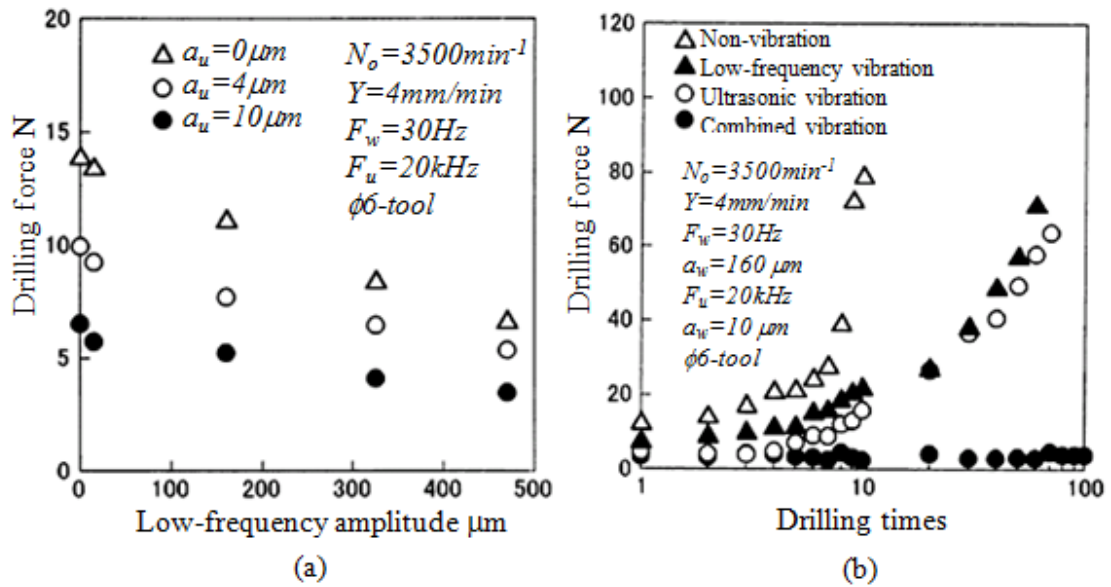


**Figure 2-11 : (a) Relationship between the drilling force and low ultrasonic frequency vibration (b) Drilling force vs. drilling time continuous drilling (Ishikawa et al. 1998)**

Generally, activities in turning development have been directed at improving machining characteristics for intractable materials like nickel and titanium alloys. Mitrofanov et al. (Mitrofanov et al. 2003; Mitrofanov et al. 2004) conducted several studies on ultrasonic assisted turning of nickel based super alloy inconel 718. He observed that the hardness of the layer machined with ultrasonic technology was half that of the conventional turning surface and closer to the hardness of untreated material. In addition to the improved cutting force characteristics, a pattern of intermittent contact between the cutter and work-piece surface was introduced. Figure 2-12a shows that in conventional turning the cutting tool stays in a permanent contact with the chip throughout the whole process, while in ultrasonic turning, the cutter remains in contact with the chip only during penetration and unloading phases. This intermittent contact in

ultrasonic turning led to significantly lower tool temperatures (Figure 2-12b). Lastly, it was determined that the average surface roughness was reduced by ~50% for specimens machined with ultrasonic assisted turning; these results were verified by comparison of simulations with and without friction.

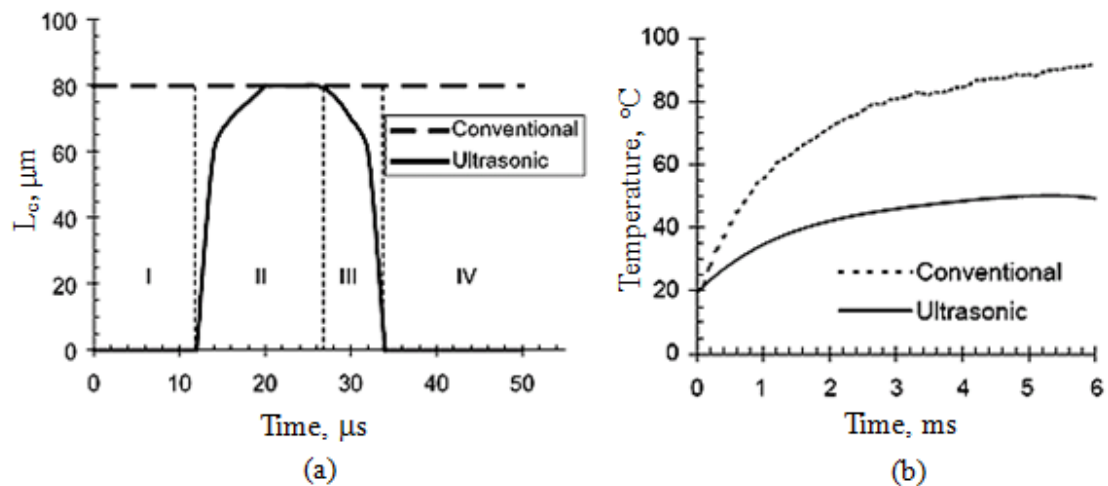


**Figure 2-12 : (a) Simulated contact lengths; approaching (I) penetration (II) unloading (III) withdrawal (IV) (Mitrofanov et al. 2003) (b) Temperature evolution for the cutting tip (Mitrofanov et al. 2004)**

Xiao et al. (Xiao et al. 2003) investigated the effect of a tool nose radius in ultrasonic cutting of hard metal. Hardened steel and Ni-based alloys generally cause machining problems such as tool chatter and unusual wear. He observed that ultrasonic assisted cutting suppresses tool chatter that is normally found in conventional cutting processes. In the case of conventional cutting, a slight increase in tool nose radius makes the machining accuracy worse due to the occurrence of this chatter. Therefore, ultrasonic assisted cutting should enable the use of larger tool nose radii than conventional cutting while improving tool wear characteristics.

Several studies on ultrasonic assisted electrical discharge machining have also been reported. Guo et al. (Guo et al. 1997) observed the reduction of the surface residual tensile stress with ultrasonic excitation. Gao and Liu (Gao and Liu 2003) applied ultrasonics to the workpiece for micro EDM and found that the removal rate decreased when the workpiece thickness was increased and that the removal rate of the ultrasonically aided micro EDM was larger than that of traditional EDM.

### **2.2.3 ULTRASONIC WELDING**

Ultrasonic welding is a solid state process in which two materials are joined by the application of ultrasonic vibrations under moderate pressure. Little or no heat is applied and the material remains near 50% of its melting temperature. This process permits welding of thin to thick sections of material with lower pressures than used in fused deposition or hot isostatic pressing welding. However, there are limitations in terms of the thickness of component and butt welds. Materials suitable for ultrasonic welding include nonferrous metals and their alloys while materials such as zinc, lead, and tin have yet to be shown to be successfully welded. The most widely used system for ultrasonic welding is shown in Figure 2-13 where a static normal force is applied perpendicular to the interface between the workpieces and the contacting sonotrode oscillates parallel to the material interface surface (Edgar de Vries 2004). The combined effect of static and oscillating forces produce deformation which promotes welding. Chang and Frisch (Chang and Frisch 1974) developed the understanding of the bonding mechanism and explained the evolution of bonded area due to the ultrasonic vibration as shown in Figure 2-14. He theorized that bonding is accomplished via two different processes: interfacial slip and sublayer plastic deformation along with a localized temperature rise at the weld.

The maximum average interfacial temperature produced in the weld zone ranges between 35 to 50% of the absolute melting temperature of the material.

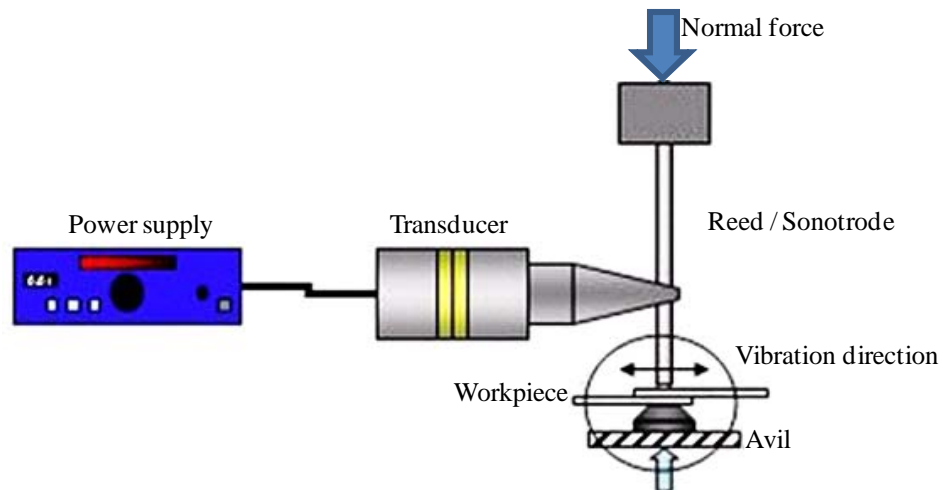


**Figure 2-13 : Principle of ultrasonic welding set up for spot welding (Edgar de Vries 2004)**

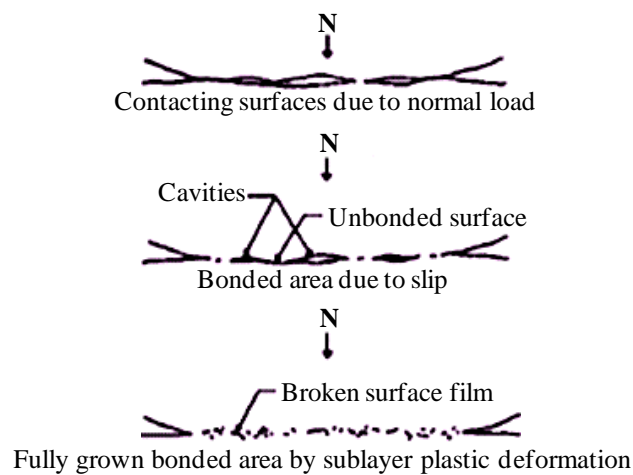


**Figure 2-14 : Evolution of bonded area due to ultrasonic vibration (Chang and Bone 1974)**

Jones and Powers (Jones and Powers 1956) explained three different phenomena to describe the mechanism of ultrasonic welding: stress distribution in the weld zone, net

energy delivered to the weld zone and the localized temperature rise developed within the weld zone. They found external deformation was on the order of 0-5% of the total thickness of the sheets being welded while internal deformations amounted to as high as 80%. It has also been theorized that the oscillatory energy generated at the weld interface causes internal stresses which in turn produces additional elastic and plastic deformation in the weld zone.

Tsujino et al. (Tsujino 1995; Tsujino et al. 1996) conducted research on ultrasonic welding in order to propose effective ultrasonic welding parameters based on the size of the workpieces. For welding of thick and large metal specimens, an ultrasonic butt welding system was developed. A conventional ultrasonic lapped spot welding method allows welding up to 2 or 3mm thick plate specimens. Aluminum plates of 6mm thickness have been joined end to end by shifting the welding tip driving position to run along the specimen width. For welding of medium to large metal specimens, a welding method of using two vibration systems was proposed. This involved the use of an upper vibration system with welding tips located at its center as well as a mirrored lower vibration system. Welding specimens were then inserted between the upper and lower welding tips under static clamping force. For medium size metal welding specimens, it was claimed that the weld strengths obtained by using a welding tip of circular locus were larger than those joined by a conventional welding system where the welding tip vibration was linear. Lastly, an ultrasonic wire bonding system is effective for welding small metal specimens.

## CHAPTER 3 - PRELIMINARY EVALUATION FOR ULTRASONIC ASSISTED FRICTION STIR WELDING

### 3.1 OVERVIEW OF FRICTION STIR WELDING EXPERIMENTAL SET-UP AND ITS OPERATION

Since the first friction stir welds were carried out at TWI (The Welding Institute) in 1991, a conventional milling machine has been demonstrated capable of performing FSW. Our experiments were similarly established using Moriseiki CNC machining center (TV-30) as shown in Figure 3-1.



**Figure 3-1 : FSW equipment by the use of Moriseiki CNC machining center**

A standard machine vice was employed to hold the workpieces securely without any

lateral movement during welding process. A steel block was used as a backing plate and to prevent trembling of the machine as shown in Figure 3-2.

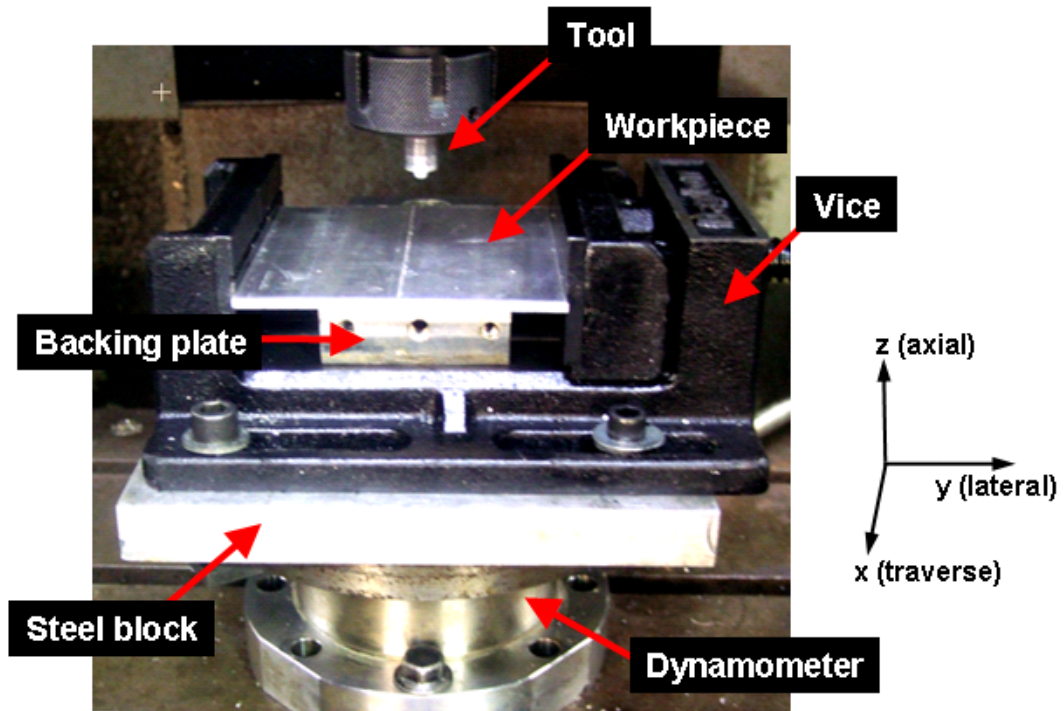


**Figure 3-2 : Schematic of fixture**

Aluminum alloy 6061-T6511, which has good weldability for FSW, was used. A 3.175mm thickness aluminum alloy sheet was cut to 50mm × 70mm rectangle plates and milled with square mating edges, whose chemical composition and mechanical properties were listed in Table 3-1 and Table 3-2.

**Table 3-1 : Nominal compositions of aluminum alloy 6061-T651**

Comp	Al	Cr	Cu	Fe	Mg	Mn	Si	Ti	Zn
Wt. %	98	0.04- 0.35	0.15- 0.4	Max 0.7	0.8- 1.2	Max 0.15	0.4- 0.8	Max 0.15	Max 0.25



**Table 3-2 : Mechanical properties of aluminum alloy 6061-T651**

Tensile strength (MPa)	Yield strength (MPa)	Elongation (%)
228-283	193-262	10-11.62

**Table 3-3 : Guideline for tempering A2 Tool Steel**

Tempering Data			
Tempering Temperature	Typical Rockwell Hardness	Tempering Temperature	Typical Rockwell Hardness
As Quenched	63.5C-65C	500 °F	59C-59.5C
300 °F	62.5C-64C	600 °F	58C
400 °F	61C-62C	700 °F	56C-57C

For the tool, air-hardened A2 tool steel was used. Figure 3-3a shows the FSW tool used for the butt joint welds. Many papers have reported various tool designs which can influence the welding quality and addressed that care must be taken in determining geometrical variables such as the shoulder diameter, pin diameter, pin length, and pin shape. The tool consists of a typical non-threaded tapered pin shape and flat diameter. Dimensions of the tool were selected based on Arbegast's work (Arbegast and Patnaik 2005). Figure 3-3b shows the dimension of the tool used for this experiment. It has been reported in FSW that the height of the tool pin used for rotating shoulder tool is known to be around 90-95% of the material thickness (Arbegast and Patnaik 2005). Heat treatment was applied to the tool to achieve high hardness and better wear resistance. According to the guideline provided by the supplier of the tool steel (McMaster-Carr), the tool

underwent hardening, quenching, and tempering procedure to achieve hardness of HRC58 as referred to Table 3-3.

Welding was carried out at rotating speeds from 1500 to 1800rpm and welding speeds from 25 to 100 mm/min. The plunge depth, i.e., the maximum depth of the shoulder penetration below the workpiece surface was around 0.1mm.

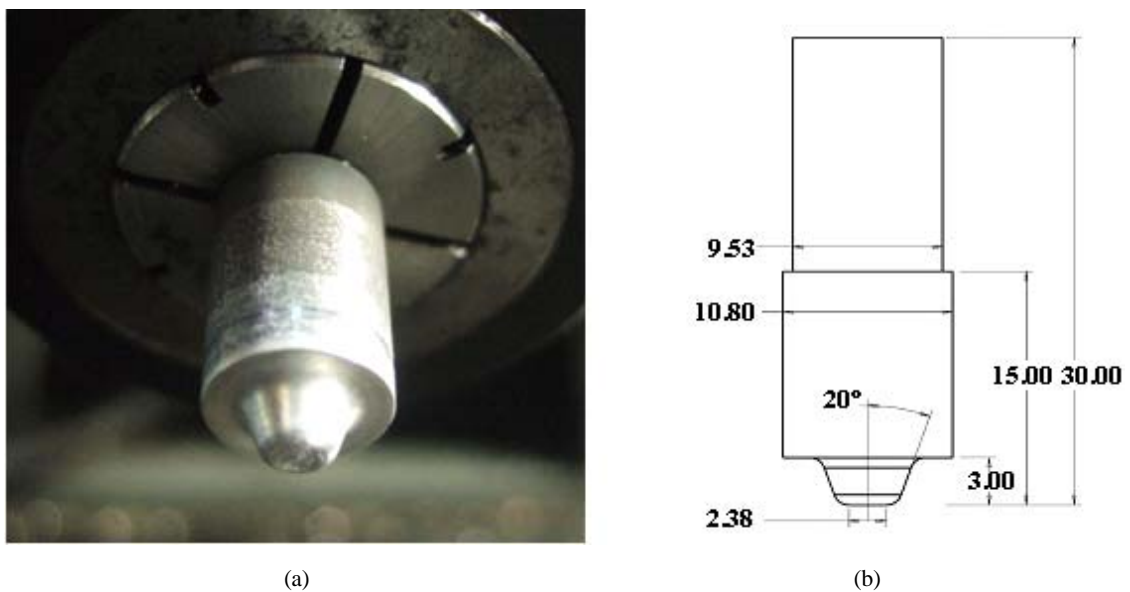


**Figure 3-3 : Friction stir welding tool (a) tool clamped in a collar (b) tool size(mm)**

### **3.2 EXPERIMENTAL INVESTIGATIONS OF THE ULTRASONIC ASSISTED FRICTION STIR WELDING PROCESS**

#### **3.2.1 FORCE MEASUREMENT DURING FRICTION STIR WELDING**

A Kistler, 4-component dynamometer (Type 9272), consists of a four-component sensor fitted under high preload between a base plate and a top plate. The four components that the dynamometer can measure are forces in X, Y and Z-direction along with the torque,  $M_z$ . In this research, two charge amplifiers, which convert the

dynamometer charge signals into output voltages proportional to the forces and moment obtained, were employed. The dynamometer was mounted with screws on the bed of the machine with help of a supporting block. The workpiece holder (vice) was clamped to the dynamometer. The operating temperature range of the dynamometer is from 0°C to 70°C. But the heat generated during welding must be much more than the operating temperature of the dynamometer. In order to reduce the heat conducted from the workpiece vice to the dynamometer, a steel plate was placed between the workpiece vice and dynamometer as shown in Figure 3-2.

The determination of the forces in such two directional forces as the axial force (z-direction) and traversing force (x-direction) provides important keys to understand and optimize friction stir welding process. The force data from a DAQ system are plotted with respect to the time step of the process.

The axial forces during the welding process were much higher than the traverse forces, as shown in Figure 3-4. It was also observed that there was a significant variation in the axial forces compared with the variation in the traverse force. Therefore, the axial force was investigated at various welding parameters such as rotational and translational speeds. Liu et al. (Liu et al. 2005) observed that the radial wear of the pin significantly differed at various locations of the pin, and the maximum wear was produced at a location of about 1/3 pin length from the pin end. From Figure 3-4, it was observed that the first peak was reached when 20~30% of the height of the pin was penetrated into the workpiece, which supports Liu's observation. Because of the frictional heat generated, the axial force drops but rises again when the shoulder of the tool is immersed into the still cold workpiece. From this, it can be expected that the preheating or fast-heating of

the workpiece would reduce the axial forces. Figure 3-5 shows the variation of the axial force with different translational speeds at constant rotational speed. It was observed that the value of the axial force increased with increase in the translational speed. Also, there is a decrease in the axial force values with the increase in the rotational speed of the spindle, which is observed in Figure 3-6. It was assured that both welding parameters such as translational and rotational speeds influenced the variation of the axial forces. Therefore, these parameters should be considered to optimize the FSW process through controlling the forces.

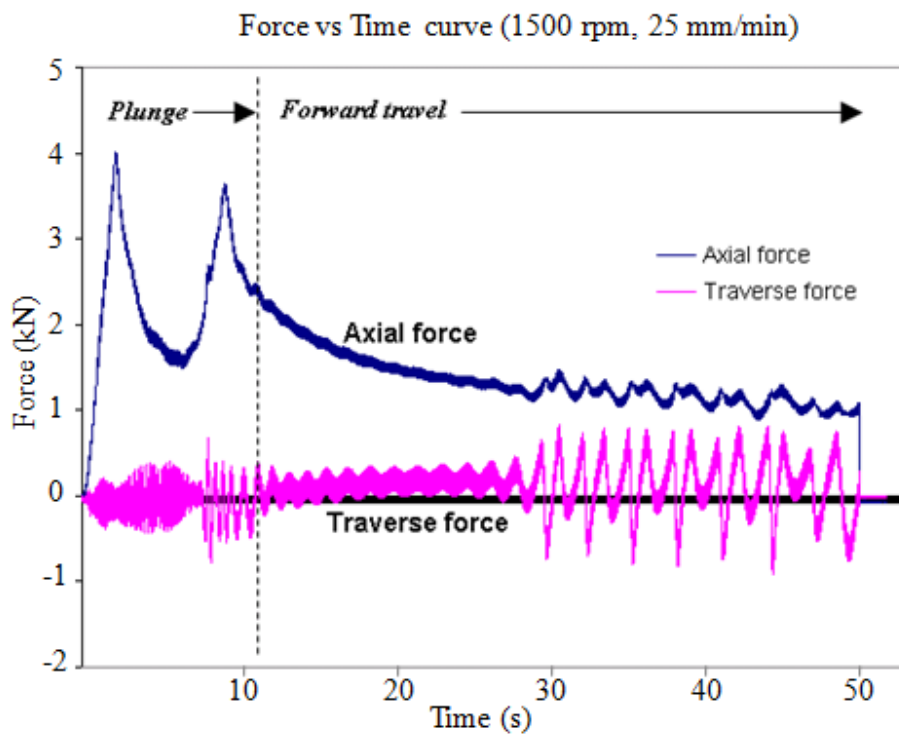
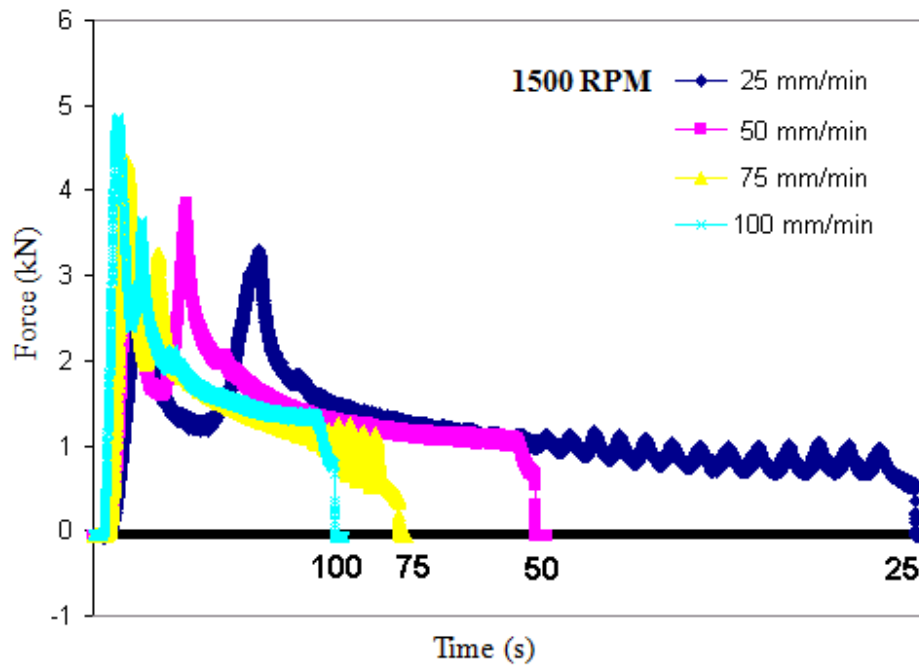
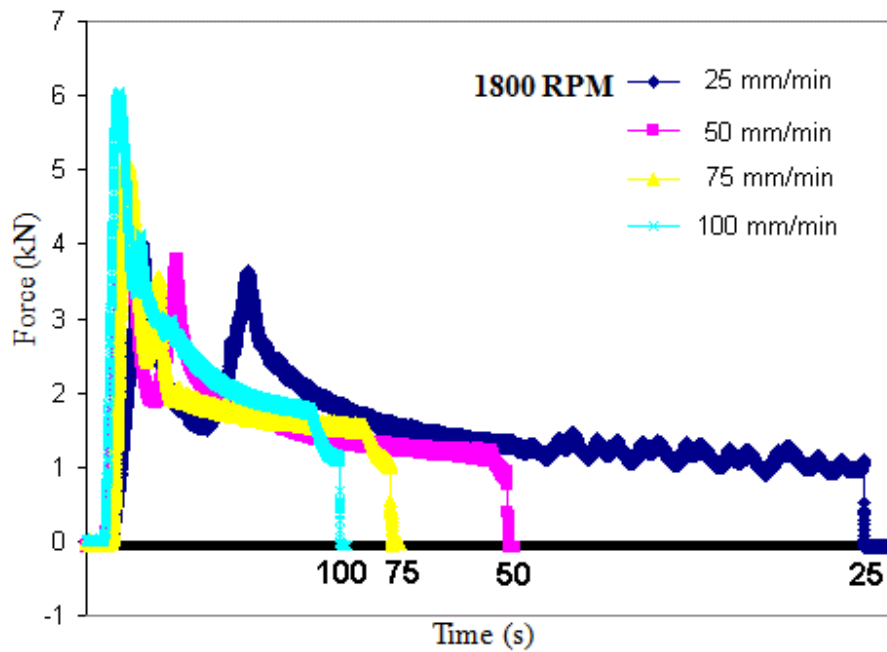


**Figure 3-4 : Axial force (z-direction) and traverse force (x-direction) with respect to time at 1500 rpm rotational speed and 1 in/min translational speed**



(a)



(b)

**Figure 3-5 : Plot of the axial force vs. translational speed (a) at constant rotation speed (1500rpm) (b) at constant rotation speed (1800rpm)**

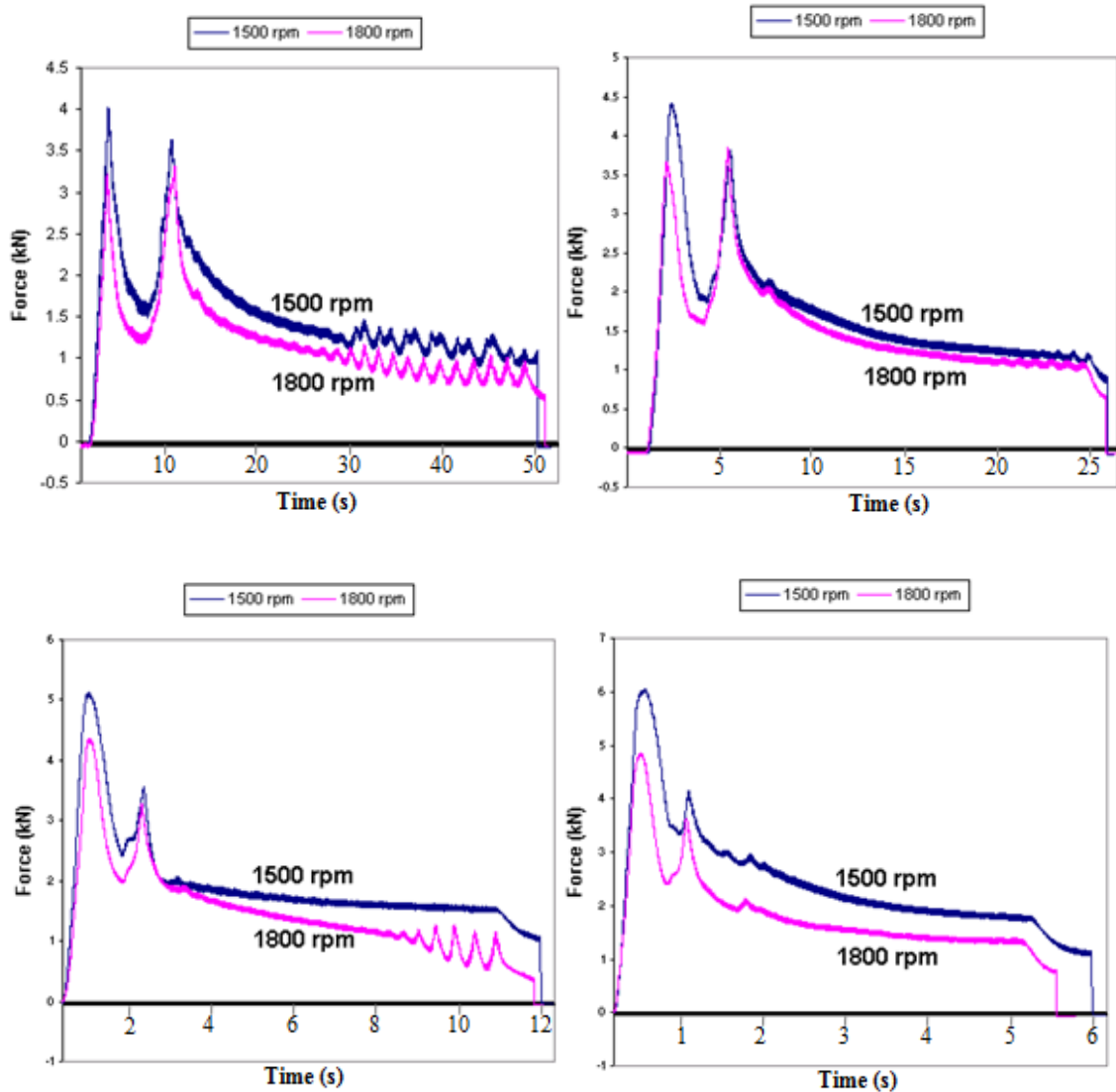


**Figure 3-6 : Plot of the axial force vs. rotational speed at constant translational speed of 25 mm/min (left top), 50 mm/min (right top), 75 mm/min (left bottom), and 100 mm/min (right bottom)**

### 3.2.2 MECHANICAL TESTING OF FRICTION STIR WELDED MATERIAL

The objective of the hardness test was to compare the hardness of friction stir welds of aluminum alloys with the original aluminum alloys. Vickers microhardness

measurements were performed at 100gf load for 15s along the centerline of the cross-section of the welds.

The objective of tensile testing was to determine the tensile yield strength and percentage of yield elongation of friction stir welds of aluminum alloys. The results were compared with the properties of original aluminum alloys. The tensile tests were performed on Instron universal testing machine. The cross-weld specimens from the welds were prepared by using EDM machine with reference to ASM guideline (Kuhn and Medlin 2000). Tensile specimens were prepared with the tensile direction, perpendicular to the welding direction, so that the weld zone is located in the middle of the specimen. The shape and dimensions of the specimen is given in Figure 3-7

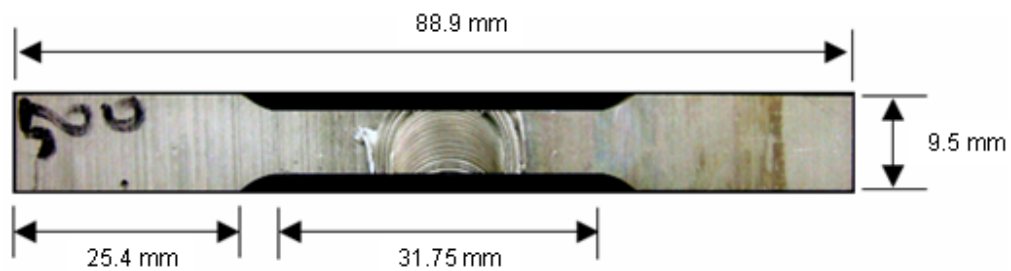
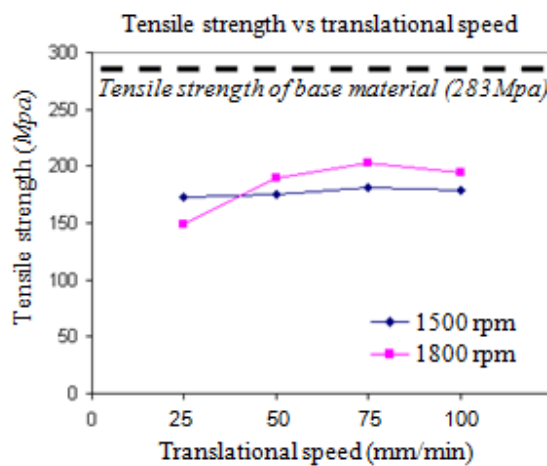


**Figure 3-7 : Schematic of a tensile test specimen**

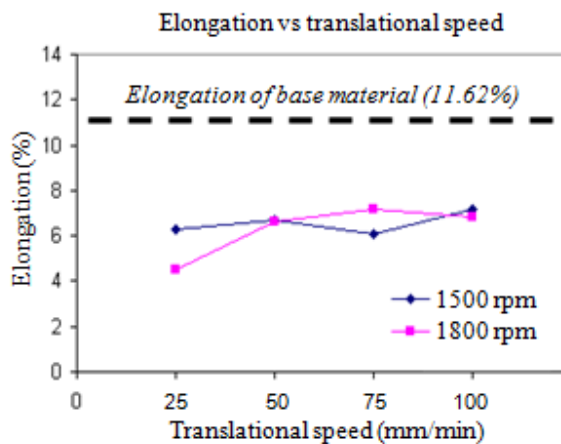
### **3.2.2.1 Tensile test**

The tensile properties of 6061-T651 Aluminum alloy are shown in Figure 3-8. It can be seen from the figure that the tensile properties of each joint are all lower than those of the base material. It was also observed that the tensile properties of the welds are influenced by the welding parameters such as the rotational speed and translational speed.

It could be seen that the tensile strength tends to increase with the increase of the translational speed at the same rotational speed. Increasing the rotational speed also tends to increase the tensile strength, even though the magnitude of the increase at 1500 rpm was not as significant as one observed at 1800 rpm. The maximum tensile strength and elongation are obtained at 1800 rpm rotational speed and 75 mm/min translational speed. In this case, the tensile strength of the joint is equivalent to 71.5% that of the base material.



(a)



(b)

**Figure 3-8 : (a) Changes in tensile strength and (b) tensile elongation of friction stir welded Aluminum 6061-T651 as a function of rotational and translational speed**



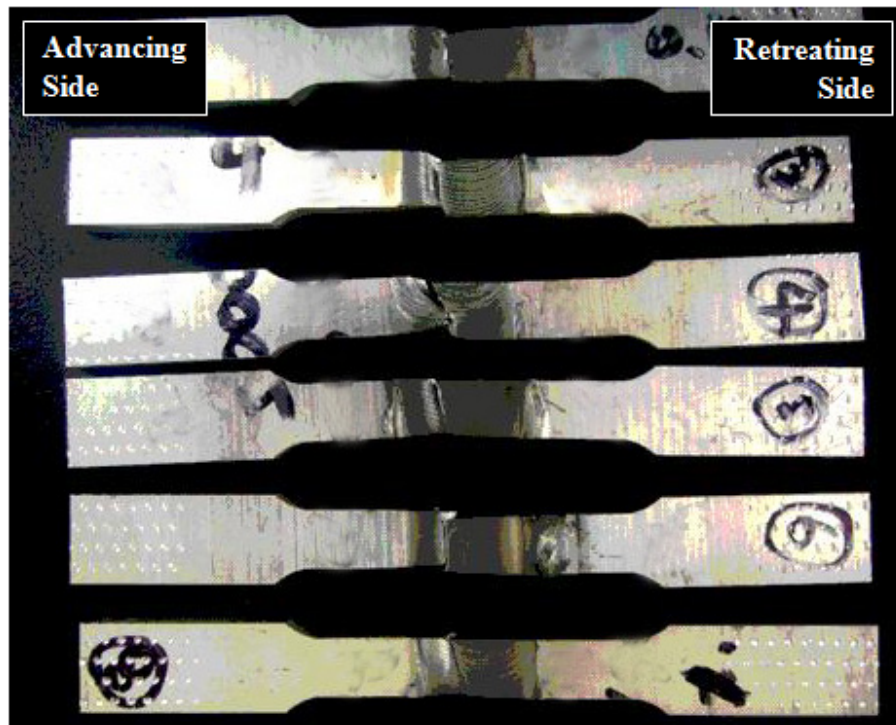


**Figure 3-9 : Top view of the failed tensile specimens showing a failure location**

Another observation was that all the failure occurred in the advancing side regardless of different welding parameters as shown in Figure 3-9. This implies that the tensile properties of the welded joints are not the same on the two sides of the weld center, and the tensile strength on the retreating side is stronger than one on the advancing side. Therefore, in order to increase the tensile properties, we should find optimal welding parameters.

### **3.2.2.2 Microhardness test**

Vickers hardness profiles were measured along the centerlines of the cross-sections of the welded material at 1800 rpm rotational speed and 75 mm/min translational speed,

which had the highest value of the tensile properties. Figure 3-10 shows the Vicker's hardness values at various locations and matching cross-section view of the specimen. It was observed that the hardness value decreased from the base material to heat-affected zone (HAZ), and that the boundary area between thermo-mechanically affected zone (TMAZ) and HAZ appeared to have the lowest hardness value. But, the hardness values of the nugget zone were higher than those of TMAZ and HAZ. It was also observed that the location of minimum hardness coincide with the failure location during the tensile test. According to Sato et al. and Zeng et al. (Sato et al. 1999; Zeng et al. 2006), the hardness profiles were affected by precipitate distribution and the grain size in the weld.

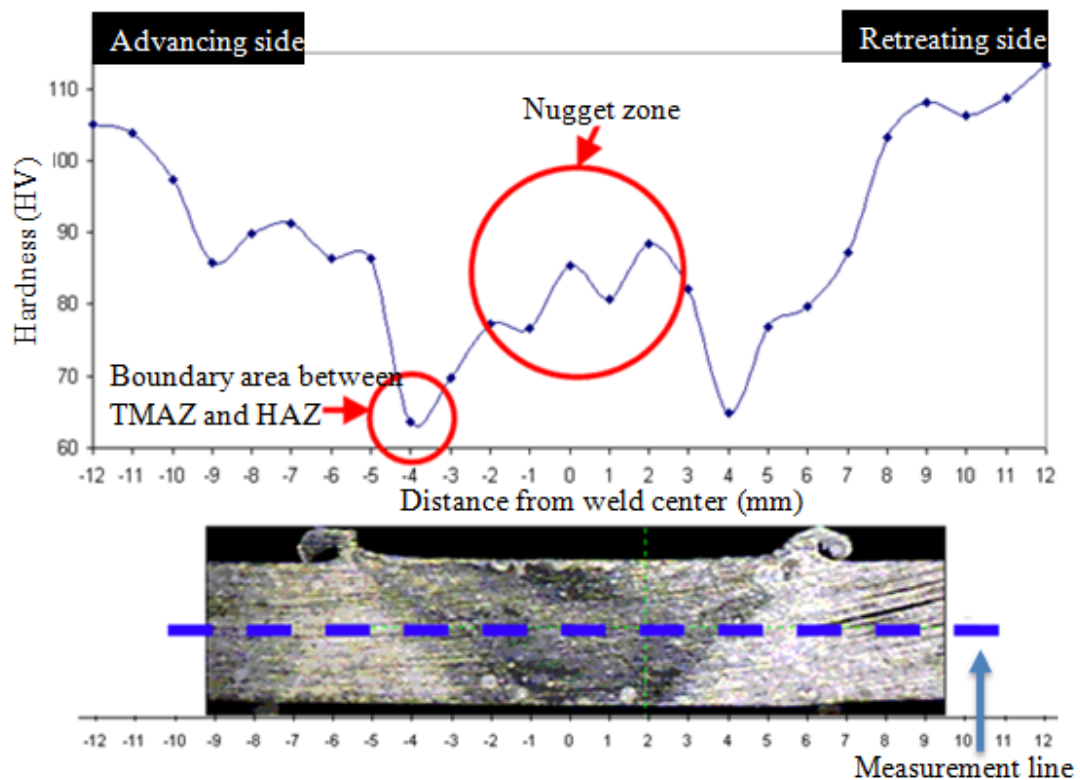


**Figure 3-10 : Vickers hardness and matching cross-section view of the weld at 1800 rpm rotational speed and 75 mm/min translational speed**

### 3.2.2.3 Defect analysis

From the experiments, a few defects have been detected with the changes of various welding conditions such as the rotational speed, translational speed, and plunge depth. From the visual examination, it was observed that the welding quality was basically affected by the plunge depth. When the plunge depth was deeper than optimized value (0.1mm), big weld flash was formed on the retreating side due to the excessive extrusion of the plastic material near the pin. On the contrary, when it was insufficient, groove type defect was generated on the advancing side. Figure 3-11 shows the good weld and two typical defects on the welded region.

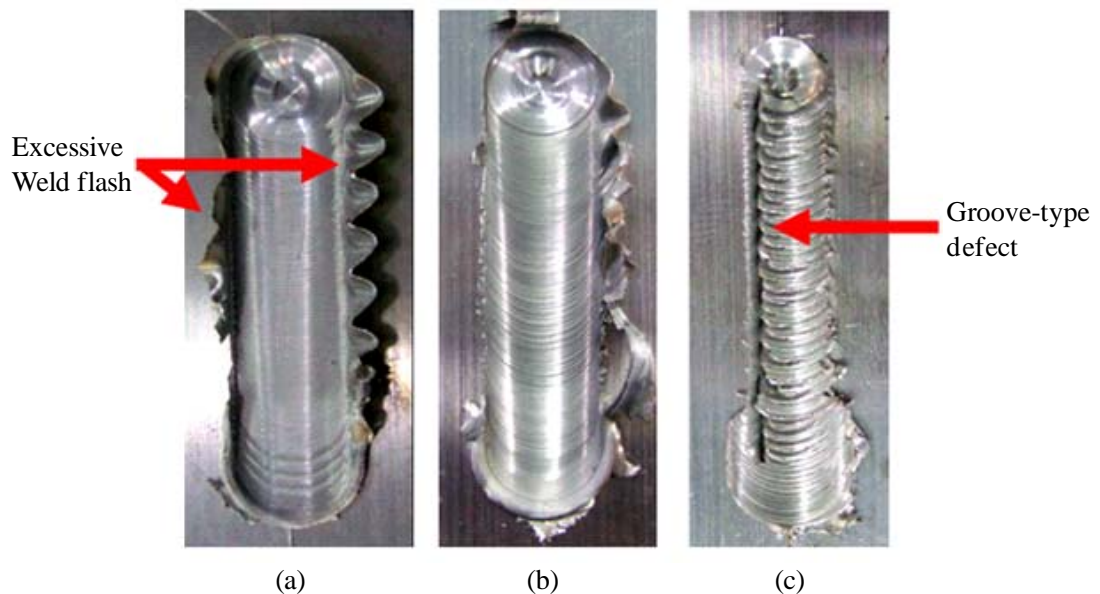


**Figure 3-11 : Surface appearances of the welds (a) weld which has excessive weld flash (b) good weld (c) groove type defect**

Even though the good-looking surface was obtained in the weld, cross-sectional views of the weld show void defect of 0.5mm in almost all the specimens. Figure 3-12

shows the void defect captured by a low magnification microscopy. It was speculated that plastically deformed material around tool pin was not sufficiently filled on the region. The geometry and size of the tool pin, rotational speed, and translational speed must influence the defect. This may be an important reason that the ductility of the welded joint decreases.

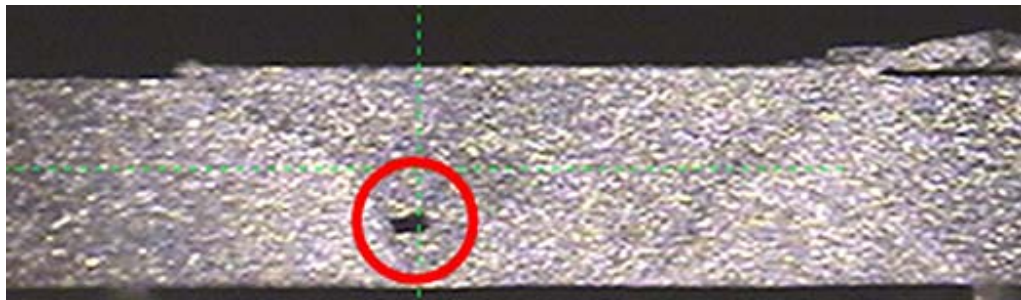


**Figure 3-12 : Void defect from the cross sectional view**

### **3.3 FE MODELING OF THE ULTRASONIC ASSISTED FRICTION STIR WELDING**

Since the invention of FSW in 1991, analytical as well as numerical models were developed in order to gain better understanding of the mechanisms of the process. As the first step to develop the numerical model of FSW process, the thermo-mechanical FE model was utilized to predict temperature distribution of the workpiece and the results were validated with experimental results (Chen and Kovacevic 2003).

#### **3.3.1 FE MODEL OF THE FRICTION STIR WELDING PROCESS**

A FE simulation model was developed for a butt weld, which joins two workpieces as shown in Figure 3-13. The FE model was performed using ABAQUS software, which enables an explicit solution of the dynamic, coupled thermo-mechanical analysis. Since the tool (A2 tool steel) was harder than the workpiece material (6061-T651 aluminum alloy), the tool was assumed rigid solid, and the workpiece was considered a ductile material having temperature-dependent properties based on reference (Alcan 1970; Chen and Kovacevic 2003). Table 3-4, Table 3-5 and Figure 3-14 show the process conditions and the material properties. At this time, we assumed that the friction between the workpiece and the tool shoulder was the major heat generation source. Moreover, due to large strain and deformation, Arbitrary Lagrangian-Eulerian (ALE) adaptive mesh technique was used to avoid excessively distorted elements.

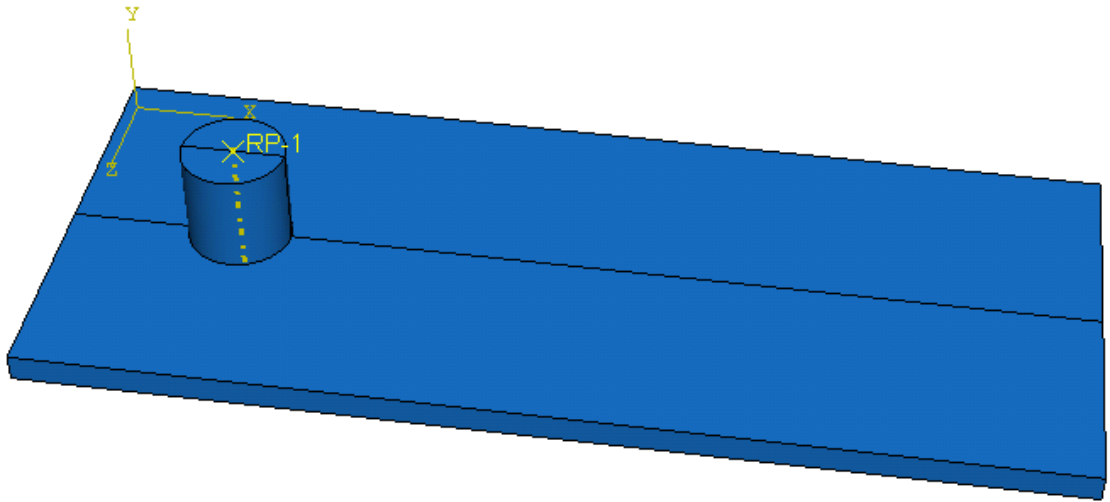


Figure 3-13 : Schematic diagram of the FSW system considered in the model

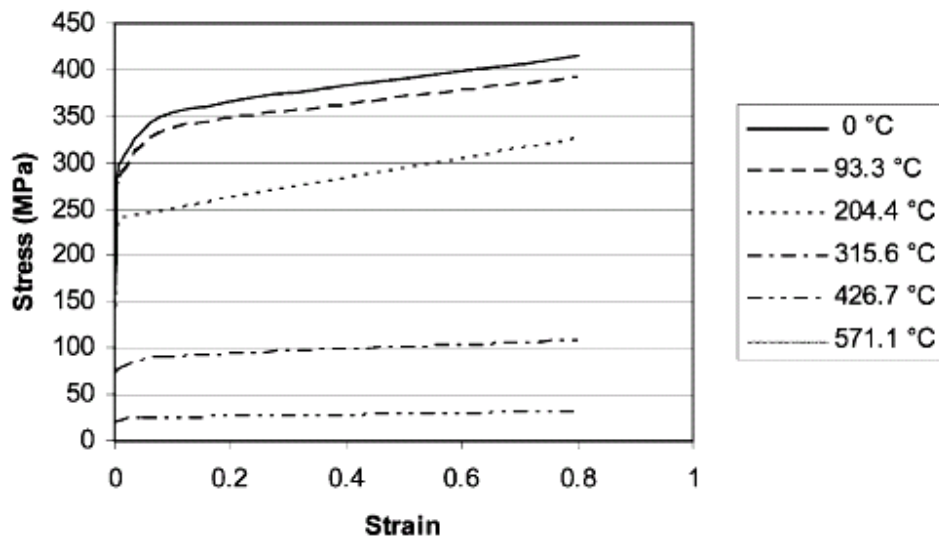


Figure 3-14 : Temperature-dependant stress-strain curve of 6061-T6 aluminum alloy [Chen and Kovacevic 2003]

**Table 3-4 : Geometry and process variables used for FEA**

<b>Variables</b>	<b>FE Model</b>
Workpiece material	6061-T651 Aluminum alloy
Workpiece size	240(long) × 50(wide) ×
Tool material	AISI A2 tool steel
Tool shoulder diameter	10.8mm
Rotational speed	500 rpm (52.36 rad/s)
Translational speed	140 mm/min
Plunge depth	0.1mm
Friction coefficient	0.1
Convective heat transfer	30W/m <sup>2</sup> (Chao and Qi 1998)
Contact heat transfer	1400W/m <sup>2</sup> K (Choi 2006)

**Table 3-5 : Material properties of A2 tool steel and 6061-T651 aluminum alloy (Alcan 1970; Chen and Kovacevic 2003)**

Material	Temp (°C)	Thermal Conductivity (W/mK)	Heat Capacity (J/KgK)	Density (Kg/m <sup>3</sup> )	Young's Modulus (GPa)	Thermal expansion (μm/K)	Poisson's ratio
A2 Steel		23.8	1096	7860	203	10.6	0.23
6061T651 Al alloy	0.0	162	917	2703	69.7	22.4	0.23
	93.3	177	978	2685	66.2	24.6	
	204.4	192	1028	2657	59.2	26.6	
	315.6	207	1078	2630	47.8	27.6	
	427.7	223	1133	2602	31.7	29.6	
	571.1	253	1230	2574	0	34.2	

### 3.3.2 HEAT GENERATION DUE TO ULTRASONIC VIBRATION

Applying horizontal ultrasonic vibration on the workpiece using a vibration table will generate heat due to the friction between the tool shoulder and the workpiece. This heat is superimposed on the heat from the existing friction stir welding process. This heat generation will affect the temperature distribution of the workpiece during the welding process, which has critical impact on the material properties.

Edgar de Vries (Edgar de Vries 2004) developed an equation for the heat generated by the friction from the ultrasonic welding process. This heat generation equation was used for adding the ultrasonic effect on the FE simulation of our welding process. Figure 3-15 shows the overview of our ultrasonic assisted FSW process.

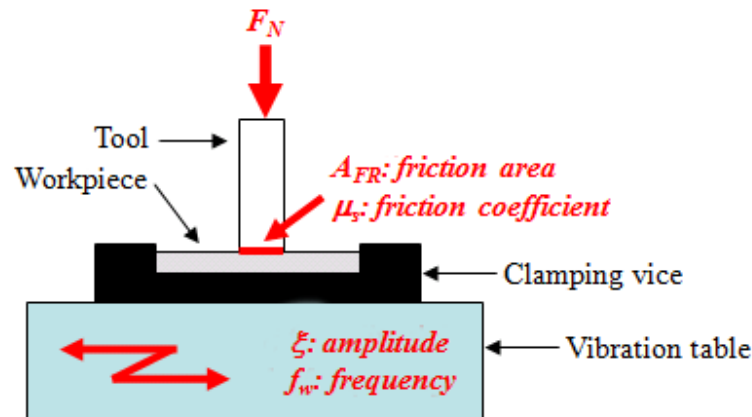


Figure 3-15 : Overview of ultrasonic assisted FSW process

The acoustic power ( $P_{FR}$ ) is calculated with the product of friction force ( $F_{FR}$ ) and the average vibration speed ( $v_{avg}$ ) in Equation 3-1.

$$P_{FR} = F_{FR} \times v_{avg} \quad (3-1)$$



The friction force is simply obtained from the product of the coefficient of friction and the axial force in Equation 3-2 and the average vibration speed is the change of amplitude with respect to time. Equation 3-3 explains the average vibration speed with amplitude ( $\xi$ ) and vibration frequency ( $f_w$ ).

$$F_{FR} = \mu_s \times F_N \quad (3-2)$$

$$\frac{\Delta \xi}{\Delta t} = v_{avg} = 4 \times \xi \times f_w \quad (3-3)$$

Substituting these two equations into Equation 3-1, we obtain an expression for the acoustic power in Equation 3-4 (Edgar de Vries 2004).

$$P_{FR} = \mu_s \times F_N \times 4 \times \xi \times f_w \quad (3-4)$$

Then, Equation 3-5 (Edgar de Vries 2004) expresses a heat flux which is the power dissipated over a friction area. This heat flux boundary condition is used on the FE simulation.

$$\dot{q}_{FR} = \frac{\mu_s \times F_N \times 4 \times \xi \times f_w}{A_{FR}} \quad (3-5)$$

### 3.3.3 RESULT AND DISCUSSION

Chen and Kovacevic (Chen and Kovacevic 2003) obtained temperatures by embedding thermal couples in one plate, which are located 1.6mm below the top surface. The temperature distribution acquired from our FE simulation was compared with their

experimental measurements. Figure 3-16 and Figure 3-17 showed the comparison of the results from our FE simulation and their experiment. A couple of missing and unmatched conditions make these two plots a little different. The plunge depth was not mentioned in the paper and the temperature of the backing plate was assumed constant in our FE simulation. However, overall, FEA prediction in the entire welding process was in a reasonable agreement with their measurement.

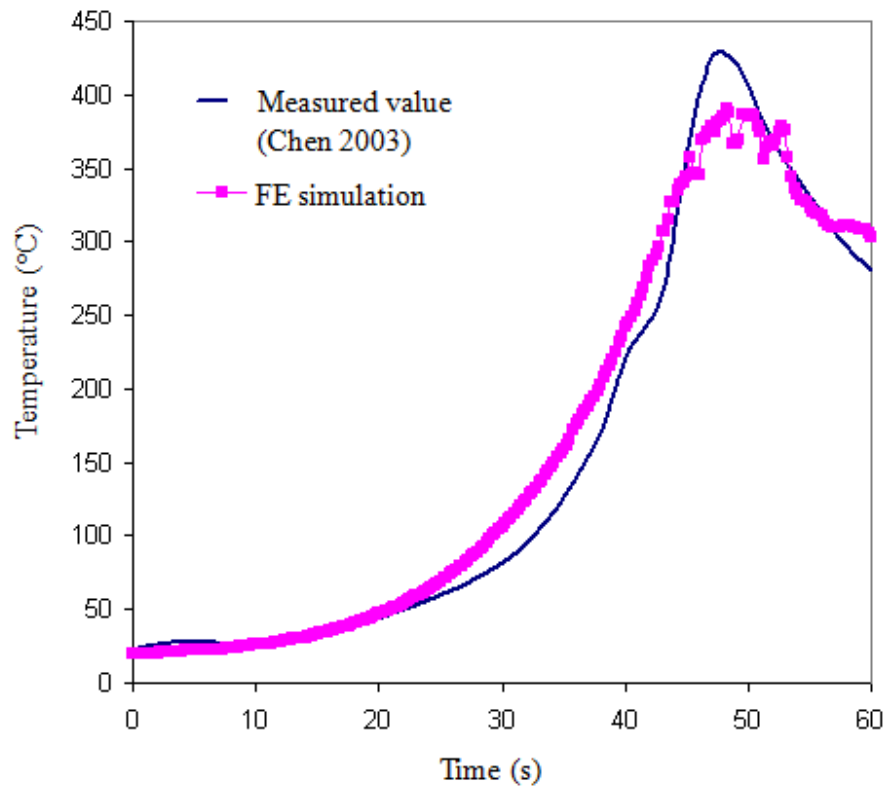


**Figure 3-16 : Comparison of temperature time curve for the location 10mm to the weld centerline and 1.6mm below the top surface of the plate**

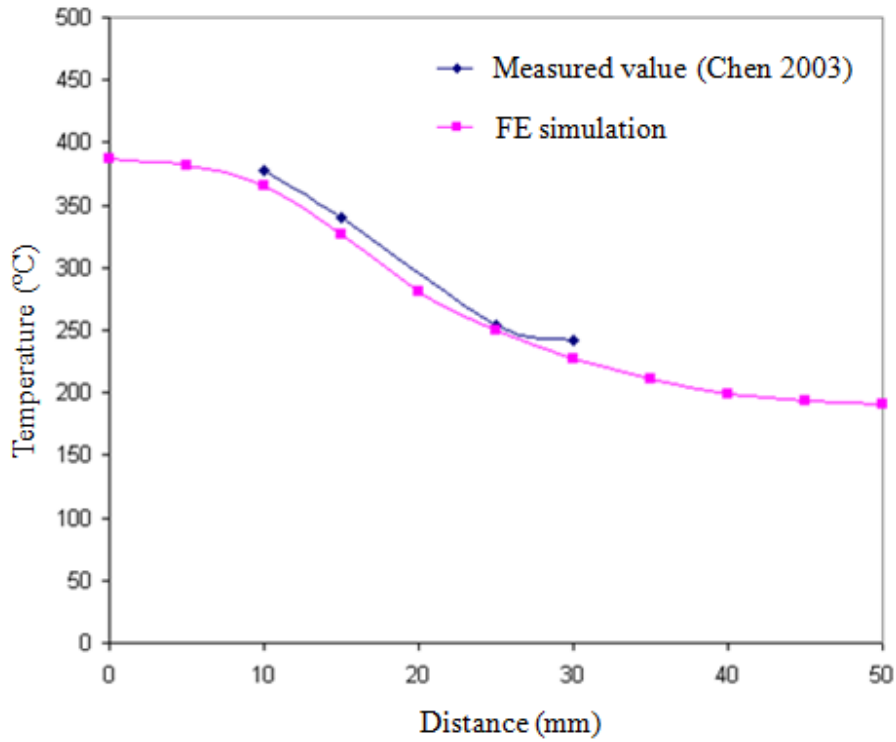


**Figure 3-17 : Comparison of temperature time curve along the lateral direction for node lists 1.6mm below the top surface of the plate (time=3.5s)**

After validating the FE model, the heat flux condition addressed in previous chapter was added to the FE model. Table 3-6 shows three different heat flux conditions which were applied to FE model of the conventional friction stir welding process. In reality, the coefficient of friction and the stress depend on temperature. Here, these variables are assumed to be constant. This simple approach is sufficient to predict the added ultrasonic effect on the normal friction stir welding process in the preliminary step.

**Table 3-6 : Heat flux conditions due to ultrasonic vibration**

	<i>Coefficient of friction (<math>\mu_s</math>)</i>	<i>Stress (<math>F_N/A_{FR}</math>)</i>	<i>Amplitude (<math>\xi</math>)</i>	<i>Frequency(<math>f_w</math>)</i>	<i>Heat flux(<math>\dot{q}_w</math>)</i>
Condition 1	0.1	50MPa	5 $\mu$ m	20kHz	$2 \times 10^6$ W/m <sup>2</sup>
Condition 2		100MPa			$4 \times 10^6$ W/m <sup>2</sup>
Condition 3		200MPa			$8 \times 10^6$ W/m <sup>2</sup>

For friction stir welding process with ultrasonic assistance, from Figure 3-18, it can be seen that the peak temperature and the curvature of the temperature profile went up according to the increase of the magnitude of heat flux by ultrasonic energy. This means that the stirring action would occur in a hotter region than in existing FSW process. That is to say, with ultrasonic assistance, less work is required by the tool to raise the temperature of the workpiece. This temperature distribution in workpiece is very important as it affects the thermal stress development. It was also observed from Figure 3-19 that the ultrasonic assistance led to the reduction of the principal stress in z-direction when compared to the FSW without ultrasonic vibration. Therefore, the axial force would decrease after adding the ultrasonic oscillation. Potentially, tool requires relatively low energy to plasticize the material and consequently has longer life as well.

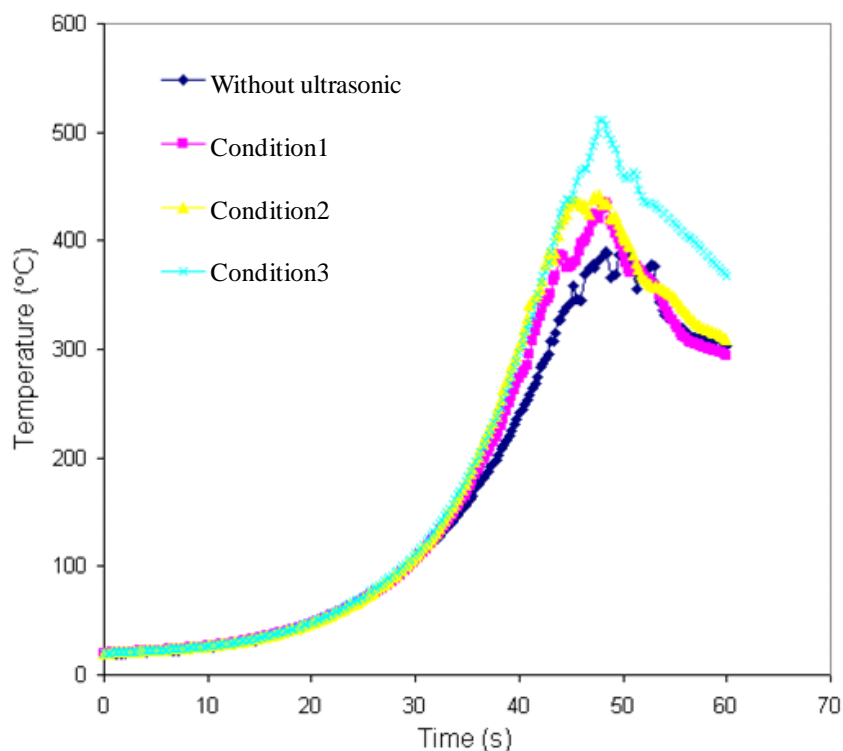


**Figure 3-18 : Comparison of temperature time curve according to different conditions at the location 10mm to the weld centerline and 1.6mm below the top surface of the plate**

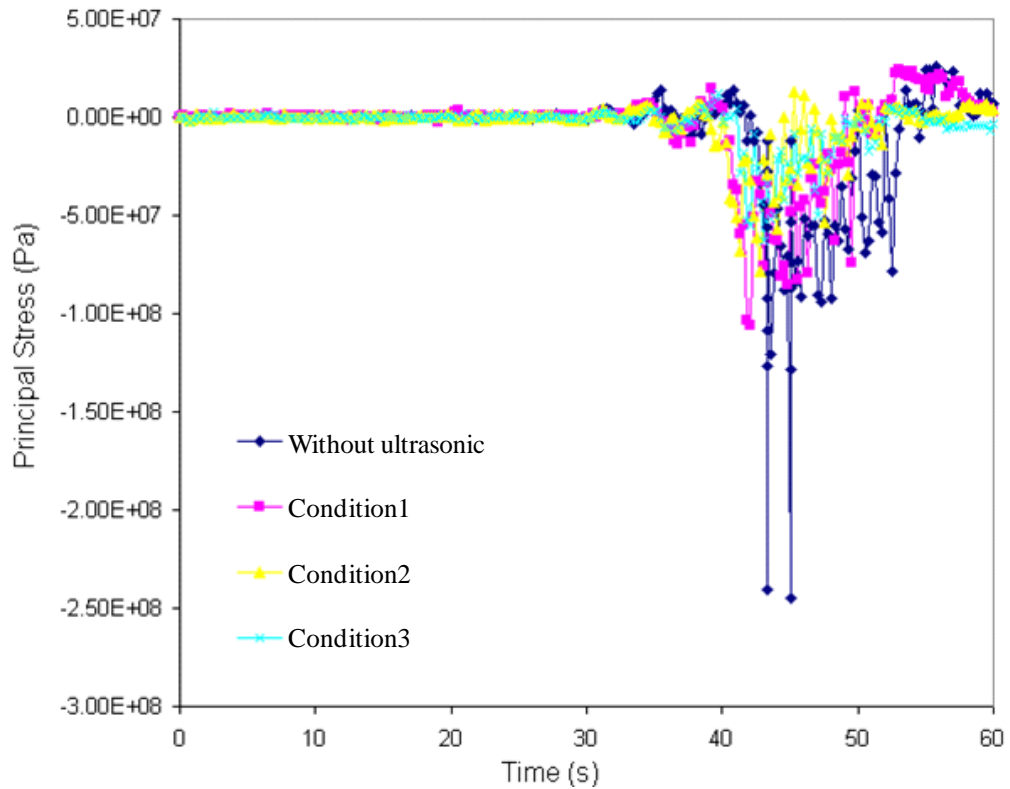


**Figure 3-19 : Comparison of predicted principal stress(z-direction) with respect to time according to different conditions at the location 10mm to the weld centerline and 1.6mm below the top surface of the plate**

### 3.4 CONCLUSIONS

In this study, we developed FSW system using the in-house CNC machine and reasonable welds were obtained for 6061-T651 aluminum alloy. The location of minimum hardness is the boundary area between thermo-mechanically affected zone and heat-affected zone, which coincide with the failure location of specimens for the tensile test. Welding conditions such as the rotational speed, translational speed, and plunge depth significantly influenced the weld quality. The experimental results agreed well with

the data published in papers. Furthermore, to verify the ultrasonic effect on FSW process, FE model was performed using ABAQUS. The model was validated and employed to analyze the temperature and flow stress from the cases with and without ultrasound. From the FE simulation with ultrasonics, it was expected that ultrasonic assistance may increase the temperature of the weld region, and consequently decrease the stress of the region as compared with FSW without ultrasonics. This would ultimately lead to the prolongation of the tool life.

## **CHAPTER 4 - THERMO-MECHANICAL FE MODEL OF ULTRASONIC ASSISTED FRICTION STIR WELDING**

Ultrasonic assisted friction stir welding (UaFSW) is a hybrid welding technique, where high frequency vibration is superimposed on the movement of a rotating tool. The benefit of using ultrasonic vibration in the FSW process refers to the reduction in the welding force and to the better welding quality. The UaFSW system is being developed and its mechanism needs to be understood using both the experiments and the numerical simulations. In this study, FE simulations of FSW and UaFSW using ABAQUS/Explicit were carried out to examine plunge forces during the plunge phase of FSW and UaFSW, respectively. The simulations of the conventional FSW process were validated. Then, simulation of UaFSW process was performed by imposing sinusoidal horizontal ultrasonic vibrations on the tool.

### **4.1 INTRODUCTION**

Friction stir welding has two different stages including a plunge and a linear welding phase as shown in Figure 4-1. In the plunge stage, a FSW tool penetrates the workpieces to be welded. In the linear welding phase, the tool moves along the joint line. The whole process adds frictional heat with intense plastic deformation to generate joints and the plunge stage of FSW process is crucial since most of the thermomechanical conditions are initiated and the highest temperature and forces are required in this stage during the whole process. The characteristic of this phase makes it difficult in observing the details

of the process. Especially, FSW welding of high melting temperature materials has tool wear problem due to high welding force during the stage (Lienert et al. 2003).

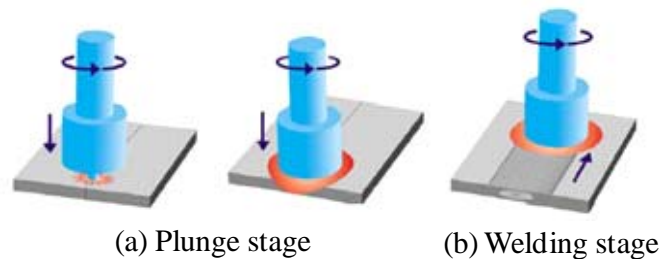


**Figure 4-1 : Friction stir welding process (Mahoney et al. 1998)**

In order to build an efficient method for FSW process, a valid FE prediction model needs to be established and many mechanics need to be understood. Few works have been carried out on the thermo-mechanical FE model developed during the plunge stage and prediction of mechanical forces. Research in FSW modeling has been carried by several researchers to better understand the thermomechanical FSW process. Schmidt and Hattel (Schmidt and Hattel 2005) developed a fully coupled thermo-mechanical three dimensional FE model in ABAQUS/Explicit using arbitrary Lagrangian-Eulerian formulation and the Johnson-Cook material law. Zhang and Zhang (Zhang and Zhang 2007; Zhang and Zhang 2008) also used a fully-coupled thermo-mechanical model to analyze the material flows and mechanical features in the FSW process. Kakarla et al. (Kakarla et al. 2005) also used ABAQUS package to develop the FE model of friction stir spot welding. Although many projects in FE modeling of the FSW process have been conducted, few efforts have been made on the validation of the experimental data for welding forces with the data obtained through simulation and prediction of the welding



forces.

Research in FE modeling of various manufacturing processes using the ultrasonic vibration techniques has been carried out. Mousavi et al. (Mousavi et al. 2007) performed FE analysis by using the explicit analysis procedure in order to study the perceptiveness of the mechanism of ultrasonic vibration extrusion. Ahmed et al. (Ahmed et al. 2007) developed transient and coupled thermo-mechanical simulations of elasto-plastic materials under conditions of ultrasonically assisted turning to study the effect of cutting parameters and friction on ultrasonic assistance. Amini et al. (Amini et al. 2008) studied turning of Inconel 738 with a tool vibrating at ultrasonic frequency by using MCS-Marc and ANSYS software. Rosochowska and Rosochowski (Rosochowska and Rosochowski 2007) created FE model of ultrasonic back extrusion using ABAQUS/Explicit to examine mechanisms responsible for the reduction in the mean forming force.

In this research, a three-dimensional solid mechanical model of FSW has been developed using the finite element analysis (FEA) ABAQUS/Explicit. The model is developed based on the actual experimental welding procedure in order to obtain the numerical steady-state solution, such as force and temperature profile of the welding. We investigated the thermo-mechanical processes in the material during the plunge phase using numerical simulation and experiments. The plunge forces during the plunge phase are considered because plunge forces in the plunge phase are higher than the plunge forces in welding phase or traverse forces. The effects of vibration properties and frictional conditions on the forces were investigated using the FE method.

## 4.2 FEM MODELING

### 4.2.1 THERMAL MODELS

In general, heat generation comes from two sources; frictional heating at the tool-workpiece interface and plastic energy dissipation due to shear deformation in the nugget zone. It has been suggested that frictional heating at the tool-workpiece interface is the main heat source while the other account for only 1-2% of the total heat generation. The governing equation for heat transfer process during the plunge phase of FSW process can be written as

$$\rho c \frac{\partial T}{\partial t} = \frac{\partial}{\partial x} \left[ k_x \frac{\partial T}{\partial x} \right] + \frac{\partial}{\partial y} \left[ k_y \frac{\partial T}{\partial y} \right] + \frac{\partial}{\partial z} \left[ k_z \frac{\partial T}{\partial z} \right] + \dot{q}_p \quad (4-1)$$

where  $\rho$  is the density  $c$  is the specific heat,  $k$  is heat conductivity,  $T$  is the temperature,  $t$  is the time,  $\dot{q}_p$  is heat generation coming from plastic energy dissipation due to shear deformation, and  $x$ ,  $y$ , and  $z$  are spatial coordinate. The density, specific heat, heat conductivity are temperature dependant parameters, which is used in this simulation to acquire accurate results.

The rate of heat generation due to plastic energy dissipation,  $\dot{q}_p$  is computed from

$$\dot{q}_p = \eta \sigma \dot{\epsilon}^{pl} \quad (4-2)$$

Where,  $\eta$  is the heat fraction,  $\sigma$  is the shear stress, and  $\dot{\epsilon}^{pl}$  is the rate of plastic strain. For inelastic heat fraction,  $\eta$ , because plasticity was assumed to heat workpieces mostly, the heat fraction of 0.9 was used in this study. (Awang et al. 2006)

Heat generation also comes from frictional heating between tool and workpieces.

(Frigaard et al. 2001) If all the shearing work at the interface is converted into frictional heat, the average heat generation per unit area becomes

$$q_f = \int_0^{M_z} \omega dM \quad (4-3)$$

where  $q_f$  is the frictional heat generation,  $\omega$  is the angular velocity, and  $M$  is the interfacial moment.

The moment required to rotate a circular tool relative to the workpiece surface under the plunging action is derived by

$$M = \int_0^{M_z} dM = \int_0^R 2\mu P \pi r^2 dr \quad (4-4)$$

where  $\mu$  is the coefficient of friction,  $R$  is the surface radius, and  $P$  is the traction.

The angular velocity can be expressed in terms of the rotational speed  $N$ . By substituting equation 4-4 and  $\omega = 2\pi N$  into equation 4-3, we derive

$$q_f = \int_0^R (2\pi N) 2\pi \mu P r^2 dr = \frac{4}{3} \pi^2 \mu P N R^3 \quad (4-5)$$

From equation 4-5, it is sure that the frictional heat generation depends on the rotational speed and the radius of the tool shoulder.

#### 4.2.2 FE MODEL DESCRIPTION

One of the primary difficulties in modeling the plunge phase is the excessive mesh distortion of the FE model leading to divergence problem. The current FE model utilizes

the ABAQUS/EXPLICIT finite element code and is based on Arbitrary Lagrangian-Eulerian (ALE) adaptive mesh technique that automatically regenerates the mesh once the elements are severely distorted due to large deformation. Adaptive meshing technique in ABAQUS/Explicit creates a new mesh and remaps the solution parameters from the existing mesh to the newly created mesh. In this study, the adaptive meshing was carried out for every three increments of the tool and five mesh sweeps per adaptive mesh increment was performed to improve the aspect ratio of distorted elements. Mass scaling technique that modifies the densities of the materials in the model and improves the computational efficiency was also used. In this study, mass scaling was carried out every 10 increments with stable time increments below a value of  $1.0 \times 10^{-5}$ .

#### **4.2.2.1 FE mesh and geometry**

A FE simulation model was performed for a butt weld, which joins two workpieces as shown in Figure 4-2. It consists of a tool, a backing plate, and 3.175mm thickness workpieces. The tool is made of A2 tool steel and consists of the shoulder and the non-threaded tapered pin. Dimensions of the tool were selected based on Table 5-2. Since the tool (A2 tool steel) and the backing plate were harder than the workpiece material (6061-T651 aluminum alloy), they were assumed rigid surfaces. The workpieces have been meshed using a biased mesh seed for better results around the moving tool. They have been modeled using element type C3D8RT, which is an 8-node thermally coupled brick having reduced integration and combined hourglass control whose stiffness-viscous weight factor is 0.5.

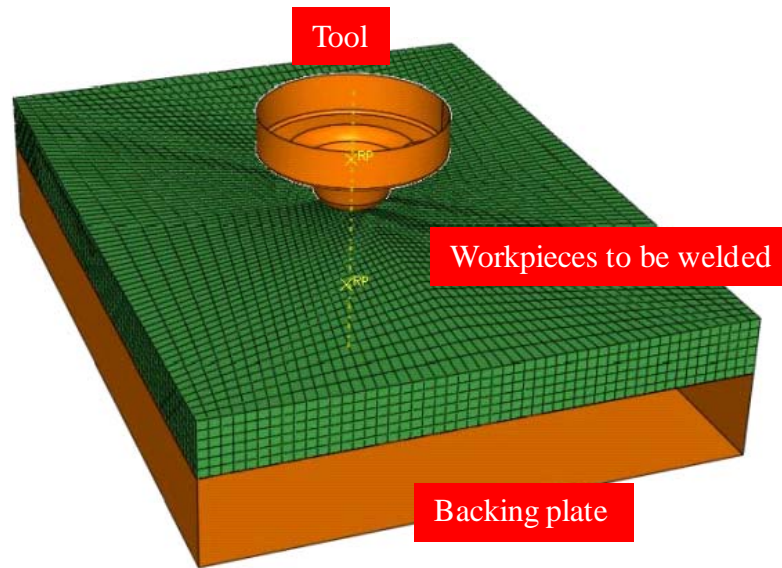


**Figure 4-2 : Finite element meshes for workpieces, FSW tool, and backing plate**

#### **4.2.2.2 Material model and interface properties**

The workpieces were modeled as a temperature dependent elastic-plastic material. Material properties used in this research are from Table 3-5. The temperature near the pin where the large plastic deformation occurs is about 430°C. The reference (Nicholas 1981) suggests the strain rate sensitivity of precipitation hardenable alloys (Al6061) is very low, particularly at this temperature range. It is reasonable to model the workpiece material as a rate-independent elastic-plastic material with temperature-dependent yielding behavior. Friction plays an important role in this process. A constant coulomb friction coefficient is used to model the interaction between the workpieces and the tool, and between the workpieces and the backing plate. The best approximation for coefficient of friction was determined by comparing to the experimental results. 90% of the heat generated by inelastic deformation (plasticity) was assumed to increase in temperature. Assumed

thermal contact conductance between aluminum and steel was 3000W/m<sup>2</sup>K (Yuncu 2006).

To determine the best approximation for coefficient of friction, the plunge forces of FE modeling were calculated for three different coefficients of friction, 0.2, 0.3, and 0.4, under 25 mm/min feed rate and 1500 rpm spindle speed. Coefficient of friction of 0.3 was the best match based on the comparison of the plunge forces of FE modeling and experimental measurement results as shown in Figure 4-3. Therefore, the FE model adopts this coefficient of friction for all the simulations in this research.

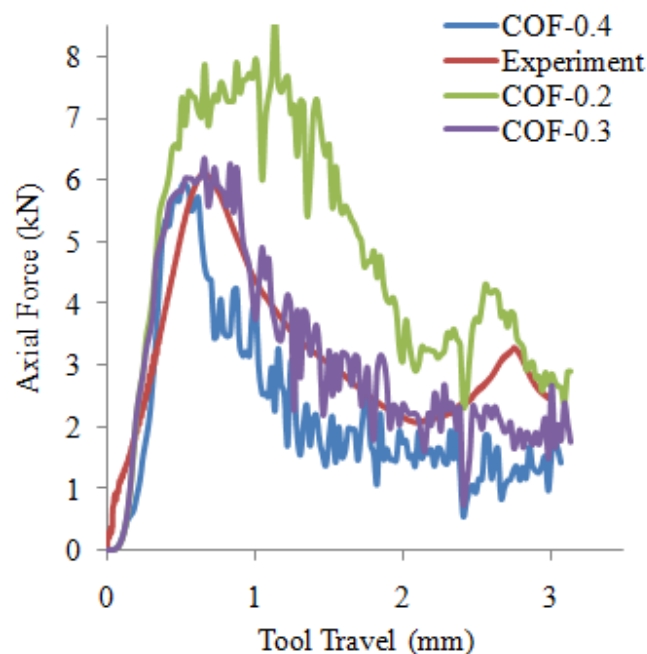


**Figure 4-3 : The effect of the friction coefficients with 0.2, 0.3, and 0.4 on the plunge forces**

The heat generated by friction between the tool and workpiece transfers to the tool and workpiece, respectively based on their thermal conductivity. ABAQUS/Explicit

requires the heat fraction of converted heat distributed to the workpiece and the value of 0.87 was set to the ratio of heat partition into the workpiece. (Miller 2006)

#### 4.2.2.3 Boundary conditions

In the FE model, the same translational and rotational speeds used in experiments were employed. The top surface of the workpiece was under free convection with convection coefficient of  $30 \text{ W/m}^2 \text{ }^\circ\text{C}$  from Awang (Awang et al. 2005) and ambient air temperature of  $22 \text{ }^\circ\text{C}$ . The backing plate and two sides of workpieces were fixed in all degree of freedom. Simulation of the ultrasonic assisted friction stir welding was performed by imposing horizontal ultrasonic vibrations on the tip of the FSW tool. Namely, the tool was subjected to ultrasonic oscillations of 20 kHz and amplitude by imposing a boundary constraint to the tip of the tool in the form of a sinusoidal displacement. The ultrasonic vibration in the model was applied in the direction of tool travel. The amplitude  $a$  is defined as a Fourier series;

$$a = A_0 + \sum_{n=1}^N [A_n \cos n\omega(t - t_0) + B_n \sin n\omega(t - t_0)] \quad (4-6)$$

where,  $t_0$ ,  $N$ ,  $\omega$ ,  $A_0$ ,  $A_n$ , and  $B_n$ ,  $n=1,2\dots N$ , are user-defined constants.

### 4.3 EXPERIMENTAL SETUP AND DESIGN

Chapter 3 and Chapter 5 address an entire experimental setup of FSW and UaFSW system. An in-house CNC machine was used to demonstrate the FSW and UaFSW and the ultrasonic horn assembly made the FSW spin tool vibrate in the horizontal direction. The determination of the axial force (z-direction) and traversing force (x-direction) provides important keys to understand and optimize the FSW process. The force data from a DAQ system are plotted with respect to the time step of the process. The plunge (axial) forces during the welding process were much higher than the traverse forces, as shown in Figure 4-4. It was also observed that there was a significant variation in the axial forces compared with the variation in the traverse force. Therefore, the axial force was investigated at various welding parameters such as rotational and translational speeds. Also, forces during the plunge phase are much higher than those in a welding travel phase. Therefore, we focused on the analysis of axial forces during the plunge phase in this FE study.

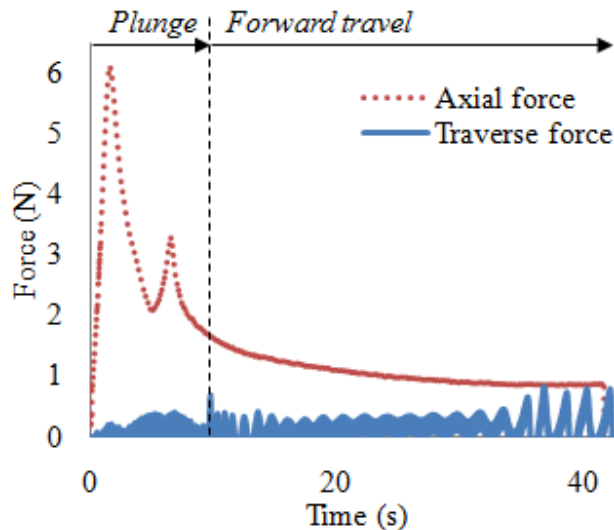


**Figure 4-4 : Axial and traverse force profiles during the plunging and welding phases**



#### 4.4 VALIDATION OF FEM MODELING OF FSW IN TERMS OF THE WELDING FORCE

For a tool feed rate of 25 mm/min and a tool rotating speed of 1500 rpm, the plunge forces during the plunge phase of FSW process were acquired in both the experiments and the simulation. The results were shown in Figure 4-5. A good agreement was obtained between the numerical results and the experimental results. The oscillations in the numerical curve were due to the computational errors in the explicit code.

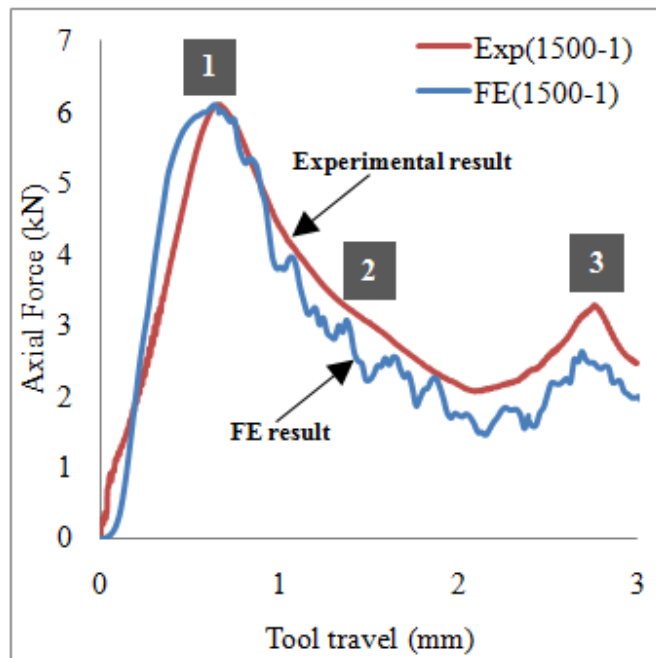


**Figure 4-5 : Comparison of forces-time curves between experiment and simulation results**

Figure 4-6 shows temperature profiles in three steps marked in Figure 4-5. Material extrusion by the FSW tool was simulated well with aid of adaptive remeshing technique and proper simulation step time.

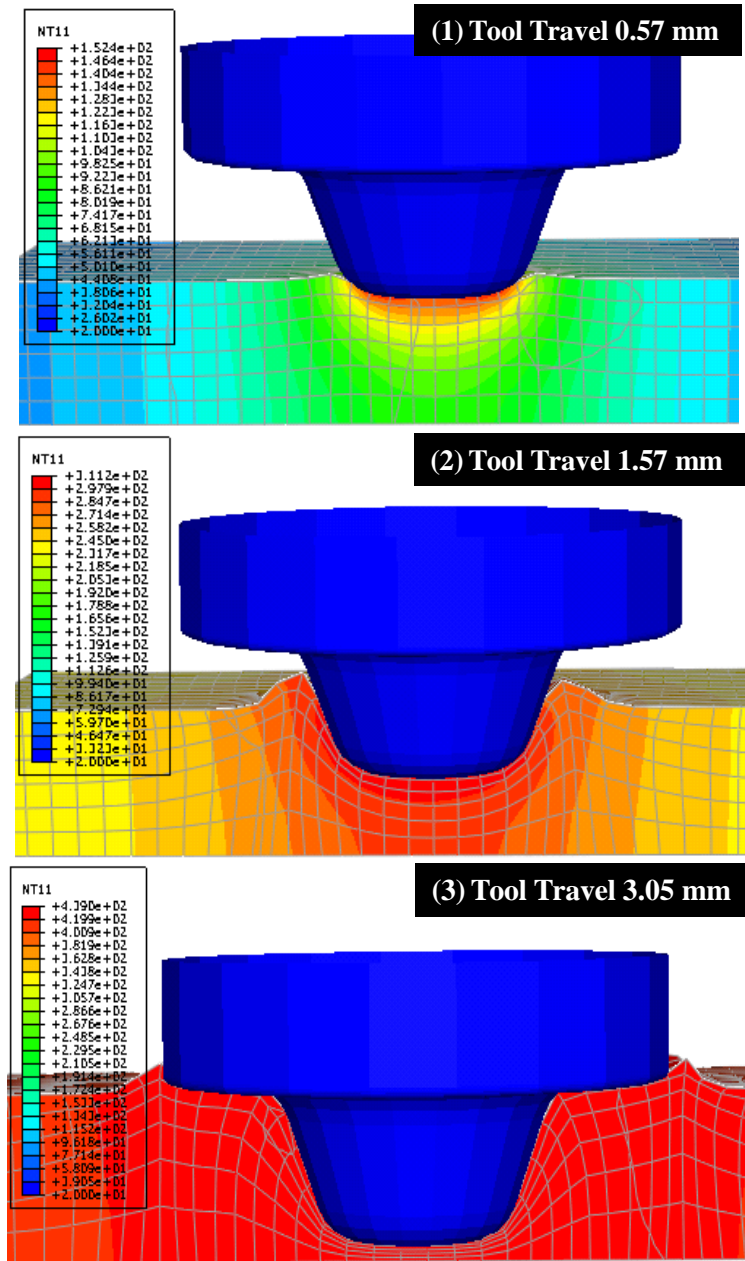


**Figure 4-6 : Temperature distribution during three steps of the tool travel**

It was observed from section 3 that both welding parameters such as translational and rotational speeds influenced the variation of the plunge forces. For a tool feed rate of 25 mm/min and 50 mm/min, and a tool rotating speed of 1500 rpm and 1800 rpm, the

plunge forces during the plunge phase of FSW process were acquired in both the experiments and the simulation as shown in Figure 4-7. For the FE model, it was assured again that the calculated force values in all the cases are in reasonable agreement with the measured values.

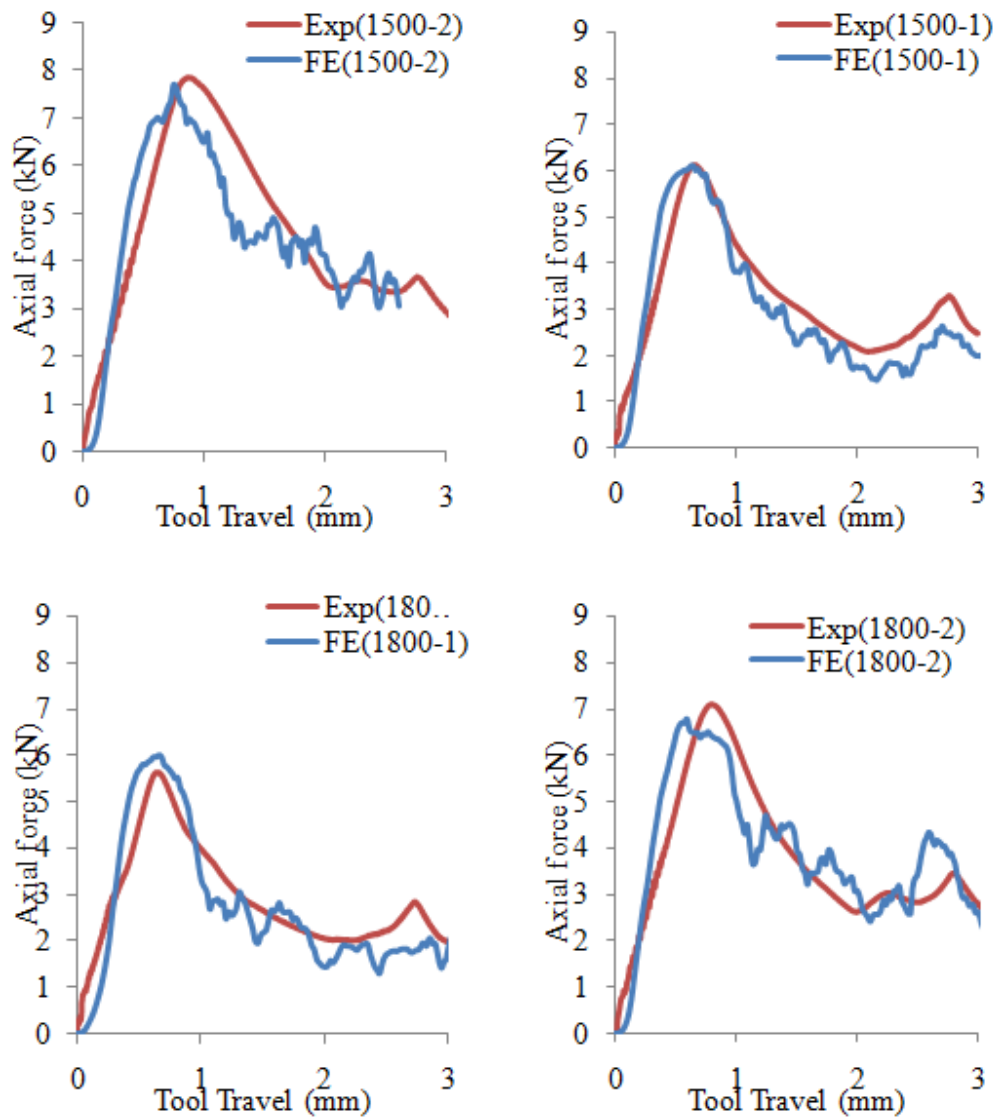


**Figure 4-7 : Comparison of the experiment vs. simulated plunge force in FSW for 1500 and 1800 rpm speed, and 1 and 2 in/min translational speed**

#### 4.5 EFFECT OF ULTRASONIC ASSISTANCE ON FSW OF LOW MELTING TEMPERATURE MATERIALS

Since the simulations of the conventional FSW process were validated, the simulation of UaFSW process was performed by imposing sinusoidal horizontal ultrasonic vibrations on the tool. The amplitude of vibrations used was varied from 5 to 10  $\mu\text{m}$  and simulated frequency was 20 kHz.

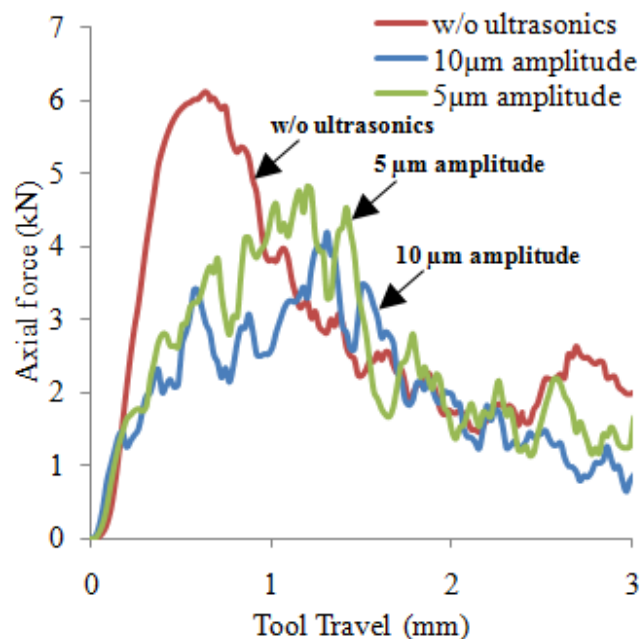


**Figure 4-8 : Variations of the plunge forces with the tool motion of 1500 rpm rotational speed and 25 mm/min feed rate by imposing ultrasonic vibrations for two amplitudes**

Simulation results indicated that the plunge force decreased with the vibration amplitude as shown in Figure 4-8. The force reduction can be obtained by increasing the amplitude of ultrasonic vibration. A 25% reduction in the welding force was obtained with  $a=5 \mu\text{m}$  and  $f=20 \text{ kHz}$ . In addition, it was observed after applying ultrasonics that

peak forces appeared in around 1.2 mm of the tool travel, while peak forces without ultrasonics appeared in around 0.7 mm of the tool travel.

In addition, Figure 4-9 shows ultrasonic assistance led to the increase in the temperature on the welding region. This temperature profiles were acquired from average values of three elements of mid-layer under the rotating FSW tool. This observation directly proves the hypothesis, where axial forces decrease with local material temperature rise.

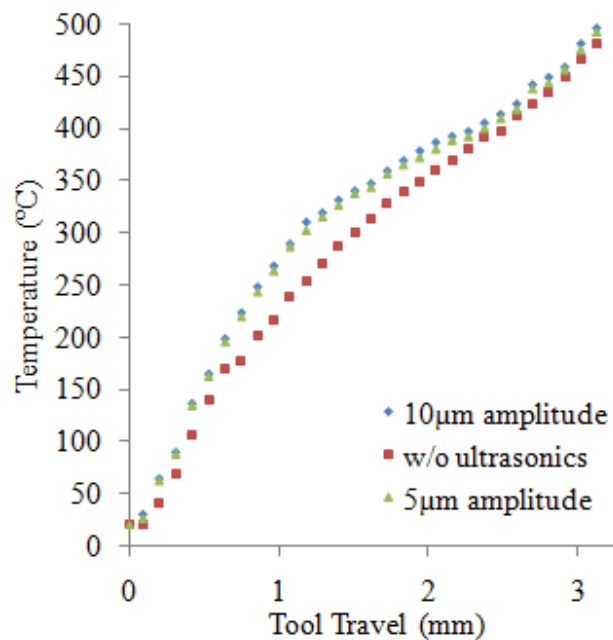


**Figure 4-9 : Temperature profiles of welding region with and without ultrasonic effect**

#### 4.6 EFFECT OF ULTRASONIC ASSISTANCE ON FSW OF HIGH MELTING TEMPERATURE MATERIALS

The FE model described in Section 4.2 was developed to investigate UaFSW of aluminum alloy. Therefore, the FE model needs to be modified for the UaFSW of high melting temperature material.

For UaFSW of steel and stainless steel, the rate-dependent constitutive model is more reasonable because the temperature by plasticization of workpiece material normally reaches up to 80-90% of the melting temperature of the workpiece material. In this study, a temperature and strain rate dependent Johnson-Cook was employed for modeling the FSW of steel and stainless steel. Schmidt and Hattel (Schmidt and Hattel w2005) and Mandal et al (Mandal et al. 2008) have successfully performed numerical analysis of the FSW process, using this rate dependent Johnson-Cook material law, which is given by:

$$\bar{\sigma} = (A + B[\bar{\varepsilon}^{pl}]^n)(1 + C \ln \frac{\dot{\varepsilon}^{pl}}{\dot{\varepsilon}_0})(1 - (\frac{\theta - \theta_{ref}}{\theta_{melt} - \theta_{ref}})^m) \quad (4-7)$$

where,  $\bar{\sigma}$  is the yield stress at nonzero strain rate,  $\dot{\varepsilon}^{pl}$  is the equivalent plastic strain rate,  $\dot{\varepsilon}_0$  is material parameters measured at or below the reference temperature, and A, B, C, n, m,  $\theta_{melt}$ , and  $\theta_{ref}$  are material parameters, given in Table 4-1, respectively. Other material properties used in this study are tabulated in Table 4-1.

Also, in this FE model, a temperature dependent coulomb friction coefficient is used to model the interaction between the workpieces and the tool as given in Table 4-2.

**Table 4-1 : Material properties and Johnson-Cook parameters for 1018 steel and 304 stainless steel used in the numerical analysis (Mori et al. 2007; Vural et al, 2003)**

Quantity	Unit	1018 Steel	304 Stainless Steel
Young's modulus	<i>GPa</i>	205	200
Poisson's ratio		0.29	0.3
Density	<i>Kg/m<sup>3</sup></i>	7870	7900
Melting temperature	<i>K</i>	1793	1673
Room temperature	<i>K</i>	293	293
Specific heat capacity	<i>J/(kg·K)</i>	486	440
Thermal expansion	<i>μm/(m·K)</i>	11.5	17.3
Fitting parameter <i>A</i>	<i>MPa</i>	560	310
Fitting parameter <i>B</i>	<i>MPa</i>	300	1000
Fitting parameter <i>n</i>		0.32	0.65
Fitting parameter <i>m</i>		0.5	1.00
Fitting parameter <i>C</i>		0.02	0.07
Fitting parameter $\dot{\epsilon}_0$	<i>s<sup>-1</sup></i>	1.00	1.00

**Table 4-2 : Temperature dependent friction coefficient of steel (Awang et al. 2005)**

Temperature(°C)	22.0	34.7	93.3	147.5	210.6	260.0	315.6	371.1	426.7	582.0
Friction Coeff, $\mu$	0.610	0.545	0.259	0.115	0.064	0.047	0.035	0.020	0.007	0.0

The UaFSW process of a butt joint between two 3.175mm thick 1018 steel was simulated under the rotational speed of 650 rpm and the translational speed of 50 mm/min. The UaFSW of 304 stainless steel used the rotational speed of 1000 rpm. These process parameters were obtained from literature sources (Lienert et al. 2003; Meran et al. 2007).

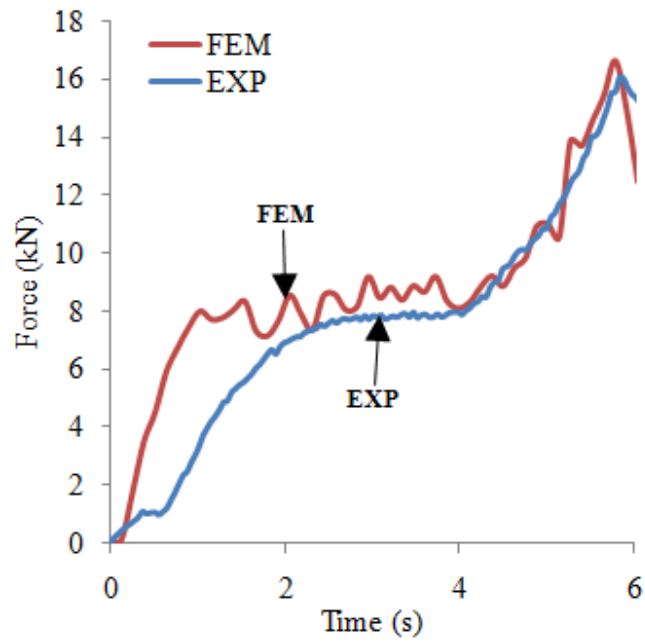


**Figure 4-10 : Axial force comparison in FSW (1018 steel, Rotational speed of 650rpm; translational speed of 50 mm/min)**

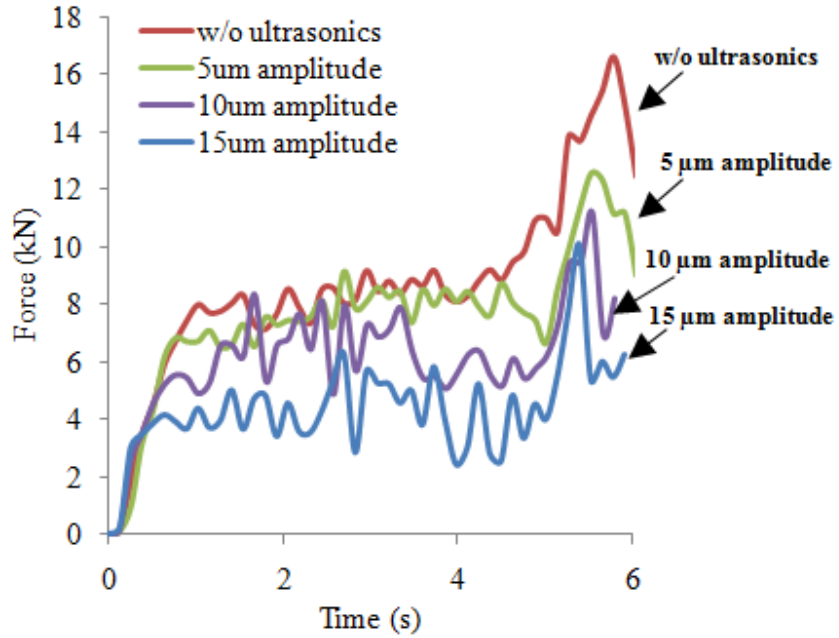


**Figure 4-11 : Axial force comparison with ultrasonic assistance (1018 steel, Rotational speed of 650rpm; translational speed of 50 mm/min)**



The modified FE model for welding of 1018 steel was validated with experimental force data. As is evident from Figure 4-10, the axial force during the plunging phase calculated from the simulation correlated well with the experimental data. Then, the simulation of UaFSW process was carried out by imposing sinusoidal ultrasonic vibrations, whose amplitudes were 5, 10, 15  $\mu\text{m}$ . A significant difference in axial forces acting on the tool has been discovered for UaFSW for same welding parameters as shown in Figure 4-11. As observed from Figure 4-8, the increase in ultrasonic amplitude results in the decrease in the welding force.

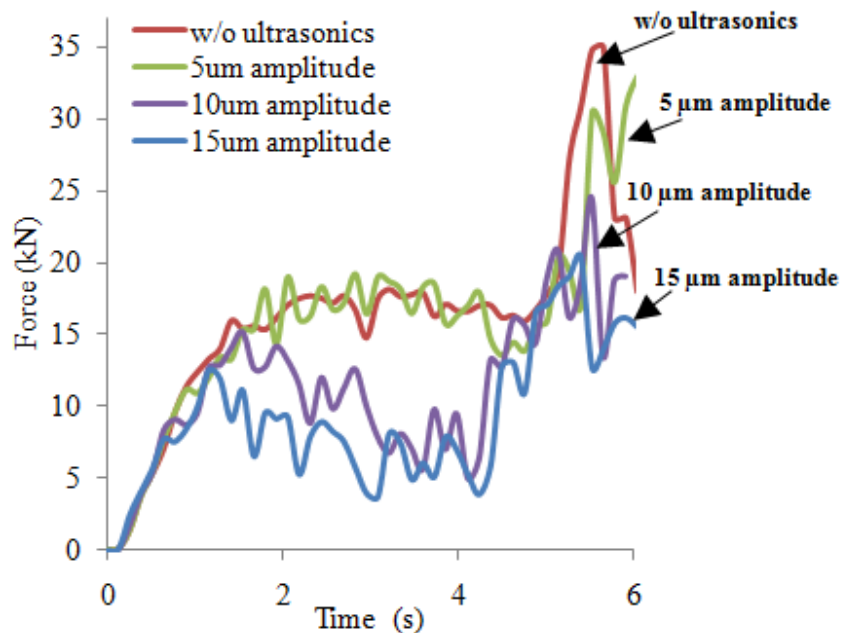


**Figure 4-12 : Axial force comparison with ultrasonic assistance (304 stainless steel, Rotational speed of 1000rpm; translational speed of 50 mm/min)**

The same simulation was performed after changing the workpiece material to a 304 stainless steel. Figure 4-12 showed the same observation as the simulation results for the 1018 steel.

#### 4.7 CONCLUSIONS

The FE analysis was used to simulate axial forces during the plunge phase of FSW and UaFSW, respectively. For FE analysis of FSW of aluminum alloy, coefficient of friction was selected based on the comparison of the plunge forces of FE modeling and experimental measurement results. The plunge forces acquired in both the experiments and the simulation showed a good agreement. Furthermore, the modified UaFSW FE model was developed using temperature and rate dependent Johnson-Cook model and temperature dependent friction coefficient for welding of 1018 steel and a 304 stainless steel. For FE analysis of UaFSW, it was observed that the plunge forces were reduced by using the ultrasonic vibrations. In addition, it was shown that the plunge forces could be decreased by increasing the amplitude of vibrations.

## **CHAPTER 5 - EXPERIMENTAL INVESTIGATIONS OF THE ULTRASONIC ASSISTED FRICTION STIR WELDING PROCESS**

### **5.1 INTRODUCTION**

The purpose of this chapter is to design and build an ultrasonic system able to integrate the ultrasonic oscillations to the FSW system. By integrating the ultrasonic to the FSW process, many benefits are expected in terms of welding quality, welding force, and tool life. Integration of ultrasonic vibration into conventional drilling and welding processes have been achieved in such a way that ultrasonic vibration is applied to the tool which is directly connected to ultrasonic transducer or horn. To overcome these disadvantages, we are introducing a method where the ultrasonic vibration is applied to a side of a rotating tool so that the welding tool can vibrate in a horizontal manner. It is much simpler and more effective than traditional way.

For designing the ultrasonic system, the natural frequency of the ultrasonic horn was considered to be as close as possible to the working frequency of the generator. The performance of the ultrasonic system is related to the amplitude of the oscillations. In this study, a laser vibrometer was applied to measure the amplitude of the ultrasonic horn. Thrust force measurement, mechanical testing, and defect analysis were used in studying the influence of the ultrasonic oscillations on the conventional FSW process.

## **5.2 DESIGN CONCEPT OF THE ULTRASONIC ASSISTED FSW PROCESS**

Ultrasonic system needs to be integrated into conventional FSW system to effectively transmit the vibrational energy to the workpiece. Ultrasonic energy can be transmitted into the welding region through various routes such as through the tool, workpiece, or a bottom support. In this study, the ultrasonic energy was applied to the rotating tool. However, compared with the commonly used method in which ultrasonic system is bolted to the tool, ultrasonic is applied to the side of the rotating tool with an aid of bearings as shown in Figure 5-1. This configuration simplifies the integration procedure since the ultrasonic transmitter can be independently designed and fabricated without changing any part of the existing FSW machine.

The ultrasonic system for this hybrid welding process consists of three components, which are ultrasonic generator, ultrasonic transducer, and ultrasonic horn. Ultrasonic generator, as shown in Figure 5-2, generates sinusoidal wave in specific frequency from the supplied power source. The high frequency signal forces the transducers to vibrate at the imposed frequency. Typical power supplies have maximum outputs ranging from a few hundred watts to several kilowatts. The ultrasonic generator by Weber Ultrasonics was used in this study. Ultrasonic transducer, as shown in Figure 5-3, converts the electrical wave to mechanical vibration which is small and must be amplified using an acoustic horn. For ultrasonic assisted friction stir welding system, the most appropriate is with longitudinal oscillations. In this study, the generator and transducer operates at a frequency of 20 kHz and 40 kHz with a variable bandwidth of 1 kHz and 4 kHz respectively. Specifications of the 40 kHz ultrasonic generator are shown in Table 5-1.

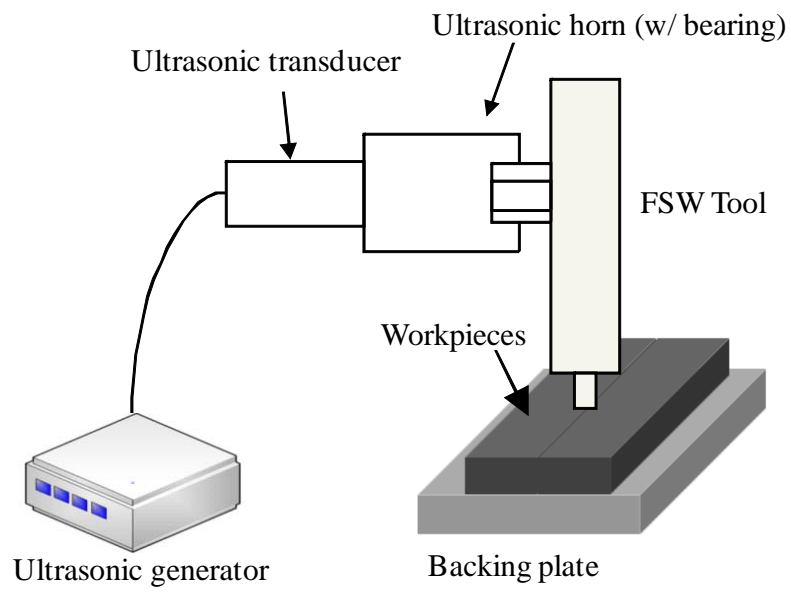


**Figure 5-1 : Concept configuration of UaFSW**

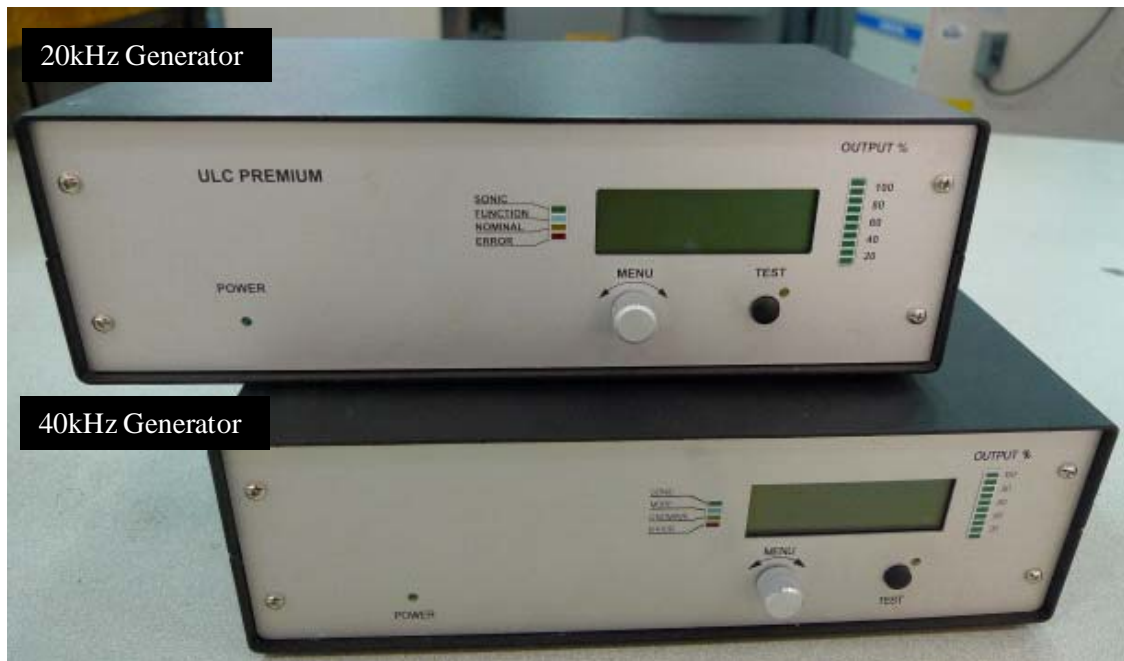


**Figure 5-2 : Ultrasonic generator by Webber ultrasonics**



**Figure 5-3 : Ultrasonic transducer**

**Table 5-1 : Specifications of the 40 kHz ultrasonic generator**

Connection voltage	Power consumption	Connected load
230-115 volt 50/60 Hz	3 A	660 VA
Ultrasound frequency	Output voltage	Output power
40 kHz	Approx. 600-1200 volt	400-1500 Watt MAX

### **5.3 ULTRASONIC HORN DESIGN AND FABRICATION**

For realization of the FSW with ultrasonic assistance, ultrasonic horn, which serves as a means of transmitting the vibrational energy to the FSW tool, should be designed and fabricated. The horn must be designed and tuned to the longitudinal mode of vibration at

an operating frequency of the ultrasonic generator and transducer. Thus, the shape, material, and dimension of the horn should be determined in such a way that the horn operates at 20 kHz and 40 kHz frequency, which is the operating frequency of the generator.

### **5.3.1 HORN DESIGN PROCEDURE**

For the horn to work properly in the UaFSW process, it should be designed and fabricated based on the following requirements. Most importantly, the desired resonance frequency of the horn must match the working frequency of the ultrasonic generator. Moreover, there must be no other effective frequency near the desired resonance frequency. During transient loading conditions, the modal coupling causes frequency shift, which leads to improper performance. Amplitude of the horn tip displacement must be maximized, and uniformity of the amplitude at the tip surface should be considered as well. Last concern is that high stress occurs in nodal area where section area varies.

The shape and size of the ultrasonic horn are restricted by the UaFSW configuration. The ultrasonic horn for this study consists of two bearings, two shafts, and a main block (horn) as shown in Figure 5-4. Design of this complex horn was performed by the FE analysis which was used to predict ultrasonic vibration frequency, amplitude, and structural stress. Such data can help design the proper horn of UaFSW with the aid of amplitude measuring data.

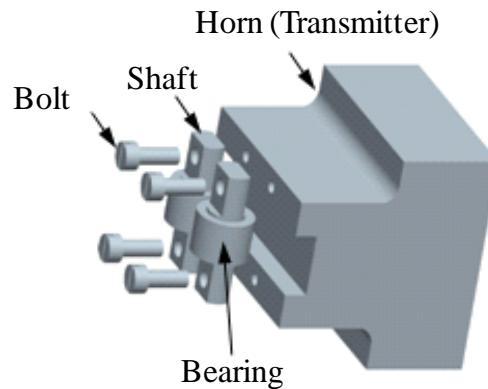


**Figure 5-4 : Assembly configuration of ultrasonic horn used in this study**

As shown in Figure 5-5, half wavelength was selected as the length of the horn so that the maximum amplitude of the tip ( $z_2$ ) can be obtained at anti-nodal point of oscillation. Moreover, the nodal point is located at the weak place of the horn so that high stress at the region where size of cross-section varies can be avoided. It was assumed that the wavelength of aluminum alloy was determined based on the wavelength of longitudinal vibration in a thin rod in the form of Equation 5-1.

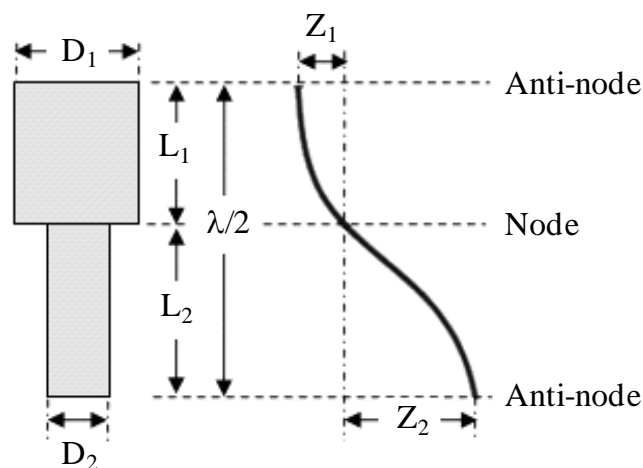


**Figure 5-5 : Criterion of horn dimension.**



$$\lambda = \frac{1}{f} \sqrt{\frac{E}{\rho}} \quad (5-1)$$

$\lambda$  is wavelength,  $f$  is resonant frequency,  $E$  is young's modulus (68.54 GPa), and  $\rho$  is density (2685 Kg/m<sup>3</sup>). Starting from the half wavelength (126.3mm) as the length of the horn, all other dimensions including  $D_1$ ,  $D_2$ ,  $L_1$ , and  $L_2$  from Figure 5-5 were determined using FE simulation.

### 5.3.2 DESIGN AND FABRICATION OF 40KHZ ULTRASONIC HORN

#### 5.3.2.1 Horn type selection

In ultrasonic application, the most common shapes are exponential, taper, and stepped types with circular or rectangular cross-section, as shown in Figure 5-6.

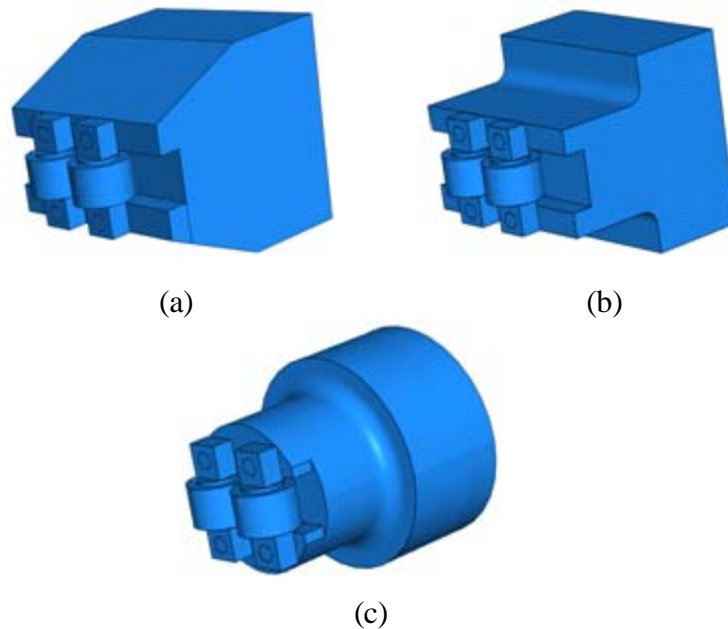
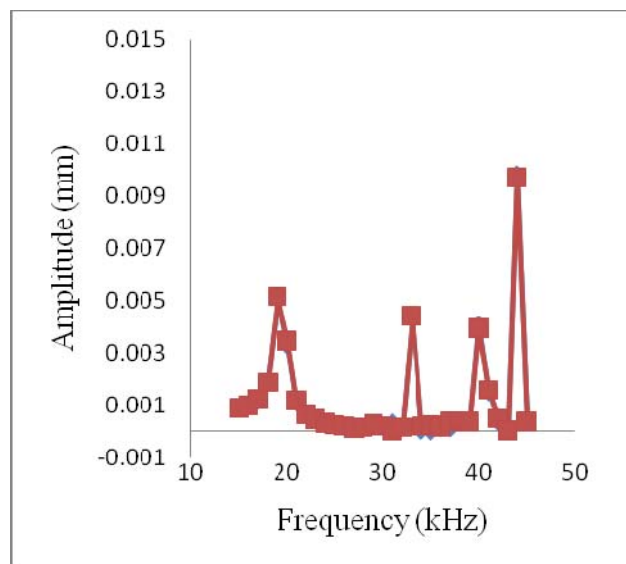
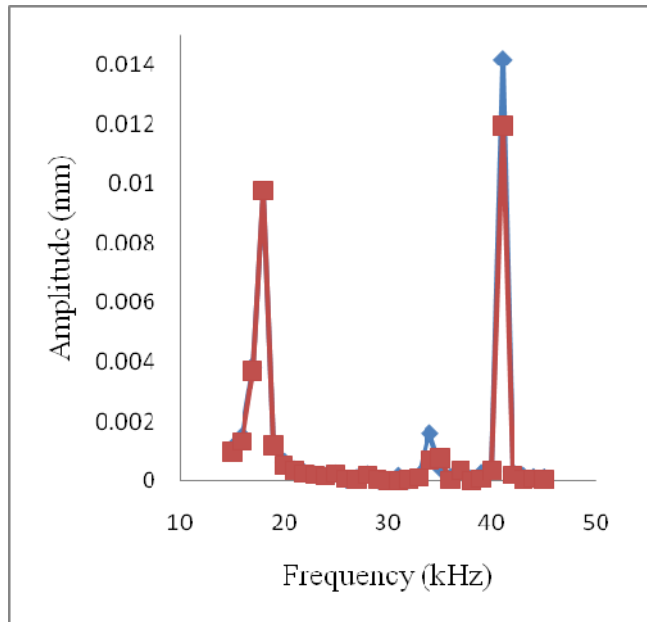


**Figure 5-6 : Different types of horn design: (a) Taper type with rectangular section, (b) Stepped type with rectangular section, and (c) Stepped type with circular section**

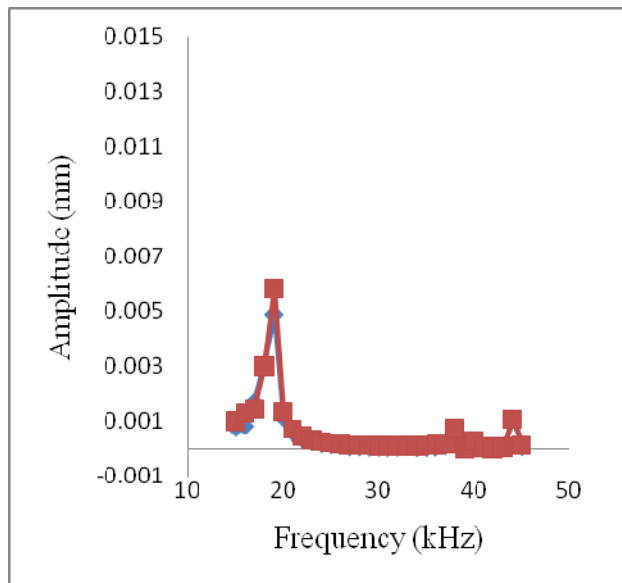
In FE model of ultrasonic application, modal analysis is employed to allow the design to vibrate at a specified frequency and then harmonic analysis is used to determine the steady state response of a structure to harmonic loads of known frequency. Figure 5 7 shows frequency response amplitudes acquired from FE harmonic analysis of each type of ultrasonic horn. In Figure 5 7, the tip amplitudes of right and left bearing were calculated within a specific range of frequency using the FE simulation. Considering the design requirements such as high amplitude, uniform amplitude, and isolation of the operating frequency, a stepped type with rectangular cross-section was selected. The stepped type with rectangular section makes amplitude maximum and uniform. Moreover, there is no undesired frequency near the desired working frequency (40 kHz) so that it can avoid modal coupling. Due to high fatigue strengths, low acoustic losses, and good machinability, aluminum alloy was used for the fabrication of the horn.



(a) Taper type with rectangular section



(b) Stepped type with rectangular section



(c) Stepped type with circular section

**Figure 5-7 : Amplitude of horn tip displacement with respect to frequency. Left and right plots describe the amplitude acquired from left and right tip of bearings, respectively**

### 5.3.2.2 Tuning process

Based on the FE simulation results, an initial horn was fabricated and assembled, which included bearings and shafts. Due to the discrepancy between the FE model and actual assembly, fabricated horn was out of the frequency range of the generator and transducer initially. The resonant frequency of the horn had to be corrected through tuning process, which involved reshaping of the horn until the resonant frequency was within the tolerance of the working frequency. Failed horn can be tuned by changing the horn size or putting slots. In our case, the change of the resonant frequency after cutting material from the horn was tested using FE simulation first. Figure 5-8 shows change in resonant frequency of longitudinal vibration mode after cutting laterally, where longitudinal direction is z and lateral one is y as described in Figure 5-8. This cutting not only increases the frequency but also makes amplitude uniform. The shortening of the longitudinal length of the horn increased the resonant frequency as shown in Figure 5-9. Following these criteria of frequency correction as described above, the horn was machined again so that the horn could have longitudinal mode at frequency of 41 kHz. As shown in Figure 5-10, the measured frequency as a result of being shortened agreed well with FE prediction of the resonance frequency. After pushing the FSW tool with this horn, the resonant frequency of the horn should be lower than one in an unloading state, which is the reason why the horn was tuned to a little higher frequency than the target one (40 kHz).

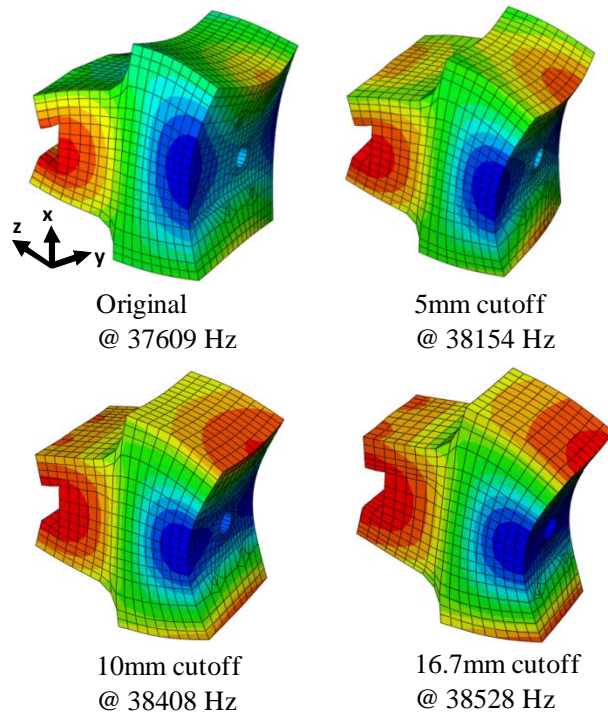


**Figure 5-8 : Change in resonant frequency of longitudinal vibration mode after cutting laterally (y-direction)**

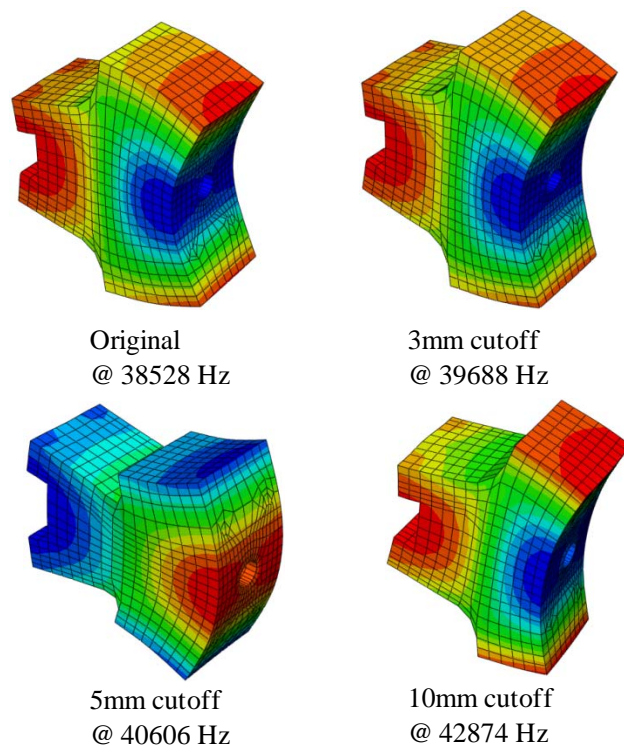


**Figure 5-9 : Change in resonant frequency of longitudinal vibration mode after cutting longitudinally (z-direction)**

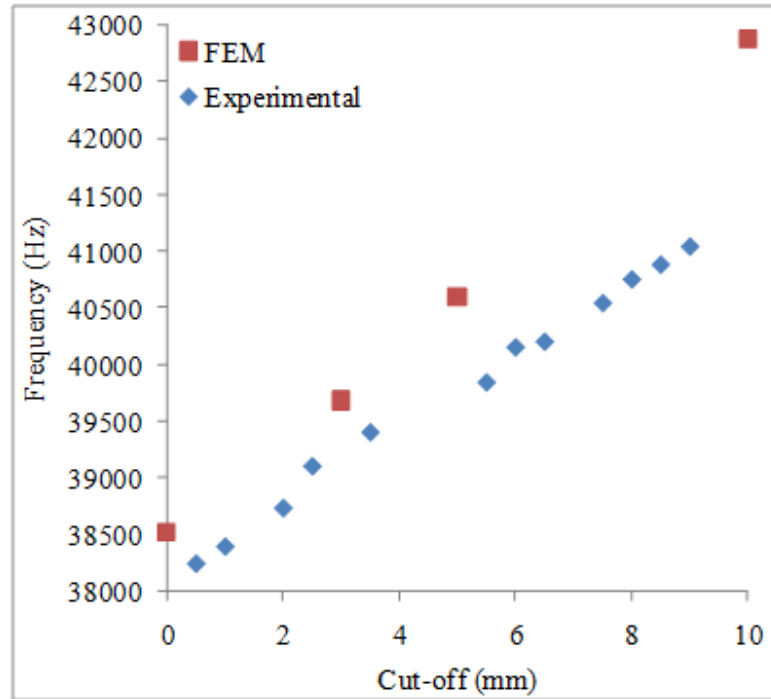
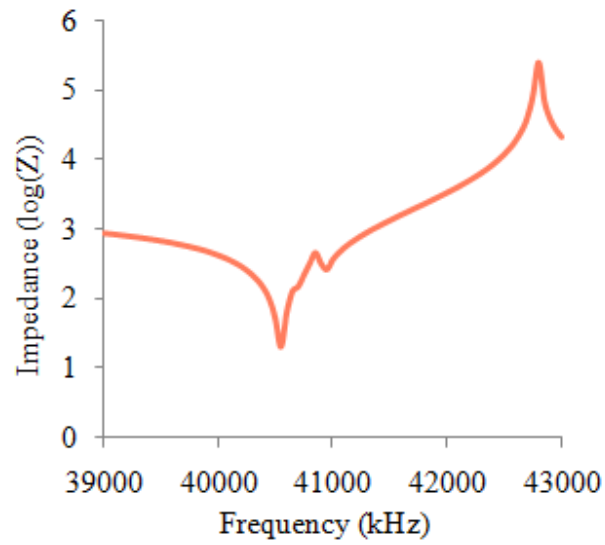


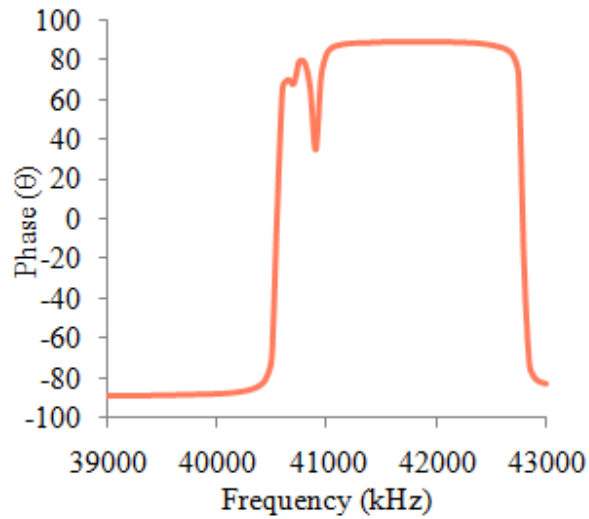
**Figure 5-10 : Estimated modal frequencies for 40 kHz horn**

### 5.3.2.3 Actual measurement of resonant frequency and amplitude

After attaching shafts and bearings on the fabricated horn, actual measurement of the natural frequency of our ultrasonic horn were made with a HP 4192A Impedance/Gain phase analyzer. The impedance analyzer is the instrument essential in every production of ultrasonic equipment for resonant frequencies measurements. Minimum impedance and phase shift occurs at the resonance frequency. Figure 5-11 shows our ultrasonic horn has resonance frequency at 40555 Hz. In tuning process, the horn without shafts and bearings was measured to have the resonance frequency at 41040 Hz. Increase in mass after adding bearings drops 500 Hz in the resonance frequency.



(a)



(b)

**Figure 5-11 : Actual measurement of (a) impedance and (b) phase using HP4192A**

The oscillatory displacement amplitude of the 40 kHz ultrasonic horn was measured using laser vibrometer (OFV-2500 modular vibrometer controller / OFV-303 Optical sensor head). It was observed from Figure 5-12 that the horn was driven at nominal peak amplitude of 2.4  $\mu\text{m}$ .

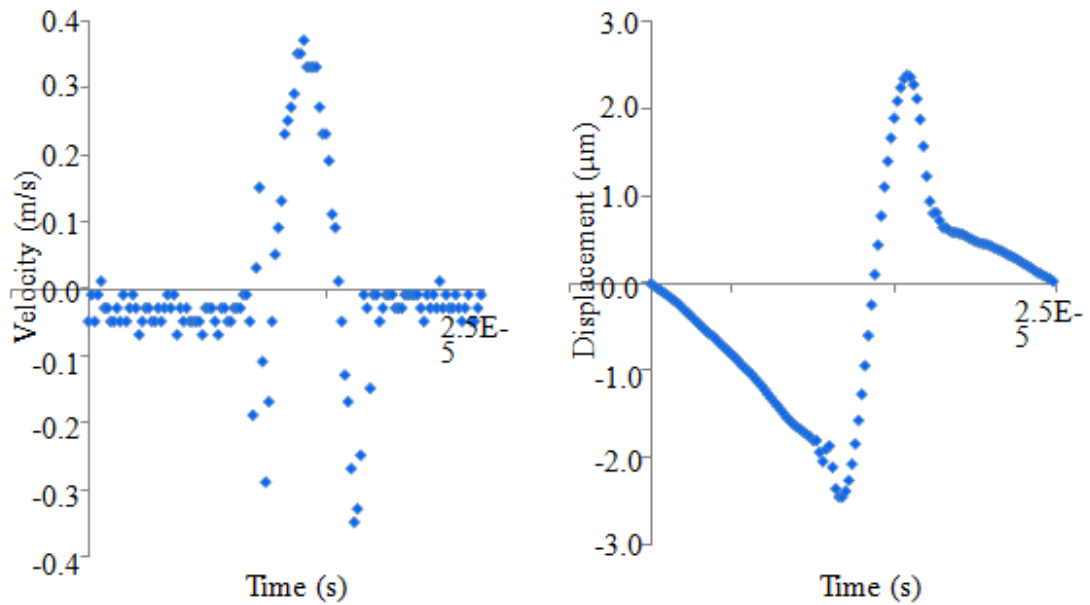


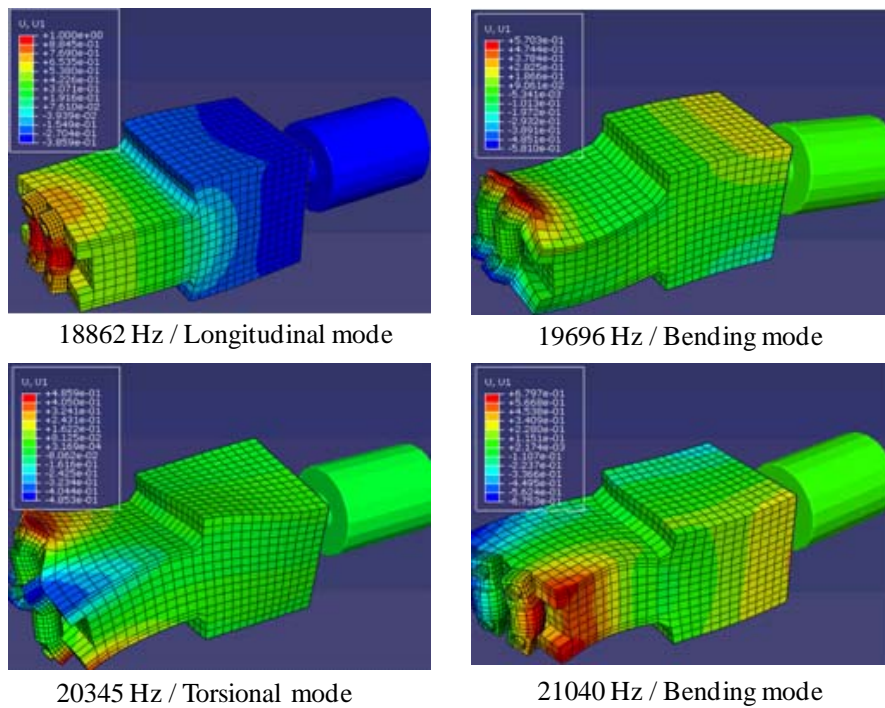
**Figure 5-12 : 40 kHz ultrasonic horn amplitude measured by laser vibrometer**

### 5.3.3 DESIGN AND FABRICATION OF 20 KHZ ULTRASONIC HORN

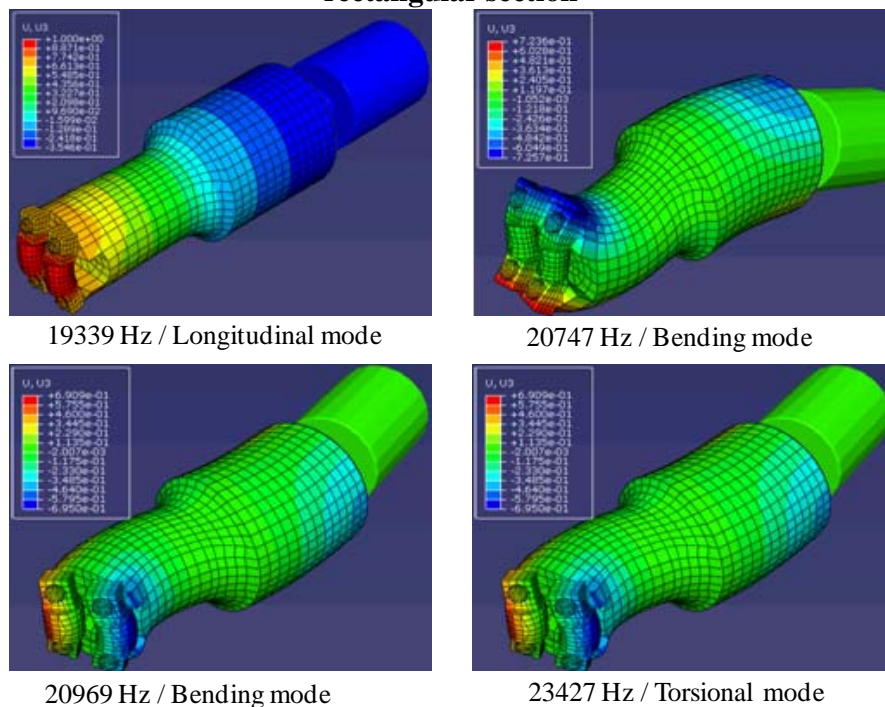
Same procedures were followed to design and fabricate an ultrasonic horn for 20 kHz application. Length of the 20 kHz horn is twice as long as that of the 40 kHz one, because the 20 kHz horn is designed based on the twice longer wavelength. As in section 5.3.2, among common shapes, stepped type with rectangular section and stepped type with circular section were considered for comparison. FE modal analysis and harmonic analysis were employed to select proper type for this application. Figure 5-13 and 5-14 show the results of modal analysis of both types. From these results, in terms of amplitude amplification and frequency spacing between vibration modes, the stepped type with circular section showed better fit to the 20 kHz application. The circular section horn showed 2.83 times amplitude magnification, while the rectangular section horn had 2.59 times amplification. In addition, the circular section horn showed 1408 Hz spacing between the desired working frequency and undesired one, while the rectangular section



horn had 834 Hz spacing.

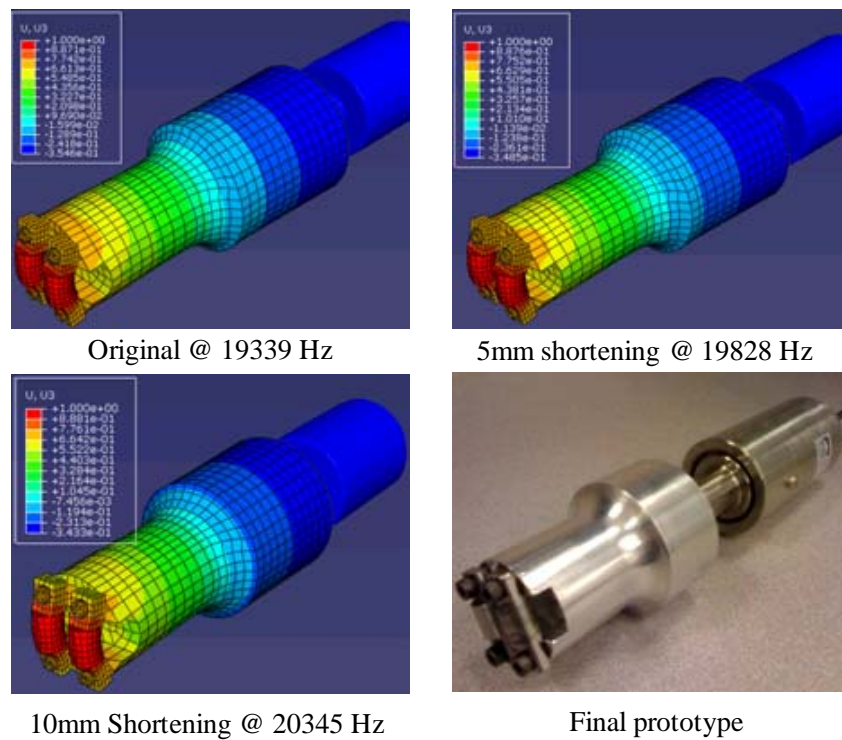


**Figure 5-13 : Result of modal and harmonic analysis of the stepped type with rectangular section**



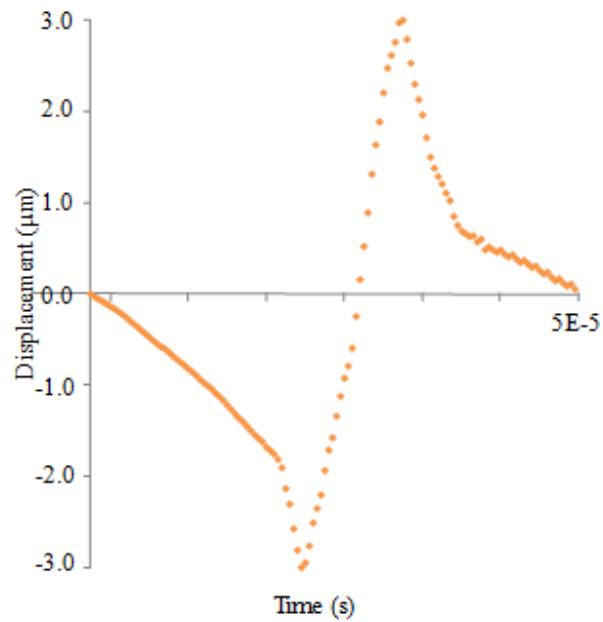
**Figure 5-14 : Result of modal and harmonic analysis of the stepped type with circular section**

Figure 5-15 shows change in resonant frequency of longitudinal vibration mode after shortening through the tuning process as described in the previous section. This cutting not only increases the resonant frequency but also amplifies the amplitude more. The FE result of 10 mm shortening showed 2.92 times amplitude magnification.



**Figure 5-15 : Change in resonant frequency of longitudinal vibration mode after shortening and the final prototype**

Due to limitation in using 20 kHz ultrasonic generator, we operated it with 50% power output. The oscillatory displacement of the 20 kHz ultrasonic horn was measured using the laser vibrometer. Figure 5-16 showed that the horn was driven at nominal peak amplitude of 3.1  $\mu\text{m}$ . It was observed that the maximum amplitude of 20 kHz horn with half power output was larger than one of 40 kHz horn with full power output.



**Figure 5-16 : 20 kHz ultrasonic horn amplitude measured by laser vibrometer**

#### **5.4 UAFSW OF 6061-T651 ALUMINUM ALLOY**

A series of the FSW tests was performed to investigate the effects of ultrasonic vibration on welding of aluminum alloy 6061-T651.

##### **5.4.1 EXPERIMENTAL SETUP**

Figure 5-17(a) shows a schematic drawing of the assembly of the horn, the transducer, and the holder. Figure 5-17(b) shows the fabricated horn, which consists of two bearings and two shafts. A fixture and a holder were also fabricated to attach the horn inside the FSW machine. During the ultrasonic operation, the transducer needs to be held firmly under the generated reacting forces. The holder consists of a housing block, a ring, and a back plate. By pushing the ring with the back plate, the ring with a slim slot can slide with a guide of the chamfer region of the housing and hold the transducer tightly.

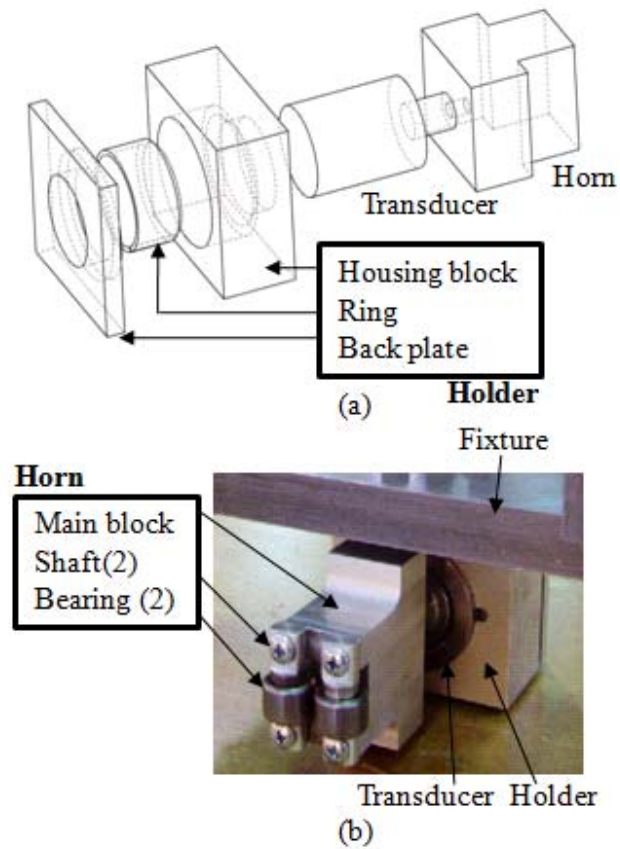


**Figure 5-17 : (a) Schematic drawing of the assembly including a holder and (b) Fabricated horn and fixture**

An in-house CNC machine was used to demonstrate the UaFSW. The FSW tool, which has a typical non-threaded cylindrical pin shape and flat shoulder, was machined and heat treated to achieve a hardness of HRC 58. Welding was carried out at rotating speeds of 1500 and 1800 rpm and translational speeds of 25 and 50 mm/min, which generated reasonable welds. Detailed processing parameters are described in Table 5-2.

**Table 5-2 : Processing parameters**

Tool	Shoulder diameter	10 mm
	Pin diameter	4 mm
	Pin extension	3.05 mm
Rotating speed		1500, 1800 rpm
Travel speed		25, 50 mm/min
Plunge depth		0.1 mm
Material (Length×Width×Thickness)		Aluminum alloy 6061-T651 (50×50×3.175 mm)
Joint type		Butt joint

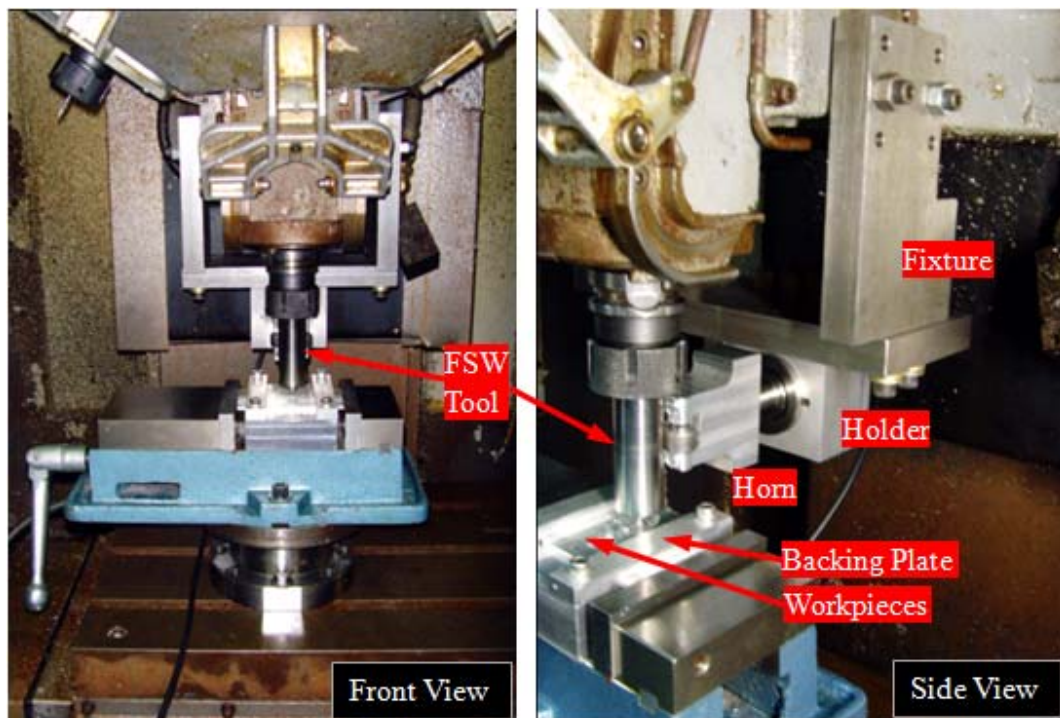


**Figure 5-18 : Experimental set-up for UaFSW using Mori Seiki CNC machine**

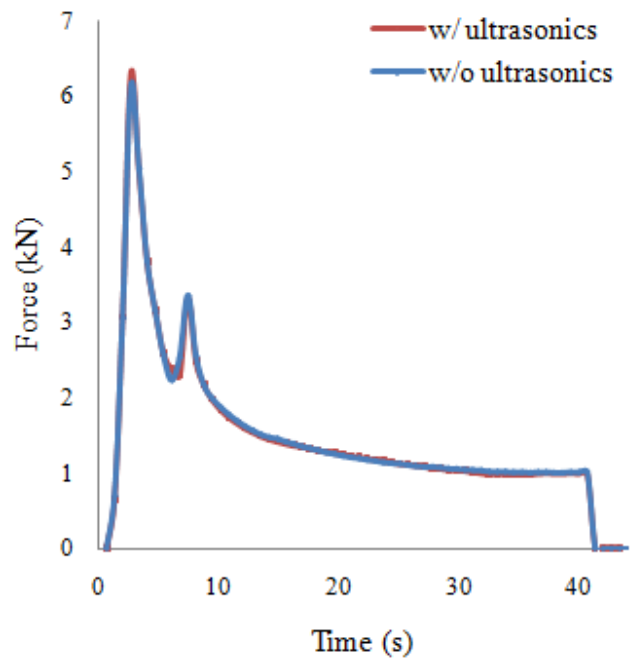
Figure 5-18 shows the total experimental setup of the UaFSW. With the aid of the fixture and the holder, the ultrasonic horn assembly makes the FSW spin tool vibrate in the horizontal direction.

A Kistler four component dynamometer (Type 9272) was used to measure the axial force during the welding process. Furthermore, tensile tests were performed on an Instron universal testing machine (Model 4502). Tensile specimens were prepared with a tensile direction, perpendicular to the welding direction, so that the weld zone is located in the middle of the specimen by using an EDM machine. Moreover, Vickers micro-hardness measurements were performed at 100gf load for 15s along the centerline of the cross-section of the welds.

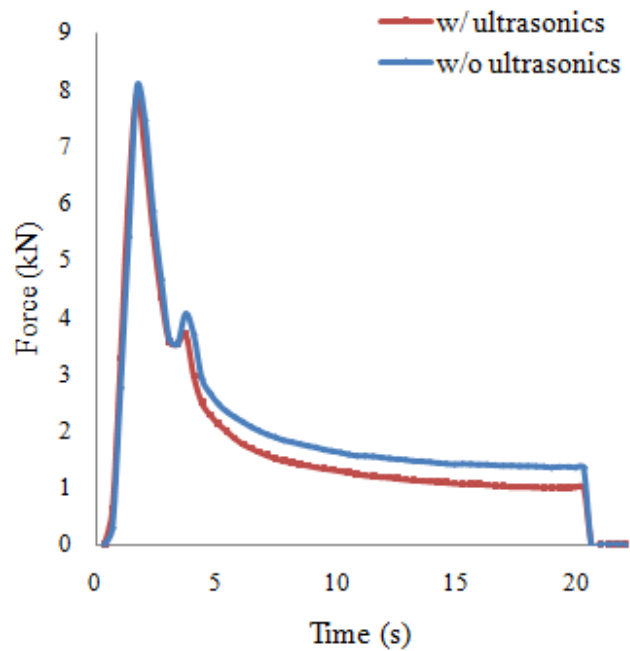
#### **5.4.2 RESULTS WITH 40 KHZ ULTRASONIC SYSTEM**

Figure 5-19 plots the axial force with respect to the time step of the process. FSW has plunging and translational portions. During the plunging motion, after the first peak was reached, the axial force drops due to the frictional heat generated. Then, it rises again when the shoulder of the tool is immersed into the workpieces. After that, during the translational portion, when the tool moves along the joint line of the butt welding configuration, the axial force stabilized.

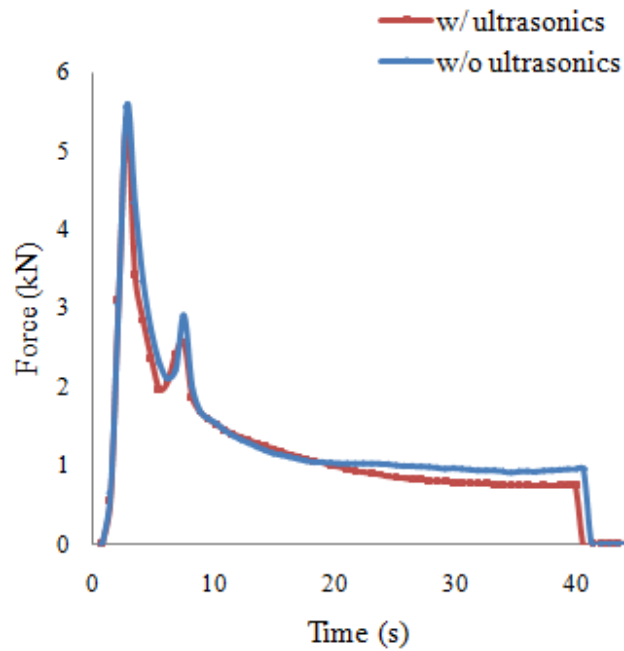
For the testing conditions of Figure 5-19 (b) and (c), the forces reduced during the translational portion. This means that the frictional heat was magnified through the shoulder part of the FSW tool due to transmission of ultrasonic energy so that less work is required by the tool to move along the joint line.



(a) Rotational speed (1500 rpm), Translational speed (25 mm/min)



(b) Rotational speed (1500 rpm), Translational speed (50 mm/min)

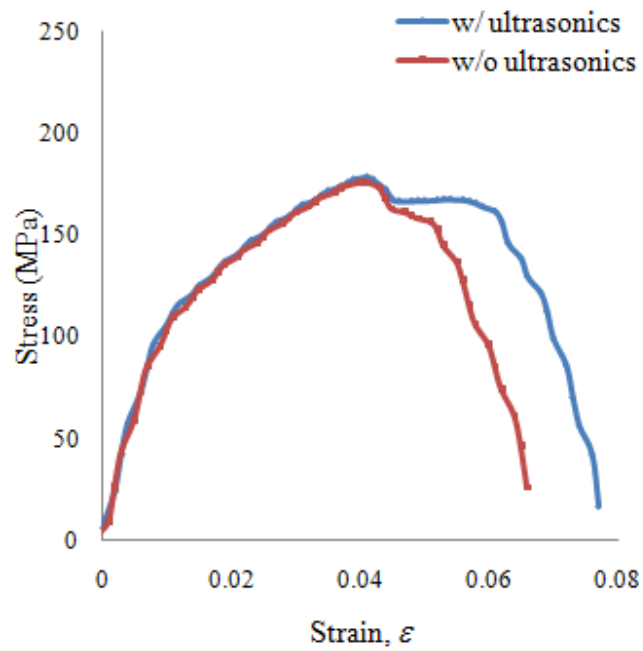


(c) Rotational speed (1800 rpm), Translational speed (25 mm/min)

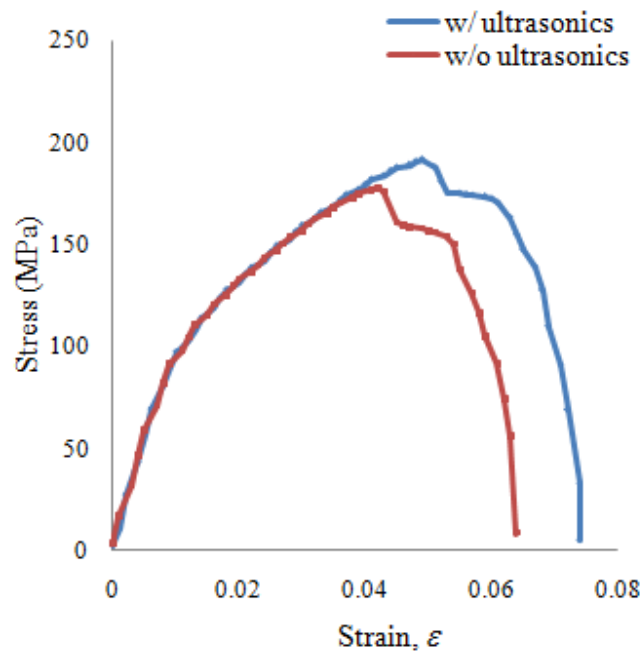
**Figure 5-19 : Axial forces with respect to time**

Tensile tests were also performed to determine stress and strain of welded part with and without ultrasonics. Figure 5-20 presents the stress-strain relationships from the tensile tests. It can be seen from the figure that by applying ultrasonics, the elongation of the weldment is 15% higher than one from only FSW process. Moreover, Figure 5-20(b) shows 10% increase in yield strength with ultrasonic assistance.





(a) Rotational speed (1500 rpm), Translational speed (25 mm/min)



(b) Rotational speed (1500 rpm), Translational speed (50 mm/min)

**Figure 5-20 : Stress strain curve of welded parts**

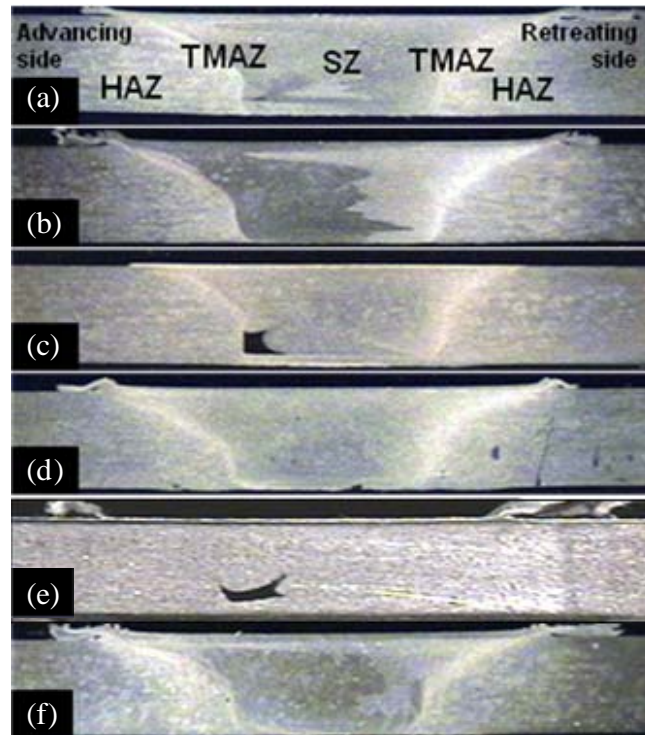
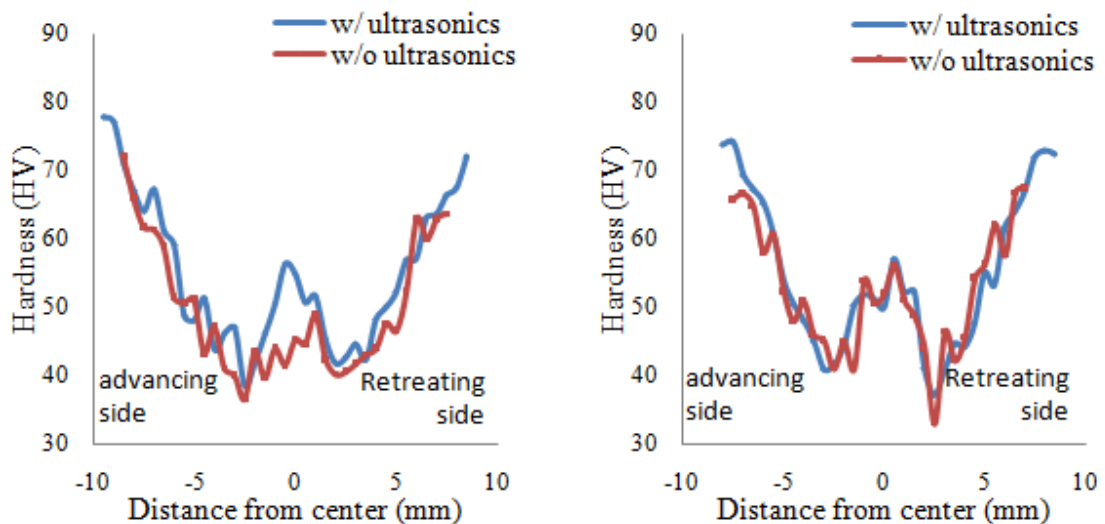


**Figure 5-21 : Macroscopic views of weld zone at (a) 1500 rpm, 25mm/min, and without ultrasonics; (b) 1500 rpm, 25mm/min, and with ultrasonics; (c) 1500 rpm, 50mm/min, and without ultrasonics; (d) 1500 rpm, 50mm/min, and with ultrasonics; (e) 1800 rpm, 25mm/min, and without ultrasonics; (f) 1800 rpm, 25mm/min, and with ultrasonics**

Enhancement of the tensile properties after applying ultrasonics to FSW process can be explained through the investigation of macroscopic view of cross section of each weldment. Figure 5-21 shows the macroscopic views of weld zone at different conditions. Despite of ultrasonic effect, all the cases have different microstructural transition regions such as heat affected zone (HAZ), thermo-mechanically affected zone (TMAZ), and stir zone (SZ). It is also observed in each case that a border of advancing side, where the direction of tool rotation is same with one of tool path, looks sharper than one of retreating side, where the direction of tool rotation is different with one of tool path. It corresponds to the fact that all the failure occurred at the border of the advancing side

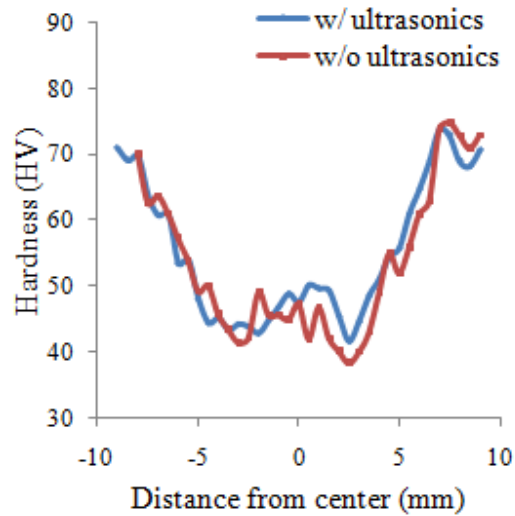
during tensile test. Furthermore, all the results coming from cases without ultrasonics have void at the advancing side. It implies that the use of non-optimal tool shape in FSW resulted in the void defect. However, it can be observed that, in UaFSW process, there is no void defect. It was demonstrated that high frequency oscillation on the FSW tool pin helps lead to sound weld.

Vickers hardness profiles were measured along the centerline of the cross-section of each weldment as shown in Figure 5-22. It was observed in all the cases with and without ultrasonics that the hardness value decreased from the base material to HAZ, and the boundary area between TMAZ and HAZ appeared to have the lowest hardness value. The hardness values of SZ were higher than those of TMAZ and HAZ. It was also observed that the location of minimum hardness coincide with the failure location during the tensile test. Ultrasonics didn't affect much on micro-hardness of the weldment. Therefore, it can be explained that difference in tensile properties is probably due to the formation of the void defect in FSW.



(a)

(b)



(c)

**Figure 5-22 : Vickers hardness profiles in weld zone along centerline at different conditions**

#### 5.4.3 RESULTS WITH 20 KHZ ULTRASONIC SYSTEM

Axial forces and stress strain curves were obtained by changing to the 20 kHz ultrasonic system under same other conditions. It was observed that the maximum amplitude of the 20 kHz ultrasonic horn was larger than one of 40 kHz ultrasonic horn. Moreover, the 20 kHz horn is heavier and stronger enough to transmit ultrasonic energy well into the FSW rotating tool than the 40 kHz one. Figure 5-23 shows the axial forces obtained under rotational speed of 1500 rpm and translational speed of 25 mm/min. It was shown that the 40 kHz ultrasonic system didn't help to decrease the axial forces under the rotational and translational speeds. However, with 20 kHz ultrasonic horn, the forces reduced during the second peak and the translational portion.

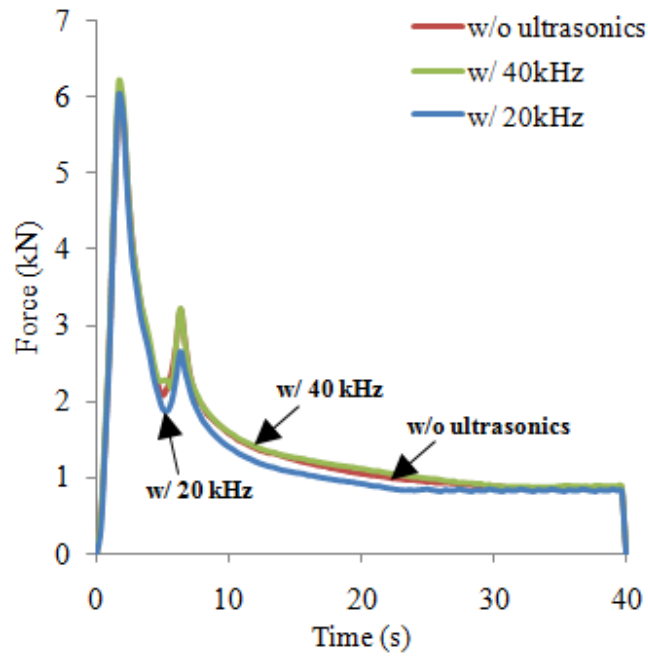


**Figure 5-23 : Axial forces with respect to time (Rotational speed of 1500rpm; translational speed of 25 mm/min)**

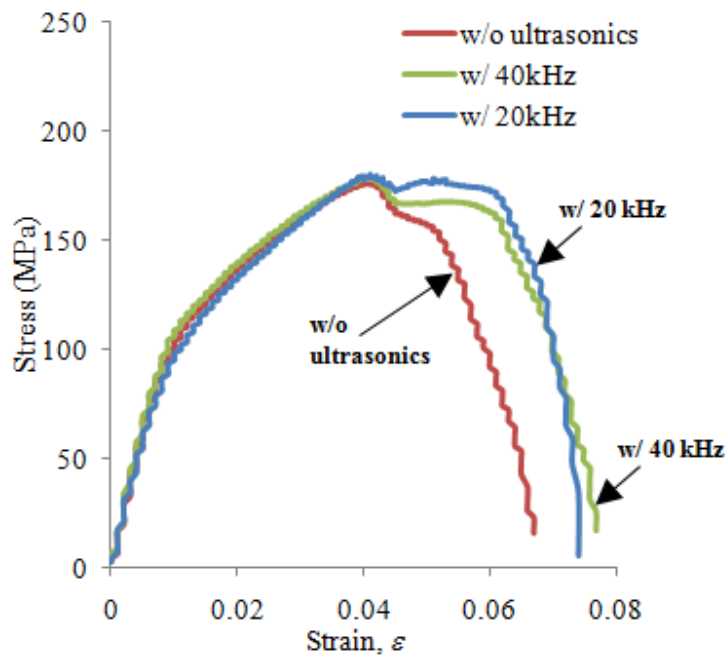


**Figure 5-24 : Stress strain curve of welded parts (Rotational speed of 1500rpm; translational speed of 25 mm/min)**

Tensile tests were carried out to determine the stress and strain of welded part. It can be seen from Figure 5-24 that by applying ultrasonics of 20 kHz and 40 kHz frequency, the elongation of the weldment is better than one obtained from FSW process.

### 5.5 ULTRASONIC ASSISTED FSW OF HIGH MELTING TEMPERATURE MATERIALS

The workpiece material was 1018 steel with nominal strength of 440Mpa. The thickness of the material was 3.175 mm.

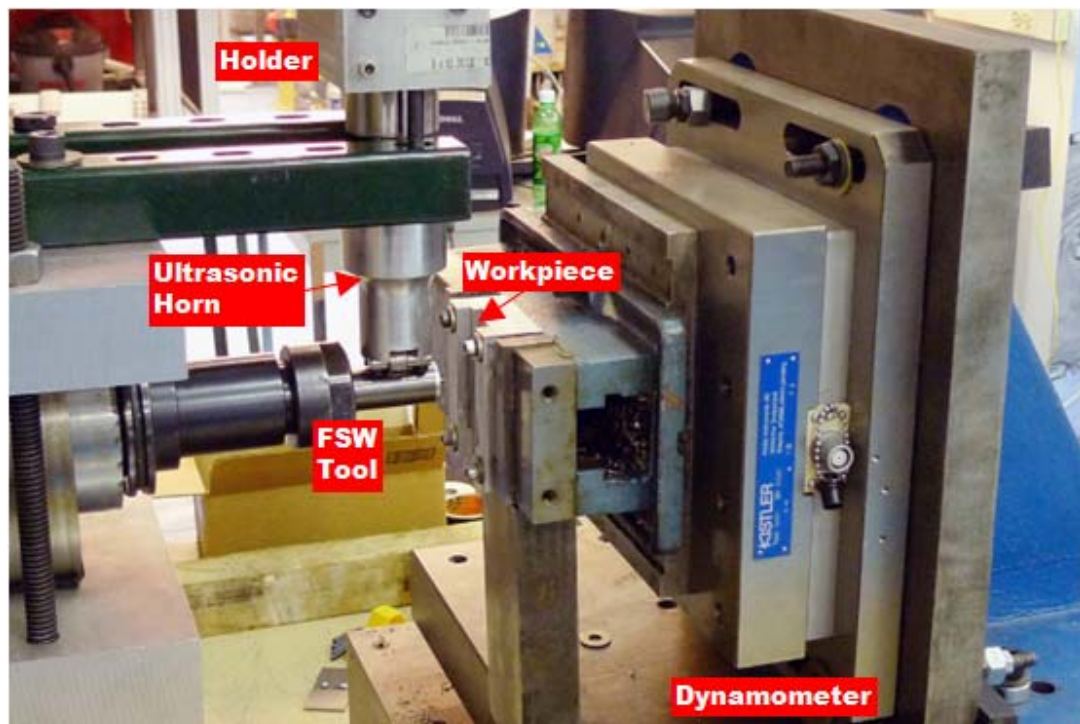


**Figure 5-25 : Experimental setup for UaFSW using horizontal CNC machine**

All of the experimental trials were performed on an in-house horizontal CNC machine (M. S. Machining Center). Figure 5-25 shows the experimental setup of the

UaFSW. With the aid of the fixture and the holder, the ultrasonic horn assembly makes the FSW spin tool vibrate in the joint direction.

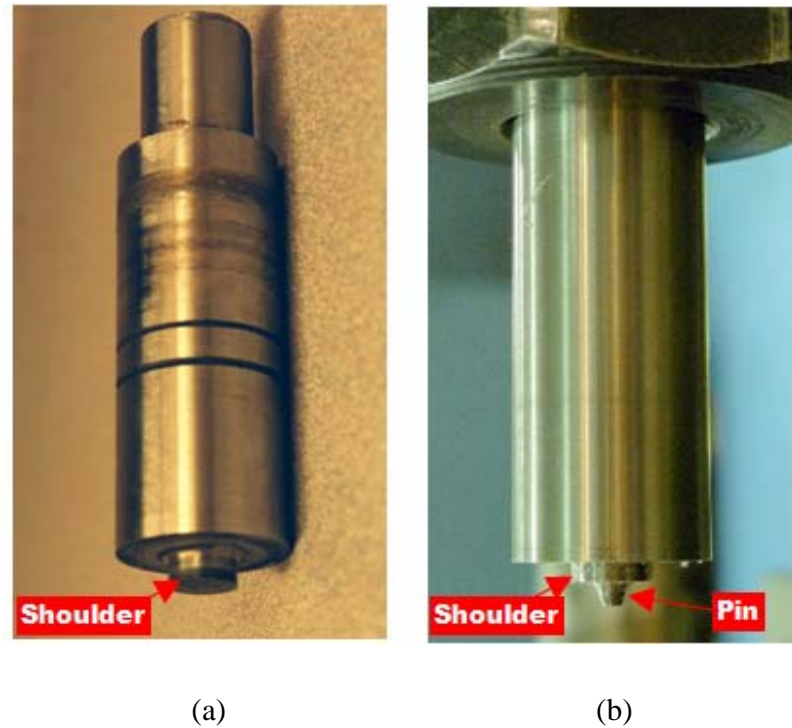


**Figure 5-26 : The view of tool used: (a) made of A2 tool steel (b) made of tungsten carbide (10% cobalt)**

The shoulder diameter of the tool was 10 mm, and the taper typed pin was changed conically 2.4 and 3.0 mm in diameter. The length of the pin was machined to be 3 mm. At the initial experimental trials, the tool made of heat treated A2 tool steel with HV 653 hardness was used. However, the pin melted down after a few trials due to high friction between the tool and steel workpiece as shown in Figure 5-26 (a). Then the FSW tool was made of tungsten carbide with HV 1650 hardness. The tungsten carbide tool can withstand high temperatures of 1200 °C. Figure 5-26 shows the tool steel FSW tool and

the tungsten carbide FSW tool. Welding was carried out at rotating speeds of 650 rpm and translational speeds of 25 and 50 mm/min, which generated reasonable welds. And a Kistler four component dynamometer (Type 9255) was used to measure the axial force during the welding process. The temperature was measured using a type E thermocouple (Omega 5TC-TT-E-36-72) on the top surface of the workpiece. The thermocouples were placed on both sides of 7 mm away from the joint line of two workpieces as a butt welding configuration and fixed on the surface using epoxy adhesive (Omega OB-101 resin and catalyst). Figure 5-27 is a top view of weldment after welding using FSW and UaFSW process. Upper joint was produced with UaFSW process, which used a 20 kHz ultrasonic system, the translational speed of 50 mm/min, and the rotational speed of 650 rpm. Two thermocouples were placed on both sides of the joint line. Lower one was produced with conventional FSW process under same parameters.

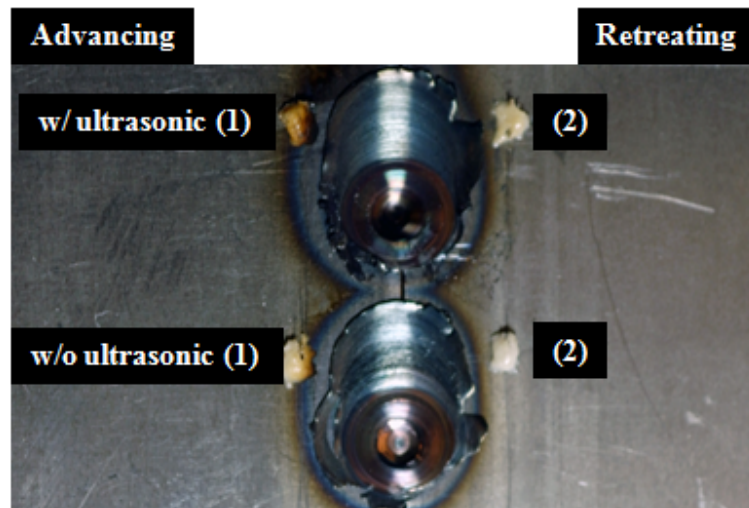


**Figure 5-27 : Top view of friction stir welded 1018 steel; Upper joint is with ultrasonic and lower one is without ultrasonic**



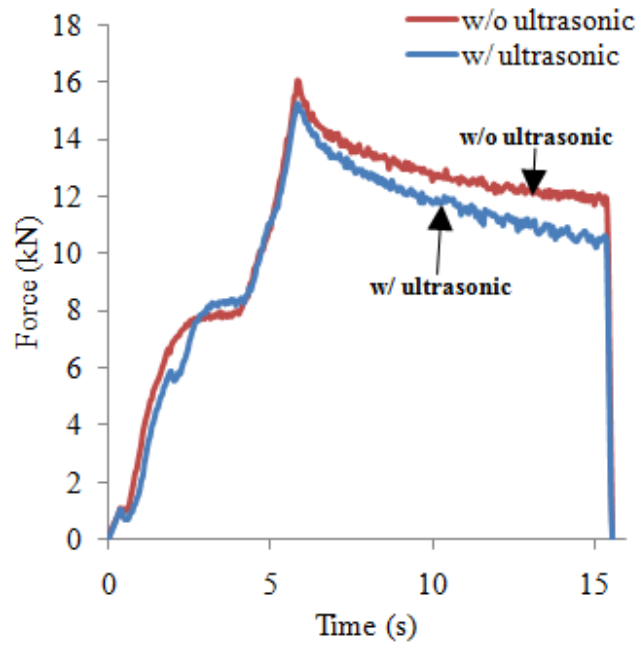


**Figure 5-28 : Effect of ultrasonic vibration on axial forces (Rotational speed of 650 rpm; translational speed of 50 mm/min)**

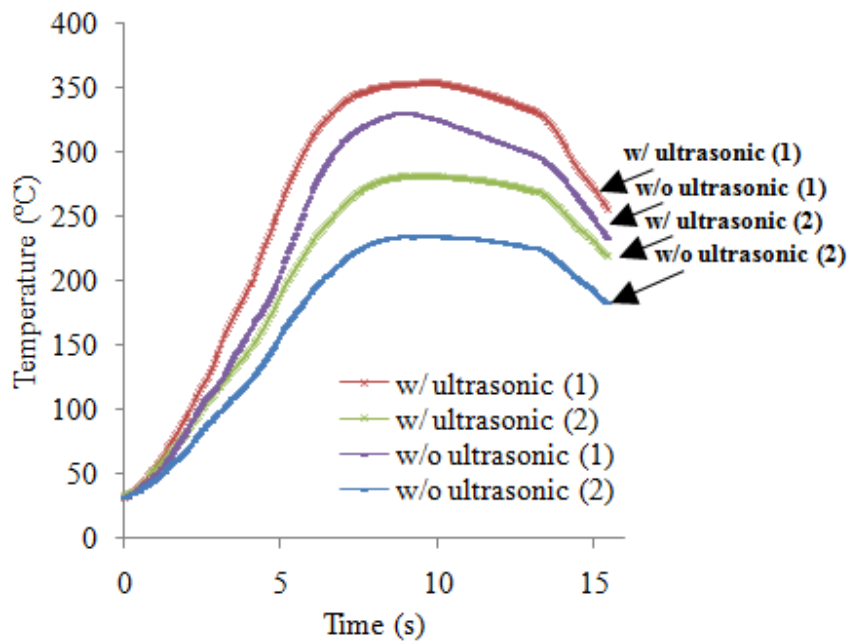


**Figure 5-29 : Effect of ultrasonic vibration on temperature profiles (Rotational speed of 650 rpm; translational speed of 50 mm/min)**

Figure 5-28 shows the effect of ultrasonic vibration on the axial forces. Measured axial forces in UaFSW are lower than those in the conventional FSW. It can be seen that the axial forces become smaller during both the peak portion and the translational one. We could obtain 6% reduction in the welding peak and around 12.5% reduction in the translational region. Figure 5-29 shows the effect of ultrasonic vibration on the temperature profiles. It can be verified for the welding of 1018 steel that the ultrasonic assistance led to the increase in temperature on the whole welding region.

Other welding trial was carried out with the translational speed of 25 mm/min as shown in Figure 5-30. This is similar to the preceding analysis. 6% reduction in the welding peak and around 20% reduction in the welding region were observed.

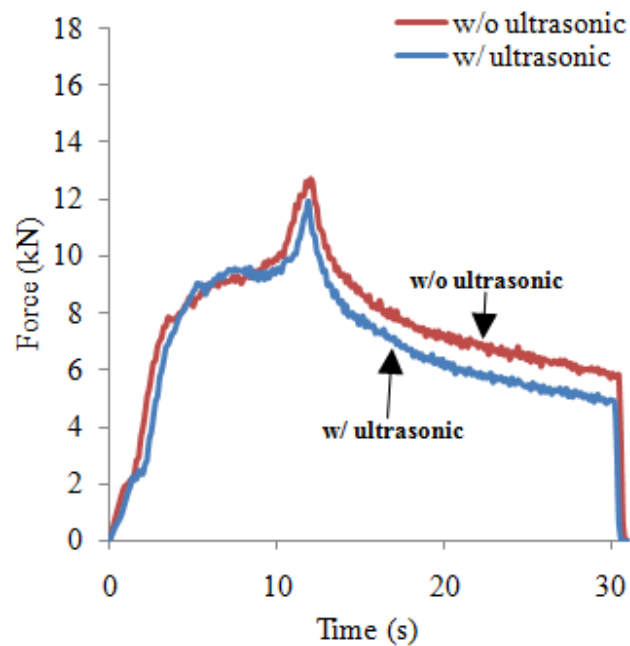


**Figure 5-30 : Axial forces with respect to time (Rotational speed of 650 rpm; translational speed of 25 mm/min)**

## 5.6 CONCLUSIONS

We proposed a development of ultrasonic assisted friction stir welding process. For integrating the ultrasonic system in the conventional FSW process, the design of stepped horn made of aluminum proved to be successful. The FE analysis was helpful to the design and tuning process of the horn structure.

Taking advantage of the characteristics of ultrasonic vibration, the UaFSW of aluminum alloys enables us to decrease the welding force and enhance mechanical properties of welded part in terms of elongation and yield strength. It was shown that ultrasonic integration on FSW tool helps to decrease the chance of formation of welding defect. Moreover, potential benefits of UaFSW process for steel workpiece include the reduction in axial forces and the increase in temperature profiles.

## **CHAPTER 6 - CONCLUSIONS AND FUTURE WORK**

### **6.1 CONCLUSIONS**

This research is focused on the development of the ultrasonic assisted friction stir welding (UaFSW) process. The feasibility of the proposed hybrid FSW process has been investigated through the experimental tests and numerical simulation.

For integrating the ultrasonic system in the conventional FSW process, the design of stepped horn made of aluminum proved to be successful. The FE analysis was helpful to the design and tuning process of the horn structure. We obtained a resonance frequency of the ultrasonic horn as close as possible to the working frequency of the ultrasonic generators. Greater amplitude and firm coupling between the horn and the FSW tool were required for successful welding.

A numerical FE model to determine the influence of the ultrasonic oscillations on the FSW process was developed. The FE analysis was used to simulate plunge forces during the plunge phase of FSW and UaFSW, respectively. For FE analysis of FSW of aluminum alloy, the coefficient of friction was selected based on the comparison of the plunge forces of FE modeling and experimental measurement results. The plunge forces acquired in both the experiments and the simulation showed a good agreement. The FE model of UaFSW of high melting temperature material was developed using temperature and rate dependent Johnson-Cook model and temperature dependent friction coefficient. For FE analysis of UaFSW, it was observed that the plunge forces were reduced by using

the ultrasonic vibrations. In addition, it was shown that the plunge forces could be decreased by increasing the amplitude of vibrations.

An in-house CNC machine was used to demonstrate the UaFSW. Taking advantage of the characteristics of ultrasonic vibration, the UaFSW enables us to decrease the welding force and enhance mechanical properties of welded part in terms of elongation and yield strength. It was shown that ultrasonic integration on FSW tool helps to decrease the chance of formation of welding defect.

## **6.2 CONTRIBUTIONS**

The major contributions of the dissertation are summarized as follows:

1. A FEM design procedure was developed for the design of a horn for friction stir welding (FSW) process. It was observed that the welding performance of an ultrasonic assisted friction stir welding (UaFSW) depends on the ability of the design of the acoustic horn.
2. Development and investigations on the UaFSW process showed a promising FSW technique for enhancement of welding quality and reduction in welding forces. Ultrasonic assistance had proven to be beneficial to avoid weld defect and to enhance the mechanical properties for UaFSW of aluminum alloys. The ultrasonic assistance on FSW of high melting temperature material helped to reduce welding forces.
3. A FE model constructed using ABAQUS software was proven feasible by

comparing with experimentally measured forces and temperature during plunge stage of the UaFSW process. The FE model supported the finding that the UaFSW could provide better weldability of high melting temperature materials than the conventional FSW. The FE model provides engineers and scientists a convenient tool to enhance the basic understanding of the FSW or friction stir spot welding (FSSW) processes.

### **6.3 RECOMMENDATIONS FOR FUTURE WORK**

To further advance the understanding of ultrasonic assisted friction stir welding (UaFSW) process few tasks that are worth pursuing in the future have been identified as follows:

1. For further enhancement of the UaFSW process, a better methodology for integrating the ultrasonic tooling system needs to be established. It may be necessary to find a method to measure energy dissipation between the ultrasonic horn and the FSW tool. Optimization of the ultrasonic horn also needs to obtain maximum benefit of the UaFSW process
2. The FE modeling should be further developed and extended to improve the modeling results. In reality, the workpiece of aluminum alloy is prone to stick to the tool so that it results in the complicated friction characteristics. A partial sliding or sticking methods should be added on the FE model.

3. To better demonstrate the feasibility of FSW of high melting temperature materials, several tool materials need to be tested by characterizing the process, microstructure, and mechanical properties of friction stir welds on high melting temperature materials. It may be necessary to measure tool wear. A better tool geometry can also help to achieve good results of the UaFSW process.
  
4. Microstructural analysis should be conducted. Based on the guidelines from this research work, it may be necessary to conduct the microstructural investigation to understand how the ultrasonic assistance influences on the friction stir welds.

## BIBLIOGRAPHY

Able, N. and Pfefferkorn, F. (2005). "Laser-assisted friction stir lap welding of aluminum." Proceedings of the ASME Summer Heat Transfer Conference, 425-429

Ahmed, N., Mitrofanov, A. V., Babitsky, V. I., and Silberschmidt, V. V. (2007). "3D finite element analysis of ultrasonically assisted turning." Computational materials science 39(1): 149-54.

Alcan (1970). Handbook of aluminum, Alcan aluminum corporation.

Amini, S., Soleimanimehr, H., Nategh, M. J., Abudollah, A., and Sadeghi, M. H. (2008). "FEM analysis of ultrasonic-vibration-assisted turning and the vibratory tool." Journal of materials processing technology 201(1): 43-7.

Arbegast, W. J. and Patnaik, A. K. (2005). "Process parameter development and fixturing issues for friction stir welding of aluminum beam assemblies." Proceedings of the 2005 SAE AeroTech Conference, Dallas, TX.

Awang, M., Mucino, V. H., Feng, Z., and David, S. A. (2005). "Thermo-mechanical modeling of friction stir spot welding(FSSW) process: Use of an explicit adaptive meshing scheme." SAE 2005 World Congress.

Biddell, D. C. and Sansome, D. H. (1974). "The development of oscillatory metal drawing equipment an engineering's view." Ultrasonics: 195-205.

Chang, S. S. F. and Bone, G. M. (2005). "Burr size reduction in drilling by ultrasonic assistance." Robotics and computer-integrated manufacturing 21(4): 442-50.

Chang, U. I. and Frisch, J. (1974). "On optimization of some parameters in ultrasonic metal welding." Welding Journal 53(1): 24-35.

Chao, Y. J. and Qi, X. (1998). "Thermal and thermo-mechanical modeling of friction stir welding of aluminum alloy 6061-T6." Journal of materials processing & manufacturing science 7(2): 215-233.

Chen, C. M. and Kovacevic, R. (2003). "Finite element modeling of friction stir welding - Thermal and thermomechanical analysis." International journal of machine tools & manufacture 43(13): 1319-1326.

Choi, H. (2006). A study on warm hydro forming of lightweight sheet material: Process



optimization. Mechanical engineering. Ann Arbor, University of Michigan. PhD.

Edgar de Vries, D. I. (2004). "Mechanics and mechanisms of ultrasonic metal welding." The Ohio State University. PhD.

Frigaard, O., Grong, O., and Midling, O. T. (2001) "A process model for friction stir welding of age hardening aluminum alloys." *Metallurgical and Material Transactions A: Physical Metallurgy and Materials Science*, 32(5): 1189-1200

Gao, C. and Liu, Z. (2003). "A study of ultrasonically aided micro-electrical-discharge machining by the application of workpiece vibration." *Journal of materials processing technology* 139(1-3): 226-228.

Guo, Z. N., Lee, T. C., Yue, T. M., and Lau, W. S. (1997). "Study of ultrasonic-aided wire electrical discharge machining." *Journal of materials processing technology* 63(1): 823-828.

Huang, Z., Lucas, M., and Adams, M. J. (2002). "Influence of ultrasonics on upsetting of a model paste." *Ultrasonics* 40(1): 43-8.

Ishikawa, K.-I., Suwabe, H., Nishide, T., and Uneda, M. (1998). "Study on combined vibration drilling by ultrasonic and low-frequency vibrations for hard and brittle materials." *Precision engineering* 22(4): 196-205.

Izumi, O., Oyama, K., and Suzuki, Y. (1966). "Effect of superimposed ultrasonic vibrations on the compressive deformation of metals." *Transaction of Japan Institute of Metal* 7: 162-167.

Johnsen, M. R. (1999). "Friction stir welding takes off at Boeing." *Welding Journal* 78(2): 35-39.

Jones, J. B. and Powers Jr., J. J. (1956). "Ultrasonic welding." *Engineers' digest* 17(10): 436-438.

Kakarla, S. S. T., Muci-Kuchler, K. H., Arbegast, W. J., and Allen, C. D. (2005). "Three-dimensional finite element model of the friction stir spot welding process", *Friction Stir Welding and Processing III. Proceedings of a Symposia Sponsored by the Shaping and Forming Committee of the Materials Processing and Manufacturing Division of TMS.*

Kohn, G, Greenberg, Y., Makover, I., and Munitz, A. (2002). "Laser-assisted friction stir welding." *Welding Journal* 81(2): 46-48.

Kremer, D. (1981). "The state of the art of ultrasonic machining." *CIRP annals* ...

manufacturing technology 30(1): 107-10.

Kuhn, H. and Medlin, D. (2000) "ASM Handbook: Volume 8: Mechanical testing and evaluation" ASM International, 10<sup>th</sup> edition

Langenecker, B. (1965). "Metal deformation in macrosonic fields." Society of Automotive Engineers – Papers, p17

Langenecker, B. (1966). "Effects of ultrasound on deformation characteristics of metals." IEEE transactions on sonics and ultrasonics 13(1): 1-8.

Langenecker, B. and Jones, V. O. (1970). "Macrosonic wire drawing and tube bending." Proceedings of 1st International Symposium High Power Ultrasonics.

Lienert, T. J., Stellwag Jr, W. L., Grimmett, B. B., and Warke, R. W. (2003). "Friction stir welding studies on mild steel." Welding Journal 82(1): 1-9.

Liu, H. J., Feng, C., Fujii, H., and Nogi, H. (2005) "Wear characteristics of a WC-Co tool in friction stir welding of AC4A+30 vol%SiCp composite." International journal of machine tools and manufacture 45, pp1635-1639

Mahoney, M. W, Rhodes, C. G., Flintoff, J. G., Bingel, W. H., and Spurling, R. A. (1998). "Properties of friction-stir-welded 7075 T651 aluminum." Metallurgical and Materials Transactions; A; Physical Metallurgy and Materials Science 29(7): 1955-64.

Mandal, S., Rice, J., and Elmustafa, A. A. (2008) "Experimental and numerical investigation of the plunge stage in friction stir welding." Journal of Materials Processing Technology 203, pp411-419

Mazda (2003). "Mazda develops world's first aluminum joining technology using friction heat." from <http://www.mazda.com/publicity/release/200302/0227e.html>.

McMaster-Carr "Guidelines for heat treating tool steel." Document 8864KAC

Mendez, P. F. and Eagar, T. W. (2001). "Welding processes for aeronautics." Advanced materials & processes 159(5): 39-43.

Meran, C., Kovan, V., and Alptekin, A. (2007) "Friction stir welding of AISI 304 austenitic stainless steel" Materialwissenschaft und Werkstofftechnik, 38(10): 829-835.

Miller, S. F. (2006). Friction drilling. Mechanical engineering. Ann Arbor, University of Michigan. PhD.

- Mishra, R. S. and Ma, Z. Y. (2005). "Friction stir welding and processing." *Materials Science & Engineering. R, Reports* 50(1): 78-78.
- Mitrofanov, A. V., Babitsky, V. I., Silberschmidt, V. V. (2003). "Finite element simulations of ultrasonically assisted turning." *Computational materials science* 28(3): 645-53.
- Mitrofanov, A. V., Babitsky, V. I., Silberschmidt, V. V. (2004). "Finite element analysis of ultrasonically assisted turning of Inconel 718." *Integration, The VLSI Journal*, 38(1): 233-9.
- Mori, L. F., Lee, S., Xue, Z. Y., Vaziri, A., Queheillalt, D. T., Dharmasena, K. P., Wadley, H. N. G., Hutchinson, J. W., and Espinosa, H. D. (2007) "Deformation and fracture modes of sandwich structures subjected to underwater impulsive loads" *Journal of Mechanics of Materials and Structures*, 2(10), pp1981-2006
- Mousavi, S. A. A. A., Feizi, H., and Madoliat, R. (2007). "Investigations on the effects of ultrasonic vibrations in the extrusion process." *Journal of materials processing technology* 187-188: 657-661.
- Neugebauer, R. and Stoll, A. (2004). "Ultrasonic application in drilling." *Journal of materials processing technology* 149(1): 633-9.
- Nicholas, T. (1981). "Tensile testing of materials at high rates of strain." *Experimental mechanics* 21(5): 177-85.
- Ohba, H., Ueda, C., and Agatsuma, K. (2001). "Innovative vehicle - The "A-train"." *Hitachi technology* 50(4): 130-133.
- Pohlman, R. and Lehfeldt, E. (1966). "Influence of ultrasonic vibration on metallic friction." *Ultrasonics* 4: 178-185.
- Reitz, V. (2002). "Causing a stir in welding." *Welding Design & Fabrication* 75(4): 46-49.
- Rosochowska, M. and Rosochowski, A. (2007). "FE simulation of ultrasonic back extrusion." *AIP conference proceedings* 907(1): 564-9.
- Sansome, D. H. (1973). "Recent developments in oscillatory metal working." *Engineering* 213(4): 243-247.
- Sato, Y. S., Kokawa, H., Enomoto, M, and Jogan, S. (1999). "Microstructural evolution of 6063 aluminum during friction-stir welding." *Metallurgical and Materials Transactions; A; Physical Metallurgy and Materials Science* 30(9): 2429-2437.

Schmidt, H. and Hattel, J. (2005). "A local model for the thermomechanical conditions in friction stir welding." *Modelling and Simulation in Materials Science and Engineering* 13(1): 77-93.

Severdenko, V. P. and Petrenko, V. V. (1969). "The temperature conditions during open die upsetting of steel in an ultrasonic field." *Izv. Akad. Nauk. B.S.S.R.*

Singh, R. and Khamba, J. S. (2006). "Ultrasonic machining of titanium and its alloys: A review." *Journal of materials processing technology* 173(2): 125-35.

Tang, W., Guo, X., and McClure, J. C. (1998). "Heat input and temperature distribution in friction stir welding." *Journal of materials processing & manufacturing science* 7(2): 163-172.

Thomas, W. M., Johnson, K. I., and Wiesner, C. S., (2003). "Friction stir welding-recent developments in tool and process technologies." *Advanced engineering materials* 5(7): 485-490.

Thomas, W. M., Nicholas, E. D., Needham, J. C., Murch, G., Temple-Smith, P., and Dowes, C. J. (1991). "Friction stir butt welding."

Threadgill, P. L. (1999). "Friction stir welding-State of the Art." TWI Report 678

Tsujino, J. (1995). "Recent developments of ultrasonic welding." *IEEE Ultrasonics Symposium. Proceedings. An International Symposium.*

Tsujino, J., Ueoka, T., Hasegawa, K., Fujita, Y., Shiraki, T., Okada, T., and Tamura, T. (1996). "New methods of ultrasonic welding of metal and plastic materials." *Ultrasonics* 34(2): 177-85.

Tsujino, J., Hidai, K., Hasegawa, A., Kanai, R., Matsuura, H., Matsushima, K., and Ueoka, T. (2002). "Ultrasonic butt welding of aluminum, aluminum alloy and stainless steel plate specimens." *Ultrasonics* 40(1): 371-374.

Tweedy, B. M., Arbegast, W., and Allen, C. (2005). "Friction stir welding of ferrous alloys using induction preheating." *Friction Stir Welding and Processing III*. 97-104

Vural, M., Ravichandran, G., and Rittel, D. (2003) "Large strain mechanical behavior of 1018 cold-rolled steel over a wide range of strain rates", *Metallurgical and Materials Transactions A*, 34(12), pp2873-2885

Winsper, C. E. (1969). Study of the mechanics of wire drawing with a superimposed ultrasonic stress. *Proc 10th MTDR Conf, Advan in Mach Tool Des and Res*: 553-65.

Winsper, C. E. and Sansome, D. H. (1969). "Fundamentals of ultrasonic wire drawing." *Journal of the Institute of Metals* 97: 274-280.

Xiao, M., Sato, K., Karube, S., and Soutome, T. (2003). "The effect of tool nose radius in ultrasonic vibration cutting of hard metal." *International journal of machine tools & manufacture* 43(13): 1375-82.

Yuncu, H. (2006). "Thermal contact conductance of nominally flat surfaces." *Heat and mass transfer* 43(1): 1-5.

Zeng, W. M., Wu, H. L., and Zhang, J. (2006). "Effect of tool wear on microstructure, mechanical properties and acoustic emission of friction stir welded 6061 Al alloy." *Acta Metallurgica Sinica* 19(1): 9-19.

Zhang, Z. and Zhang, H. W. (2007). "Material behaviors and mechanical features in friction stir welding process." *International journal of advanced manufacturing technology* 35(1): 86-100.

Zhang, Z. and Zhang, H. W. (2008). "A fully coupled thermo-mechanical model of friction stir welding." *International journal of advanced manufacturing technology* 37(3): 279-293.

Zhao, Y.-H., Lin, S.-B., Wu, L., and Qu, F.-X. (2005). "The influence of pin geometry on bonding and mechanical properties in friction stir weld 2014 Al alloy." *Materials letters* 59(23): 2948-52.